1997-03

# Lagrangian measurements of eddy characteristics in the California current system

Sires, James Gary

Monterey, California. Naval Postgraduate School

# NAVAL POSTGRADUATE SCHOOL
# MONTEREY, CALIFORNIA


# THESIS

**LAGRANGIAN MEASUREMENTS OF EDDY CHARACTERISTICS IN THE CALIFORNIA CURRENT SYSTEM**

by

James Gary Sires

March 1997

Thesis Advisor: Jeffrey D. Paduan



**Approved for public release; distribution is unlimited**

# REPORT DOCUMENTATION PAGE

Form Approved OMB No. 0704-0188



| 1. AGENCY USE ONLY *(Leave blank)* | 2. REPORT DATE | 3. REPORT TYPE AND DATES COVERED |
|---|---|---|
| | March 1997 | Master's Thesis |

| 4. TITLE AND SUBTITLE | 5. FUNDING NUMBERS |
|---|---|
| LAGRANGIAN MEASUREMENTS OF EDDY CHARACTERISTICS IN THE CALIFORNIA CURRENT SYSTEM | |
| 6. AUTHOR(S) James Gary Sires | |
| 7. PERFORMING ORGANIZATION NAME(S) AND ADDRESS(ES)<br>Naval Postgraduate School<br>Monterey CA 93943-5000 | 8. PERFORMING ORGANIZATION REPORT NUMBER |
| 9. SPONSORING/MONITORING AGENCY NAME(S) AND ADDRESS(ES) | 10. SPONSORING/MONITORING AGENCY REPORT NUMBER |

11. SUPPLEMENTARY NOTES The views expressed in this thesis are those of the author and do not reflect the official policy or position of the Department of Defense or the U.S. Government.

| 12a. DISTRIBUTION/AVAILABILITY STATEMENT | 12b. DISTRIBUTION CODE |
|---|---|
| Approved for public release; distribution is unlimited. | |

13. ABSTRACT *(maximum 200 words)*

During the Eastern Boundary Current program in 1993, 96 Argos-tracked surface drifters, drogued to 15 m depth, and satellite thermal imagery were used to provide a description of the mesoscale features in the California Current System off the northern California coast. The drifter movements and satellite images revealed a highly energetic series of filaments and eddies that dominated the summer flow field off the coast, similar to those noted in the earlier CODE, OPTOMA, and CTZ studies. Winter mesoscale activity in the region was less energetic, with the principle feature being the poleward-flowing Davidson Current.

Translation rates for mesoscale eddies were deduced from drifter trajectories in the summer period. Translation rates, vorticity, divergence and eddy center positions were also estimated for a cyclone and anticylone sampled in July and September, respectively, by constraining observed drifter velocities to a linear Taylor expansion in the least square sense. Translation rates from this technique were similar to those observed from previous shipboard surveys and drifter motions. Using observations over 7 (12) days, the cyclonic (anticyclonic) eddy was determined to have a translation rate of 3.7 (4.2) cm/s to the southwest. The least square technique, applied to shorter time periods, however, provided unreliable estimates of eddy properties when drifters were not evenly distributed around the eddy.

| 14. SUBJECT TERMS eddy, drifter buoys, ARGOS, AVHRR, California Current | 15. NUMBER OF PAGES 135 |
|---|---|
| | 16. PRICE CODE |

| 17. SECURITY CLASSIFICATION OF REPORT | 18. SECURITY CLASSIFICATION OF THIS PAGE | 19. SECURITY CLASSIFICATION OF ABSTRACT | 20. LIMITATION OF ABSTRACT |
|---|---|---|---|
| Unclassified | Unclassified | Unclassified | UL |

NSN 7540-01-280-5500

Standard Form 298 (Rev. 2-89)
Prescribed by ANSI Std. 239-18 298-102

**Approved for public release; distribution is unlimited.**

# LAGRANGIAN MEASUREMENTS OF EDDY CHARACTERISTICS IN THE CALIFORNIA CURRENT SYSTEM

James G. Sires
Lieutenant, United States Navy
B.A., Memphis State University, 1989

Submitted in partial fulfillment
of the requirements for the degree of

**MASTER OF SCIENCE IN PHYSICAL OCEANOGRAPHY**

from the

**NAVAL POSTGRADUATE SCHOOL**
**March 1997**

## ABSTRACT

During the Eastern Boundary Current program in 1993, 96 Argos-tracked surface drifters, drogued to 15 m depth, and satellite thermal imagery were used to provide a description of the mesoscale features in the California Current System off the northern California coast. The drifter movements and satellite images revealed a highly energetic series of filaments and eddies that dominated the summer flow field off the coast, similar to those noted in the earlier CODE, OPTOMA, and CTZ studies. Winter mesoscale activity in the region was less energetic, with the principle feature being the poleward-flowing Davidson Current.

Translation rates for mesoscale eddies were deduced from drifter trajectories in the summer period. Translation rates, vorticity, divergence and eddy center positions were also estimated for a cyclone and anticylone sampled in July and September, respectively, by constraining observed drifter velocities to a linear Taylor expansion in the least square sense. Translation rates from this technique were similar to those observed from previous shipboard surveys and drifter motions. Using observations over 7 (12) days, the cyclonic (anticyclonic) eddy was determined to have a translation rate of 3.7 (4.2) cm/s to the southwest. The least square technique, applied to shorter time periods, however, provided unreliable estimates of eddy properties when drifters were not evenly distributed around the eddy.

**TABLE OF CONTENTS**

## ACKNOWLEDGEMENTS

This thesis could not have been written without the help and encouragement of a number of people. My thesis advisor, Dr. Jeffrey Paduan has been nothing short of outstanding, provided me the with the help and support I needed to complete this project on time. My second reader, Dr. Pierre-Marie Poulain provided expert critique and was a ready source of assistance throughout my research. Among the many at NPS who provided me with help and guidance are Dr. Mary Batteen, Mr. Paul Jessen, Mr. Brian Brown. This thesis would never have been completed without the assistance, patience, and friendship of Mr Michael Cook, one of the best programmers I know.

From Oregon State, I wish to thank Dr. T. Strub for the AVHRR satellite imagery, Dr. M. Abbott for the drifter information on the OSU deployed buoys, and Drs. A. Huyer and M. Kosro for the hydrographic survey data.

Dr. R. Beardsley and Mr. R. Limeburner of the Woods Hole Oceanographic Institution kindly provided processed drifter data and Dr. M. Swenson of NOAA/AOML provided specially filtered drifter data that made it possible to assess the impact of high-frequency motions.

Only through the love and patience of my wife, Ann, and our children, Rachael, Gordon Nichole and Sarah was the completion of this thesis possible. This work is dedicated to them.

# I. INTRODUCTION

As the United States Navy sails into the twenty-first century, the capabilities of its allies and potential adversaries are nearing its own. Only through a thorough understanding of the oceanic environment in which it operates, and the ability to take advantage of that environment, will the Navy of tommorrow remain as superior a force as it is today. Programs such as the Eastern Boundary Current research initiative, which focused on the mesoscale field off the coast of California, provide an important base of knowledge from which tactical and strategic decisions aids (models) can be formulated.

Knowledge of the mesoscale features are of particular importance to naval operations. Important parameters such as acoustical ranges for surface and submarine operations, as well as amphibious and mine/countermine operations, can be directly impacted by eddies, jets, filaments and coastal upwelling regions. This thesis is written with the hope of further increasing our knowledge and understanding of mesoscale variability in near-coastal regimes.

## A. THE CALIFORNIA CURRENT SYSTEM

The California Current System (CCS) represents the eastern limb of the anticyclonic subtropical gyre in the North Pacific. The CCS is a complex system of jets, filaments and eddies that, along with the general wind driven circulation, comprise the southward flow. The dominant scales and dynamics of the circulation over much of the CCS are set by several

general characteristics of the physical environment, namely: 1) strong wind stress forcing, 2) large alongshore scales for both the wind field and bottom topography and 3) a relatively narrow and deep continental shelf (Hickey, 1996). The CCS can be broken down into three principal parts, the California Current, the California Undercurrent and the Davidson Current (Figures 1.1-1.3).

### 1. California Current

The California Current (CC), as traditionally defined, flows equatorward year round offshore of the U.S. west coast from the shelf break to a distance of 1000 km from the coast. The current is a surface current (0-300 m deep) with speeds typically less than 25 cm/s with characteristics of low temperature, low salinity and high dissolved oxygen (Lynn and Simpson, 1987; Hickey, 1996). Whether the current itself is comprised of eddies and jets or whether they are mesoscale features superimposed onto the general southward flow is still debated. Recent studies (Strub et al., 1991; Strub and James, 1995) have shown a strong offshore southward-flowing jet that carries most of the transport of the California Current during the spring and summer months with filaments and eddies inshore of the jet.

### 2. California Undercurrent

The California Undercurrent (CU) is a relatively narrow feature (10-40 km) that flows poleward over the continental slope from Baja California to at least Vancouver Island, occasionally interrupted by eddy-like features (Hickey, 1996). Water in the CU is of equatorial origin, high in temperature and salinity with maximum speeds up to 50 cm/s and seasonal means of about 10 cm/s (Lynn and Simpson, 1987; Hickey 1996).

### 3. Davidson Current

The Davidson Current, also called the inshore surface current (IC) by Lynn and Simpson (1987), is the poleward flowing surface current over the shelf and slope. The IC, which may be a seasonal surfacing of the CU, can extend to 100 km or more in width and can be as strong as or stronger than the corresponding poleward undercurrent (Lynn and Simpson, 1987; Hickey, 1996). Interannual variations in the IC appear primarily due to remote forcing by poleward propagating coastally trapped waves originating in the tropics and to local forcing by anomalous onshore Ekman transport in winter (Rienecker and Mooers, 1989a).

### 4. Wind Fields over the CCS

A major driving force behind the CCS is strong wind stress forcing. Nelson (1977) described the wind field in the CCS as being seasonal in nature. Summer wind stress fields show a strong southerly flow throughout the CCS (Figure 1.4). Winter wind stress patterns (Figure 1.5) show flow dividing in the vicinity of Cape Mendocino. Winds to the north of Cape Mendocino generally flow northward along the coastline. South of San Francisco Bay, the winds change only in magnitude, not direction from their southerly flow. The area between Cape Mendocino and San Francisco Bay is marked by generally weak and variable winds during the winter months. The transition from the winter to summer wind fields, known as the spring transition (Huyer et al., 1979) is a rapid transition, occurring over the course of only one to two days. The corresponding fall transition back to winter winds is a more graduate, less dynamic change.

## B. PREVIOUS EXPERIMENTS IN THE CCS

### 1. CalCOFI Program

In response to the collapse of the lucrative sardine fishing industry, the California Cooperative Oceanic Fisheries Investigation (CalCOFI) program was begun. Since 1950, the stations established by the program have been repeatedly occupied at varying intervals based on a geographically fixed grid. These stations run from just offshore to approximately 700 km off the coast, from Point Reyes to the southern Baja Peninsula. Spacing between stations is approximately 74 km (Lynn and Simpson, 1987).

The CalCOFI dataset is the most complete decades-long oceanic time series in the world. The data from this project was the key source for numerous oceanic studies up until the 1980s and remains an important source of data to reinforce current studies. Although the longevity of this dataset helped to answer many questions, the coarse spatial resolution of the dataset also raised many questions.

### 2. OPTOMA Experiments

The OPTOMA (Ocean Prediction through Observations, Modeling and Analysis) program aimed to provide an improved description of the mesoscale variability of the CCS in order to gain a better understanding of its governing dynamics. It also aimed to investigate the feasibility and practical limitations of mesoscale ocean predictions. Results of the CalCOFI project showed that the CC may have mesoscale features such as jets and eddies embedded in the equatorward flow (Riencher and Mooers, 1989b). As a result, OPTOMA researchers from the Naval Postgraduate School and Harvard University conducted a series

of experiments over four years (1982-1986) off the coasts of northern and central California, concentrating mainly on the region off Point Arena and Point Reyes. A series of 45 oceanographic surveys were conducted with observations acquired primarily from ship surveys; aircraft surveys were used to obtain synoptic descriptions and thus test whether the asynoptic surveys were aliasing the signal to an inappropriate description of the variability (Rienecker and Mooers, 1989b).

The OPTOMA program also included current meter observations from three moorings off Point Arena separated by 100 km from one another. The moored current meter spanned the water column from 150 m below the surface to 200 m above the ocean floor in depths of 3500 m-4300 m. These moorings were set, from October 1984-July 1985, to investigate current variability and its relation to the variability inferred from maps of dynamic height, the temporal and spatial relationship between barotropic and baroclinic flow and the relation between ocean variability and wind forcing (Rienecker and Mooers, 1989a). The OPTOMA program can be separated into three parts: a) shipboard and aircraft surveys, b) the moored current meter observations and c) the modeling efforts conducted with the dataset.

### *a. OPTOMA Shipboard Observations*

A series of dynamic height charts from shipboard and aircraft observations relative to 450 db were compiled showing the seasonal mesoscale variability in the CC. Forcing from alongshore wind stress produced positive values of wind stress curl in the summer months and negative values in the winter. By comparing the forcing parameters

with the dynamic height charts, the researchers were able to draw the following conclusions (Rienecker and Mooers, 1989a):

1) Eddies are ubiquitous features of the CCS

2) The main difference between summer and winter regimes is the presence of an intense, near-shore current filament associated with the summer coastal upwelling regime.

3) Current meanders in the summer are sharper, so they have a smaller horizontal scale.

### *b. OPTOMA Current Meter Data*

The current meter data variability was seen to be consistent with that from the quasi-synoptic surveys. The circulation within the array appeared to be influenced by eddies, as seen by the lack of large-scale coherence between velocity and temperature variations at the different stations. The array did provide some evidence that the eddies move offshore, but it provided no firm evidence that the eddies proceeded southward (Rienecker and Mooers, 1989a).

### *c. OPTOMA Modeling Efforts*

The final goal of the OPTOMA experiments was to identify the feasibility and limitations of open ocean forecasting. Three of the OPTOMA surveys were designed specifically for ocean prediction experiments. From these surveys, several forecast experiments were conducted by initializing a dynamic model with observed fields and allowing the model to evolve the fields according to assumed dynamics and various boundary data. It was found, if given accurate initial, boundary and surface forcing data, that the

mesoscale fields of the CCS could be predicted with quasi-geostrophic dynamics. Dynamic instability processes were shown to operate and the importance of wind stress curl was identified (Rienecker and Mooers, 1989a).

### 3. CODE Experiments

As the OPTOMA experiments were just beginning another detailed study, this one on the continental shelf, was concluding. Entitled the Coastal Ocean Dynamics Experiment (CODE), it was designed to identify and study those dynamical processes which govern the wind-driven motion of water over the continental shelf. Conducted in two parts over the summers of 1981 and 1982, the study concentrated on the shelf region off of Point Arena (Beardsley and Lentz, 1987).

Comprehensive hydrographic surveys of the region were conducted during both segments of the project. CODE I (the first segment) showed that the current field was highly coherent in the vertical, but exhibited larger-than-expected horizontal mesoscale variability over the shelf and slope. This variability may have been strongly influenced by offshore eddy features, distant and local wind forcing and local topographic features such as Point Arena. CODE II was then designed with reduced vertical, but increased horizontal sampling to study the mesoscale variability in all parameters (Beardsley and Lentz, 1987).

Drifter observations during CODE showed rapid and direct communication between the shelf and slope regions (Davis, 1985a). The means of offshore transport, jets, squirts and filaments were found to be more representative of transient features than permanent structures. The drifters showed a much more complex view of the flow field than previously thought (Davis, 1985a, b).

Results from CODE showed that, associated with cold filaments, such as the one off Point Arena, the strong current jets noted by Davis (1985a,b) extended 100 m or more below the surface with core speeds in excess of 50 cm/s. These strong filaments had the equivalent transport of the wind-driven offshore transport over a 1000 km section of the coast (Beardsley and Lentz, 1987). In terms of the ocean mesoscale, this proved to be the most significant finding of the study. Other results of CODE included detailed studies of the separate contributions of local and remote wind forcing and numerous modeling efforts, in particular models based on coastally trapped waves (Hickey, 1996).

Although the CODE study was concentrated on the shelf, it still left some important questions unanswered. It failed to resolve the oceanic boundary layers enough to study the detailed physics of the region. Additionally, it failed to study the filaments it had "discovered" in any real detail, specifically the offshore transport and onshore return flow. It was these unanswered questions that led to the most detailed oceanographic study conducted to date off the Northern California coast.

### 4. CTZ Experiments

The Coastal Transition Zone (CTZ) experiments were the first truly interdisciplinary studies conducted in the CCS with focus on the ocean mesoscale. The CTZ programs combined the use of satellite, airplane and shipboard measurements and drifting buoy and current meter observations as well as numerous modeling efforts to address the unanswered questions from both OPTOMA and CODE. Specifically, the experiments addressed the physical and biological nature of filaments, the causes of filament formation and the physical and biological characteristics of a filament (Brink and Cowles, 1991).

The CTZ experiments were conducted in two parts, a pilot program in 1987, and the main program conducted in the summer of 1988. It was conducted off the continental shelf between 37.5 N and 41.5 N, focusing on the filament off of Point Arena (39 N) for the main program. Surveys included both a large-scale (approximately 400 km alongshore by 150 km acrosshore) grid sampled seasonally in 1987 as well as a somewhat smaller grid (approximately 200 km by 200 km) that was more frequently sampled during the 1988 upwelling season (Brink and Cowles, 1991; Hickey, 1996).

### *a. The 1987 Experiments*

The 1987 experiments were conducted over the course of four cruises, two during winter months (February and March), and two during summer months (May and June). During the winter months, the CTZ group found no coherent flow pattern and little eddy activity with no obvious filaments, reinforcing the earlier studies done by the OPTOMA group. During the summer months, however, a meandering, energetic southward flowing core of the CC was clearly present and the Point Arena filament was seen to be a surface expression of the offshore-directed flow in a meander (Brink and Cowles, 1991). Paduan and Niiler (1990), using drifter and hydrographic observations, estimated the transport in the filament to be approximately 2 Sv, that is, of the same order of magnitude as the total southward transport in the CC. Eddy variability was found to be substantially stronger in the summer surveys. Flow appeared as a complex system, not dominated by a single process or sense of energy conversion. One obvious question was raised: Why is the offshore-directed filament so much colder than those in the onshore-directed meanders (Brink and Cowles, 1991; Strub et al., 1991)?

### *b. The 1988 Experiments*

The main CTZ program was conducted in a series of five successive surveys between mid-June and early August 1988. This phase of the experiment concentrated on one filament, the Point Arena filament (which has become known as the CTZ filament because of these intensive studies), documenting its temporal evolution and the processes that maintained its structure. Dynamic height charts show the Point Arena filament as a surface expression of the offshore-directed flow in a meander.

The CTZ program also resulted in a number of biological, chemical and physical results that helped describe the coastal filaments found in the CCS. Among the key findings were that filament core water originates from upstream and is not just a mixture of coastal and offshore waters. It also showed that a common feature of filaments is a subduction process with distance from the coast. Others found that wind stress plays a part in the near-surface and sub-surface evolution of the CCS. More recent modeling efforts by Batteen (1997) and others confirmed CTZ findings that instabilities play a key role in filament formation, alongshore spacing and strength (Brink and Cowles, 1991; Strub et al., 1991; Hickey, 1996; Batteen, 1997).

The CTZ program is considered one of the most successful studies conducted in the CCS. It concluded that the summertime, southwestward flowing CC core is unstable, leading to a meandering jet surrounded by persistent eddies. Filaments may represent the offshore-directed branches of these meanders (Brink and Cowles, 1991).

## 5. NCCCS Experiments

Off the coast of Cape Mendocino, contemporaneous with the CTZ experiments, the Northern California Coastal Circulation Study (NCCCS) was conducted. This study set out to examine the structure and variability of density and velocity over the northern California shelf, slope and transition region of the CC. Specific objectives of the study were to obtain a comprehensive set of current observations over the shelf and slope, provide a quantitative description of surface circulation and to improve the understanding of the forcing mechanisms (Bray and Greengrove, 1993).

To achieve these goals, seven hydrographic sections extending to 1500 m depth and 70 km offshore were occupied seven times during the study period between March 1987 and October 1989 (Bray and Greengrove, 1993). The deeper level sampled by this study (1500m instead of the usual 500 m) allowed investigation of the seasonal variability of flow at deeper depths over the slope than was previously possible (Hickey, 1996). Additionally, shelf moored current meters, surface drifters and local hydrography were used to study current fluctuations.

The objectives of the NCCCS were to describe a variety of features with alongshore and temporal scales that were not well resolved by CODE. Its most noteworthy result concerned the alongshore and seasonal variation in coastal upwelling. An additional result of the NCCCS was the resulting 2.5-year time series obtained from the shelf moorings. This moored time series was the longest record associated with a comprehensive study on the west coast prior to the moored observations in the Eastern Boundary Current Experiment (Largier et al., 1993; Hickey, 1996).

### 6. EBC-ARI Program

The most recent large-scale study conducted in the CCS was the Eastern Boundary Current (EBC) Experiment conducted between 1992 and 1996. Previous studies, (OPTOMA, CODE, CTZ, NCCCS) revealed abundant mesoscale features whose structure, origin, evolution and importance were not well understood. The purpose of EBC was two-fold, first to understand the physical and biological dynamics of mesoscale interactions in weakly non-linear regimes (i.e., Eastern Boundary Currents) and second, to consider the CC as a prototype system for ocean prediction, with emphasis on mesoscale eddy structures in the upper ocean.

Like the CTZ experiments, EBC was an interdisciplinary study that used a variety of techniques to study the CC. Researchers carried out shipboard surveys with SEASOAR and Acoustical Doppler Current Profiler (ADCP) instruments, satellite imagery and altimetry data and drifter observations. In addition, a moored current meter array was kept in place for three years and a program of intensive modeling was, and continues to be, conducted using the observations.

## C. PREVIOUS MESOSCALE EDDY RESEARCH

In early oceanographic studies, eddies were unknown, ignored or not singled out by any surveys. Not until the 1960s was the growing need to study eddies identified. The decade of the 1960s was characterized by relevant and essential instrumental and technical developments, the detection of some eddy signals in data and a growing awareness of the

necessity of scientific pursuit of the mesoscale variability (Robinson, 1983). The 1970s began with the Soviet experiment POLYGON-70. That study measured eddy currents for several months in the North Atlantic Equatorial Current from a series of moored current meters and extensive hydrographic surveys.

In 1973, the next major ocean experiment, the Mid-Ocean Dynamics Experiment (MODE) was conducted. The study became a milestone for research on mesoscale currents in that a substantially more complete, four-dimensional description of a few mesoscale eddies was obtained. The experiment, centered southwest of Bermuda, intercompared a number of instruments and systems initiated by a series of long-time Eulerian and Lagrangian statistical measurements (Robinson, 1983).

Following MODE was the joint US-USSR POLYMODE program. The field portions of the program were conducted between 1974-1978 at several locations in the western and central North Atlantic Ocean. The program was broken down into three experiments, a synoptic dynamical experiment (SDE), a local dynamic experiment (LDE) and a statistical geographical experiment (SGE). As planned, the center of the experimental area coincided with the center of the earlier MODE experiment. The results consisted in a thorough mapping of this section of ocean and a comparison dataset of eddies that passed through the study region during the experiments (Robinson, 1983).

### 1. Rings Experiments

While these studies were taking place, other research initiatives concentrating on Gulf Stream rings were underway. A group of researchers known as the Ring Group began the first multidisciplinary studies of Gulf Stream rings. Conducted from December 1976-

November 1977, the rings were tracked by free-drifting surface buoys, sub-surface floats, expendable bathythermagraphs (XBT) and conductivity-temperature-depth (CTD) measurements (Ring Group, 1981). This marked the first time a large-scale study had been dedicated to studying rings (eddies) and the first time a large study had used drifting surface buoys to specifically study mesoscale features.

Observations, particularly from drifting buoys and satellite imagery, helped lead to estimates of translation rates and decay rates of rings. By measuring the amount of time for the buoy to loop around the ring, the group was able to conclude that the rotation rate was gradually slowing, indicating the ring's decay rate (Ring Group, 1981). Ring translation was measured using drifting buoy positions as well as thermal satellite imagery.

An even more detailed study of Gulf Stream rings was conducted five years later. The study, called the Warm Core Ring Experiment (WCRE), tracked three warm-core Gulf Stream rings using satellite imagery, XBT/CTD data and surface drifters. The researchers concentrated on one warm-core ring, designated ring 82B, the second warm-core ring of 1982 (Joyce, 1985). The researchers chronologized the ring's life history. Some of them studied it mainly from satellite imagery (Evans et al., 1985). Others presented a more dynamical approach. Olson et al. (1985) studied changes in ring volume, momentum and energetics by utilizing a two-layer diagnostic model from CTD and XBT data. Flierl and Mied (1985) used both numerical and analytical models to examine frictionally driven spin-down (decay) of warm-core Gulf Stream rings. Hooker and Olson (1984) used data from in-situ and drifter measurements to determine the accuracy and nature of satellite imagery.

Chemical and biological analyses of the rings were also made. The multidisciplinary studies of the WCRE and the Ring Group represented the first dedicated large-scale studies of eddies and rings. As a result, it became apparent that a detailed accounting of the mesoscale, and of eddies in particular, was required, thus providing part of the empetus for the EBC experiment.

### 2. Drifter-Based Initiatives

By the mid-1970s, regression techniques gathered from drifting buoy data to determine differential kinematic properties (DKP) of fluid flow (divergence, vorticity, shearing deformation rates and stretching deformation rates) and to describe ocean current kinematics and dynamics had been developed (Molinari and Kirwan, 1975). By the mid-1980s, Kirwan et al. (1984) were able to improve on the previous models by using a paradigm that fixed the flow center to the drifter cluster centroid. Just four years after this model was introduced, Kirwan (1988) pointed out serious bias problems with this paradigm and demonstrated that his regression techniques gave fundamentally unreliable estimates of the DKP under certain flow conditions. Poulain and Niiler (1989) use regression techniques for estimating the DKP in filaments of the southern CCS.

By 1992, Kirwan had found an alternative method for calculating DKP from drifter trajectories (Kirwan et al., 1988; 1990; Kirwan 1992). He assumed that drifters were near an isolated flow field singularity and then inverted the solution to obtain the DKP from individual drifter trajectories. His method allowed for solving DKP of an eddy from as few as one drifter. The method, however, requires determining high-order time derivatives of the

drifter trajectory and required smoothing after each differentiation (Halide and Sanderson, 1993).

In an effort to simplify Kirwan's model, Halide and Sanderson (1993) proposed a linear regression model, later improved by Sanderson (1995), that will be discussed below. The emphasis of this thesis deals with the estimation of the DKP following Sanderson technique using data acquired from coherent drifting buoy deployments during the EBC experiment in the summer of 1993. This thesis also serves as an independent validation of the Sanderson technique in the CCS.

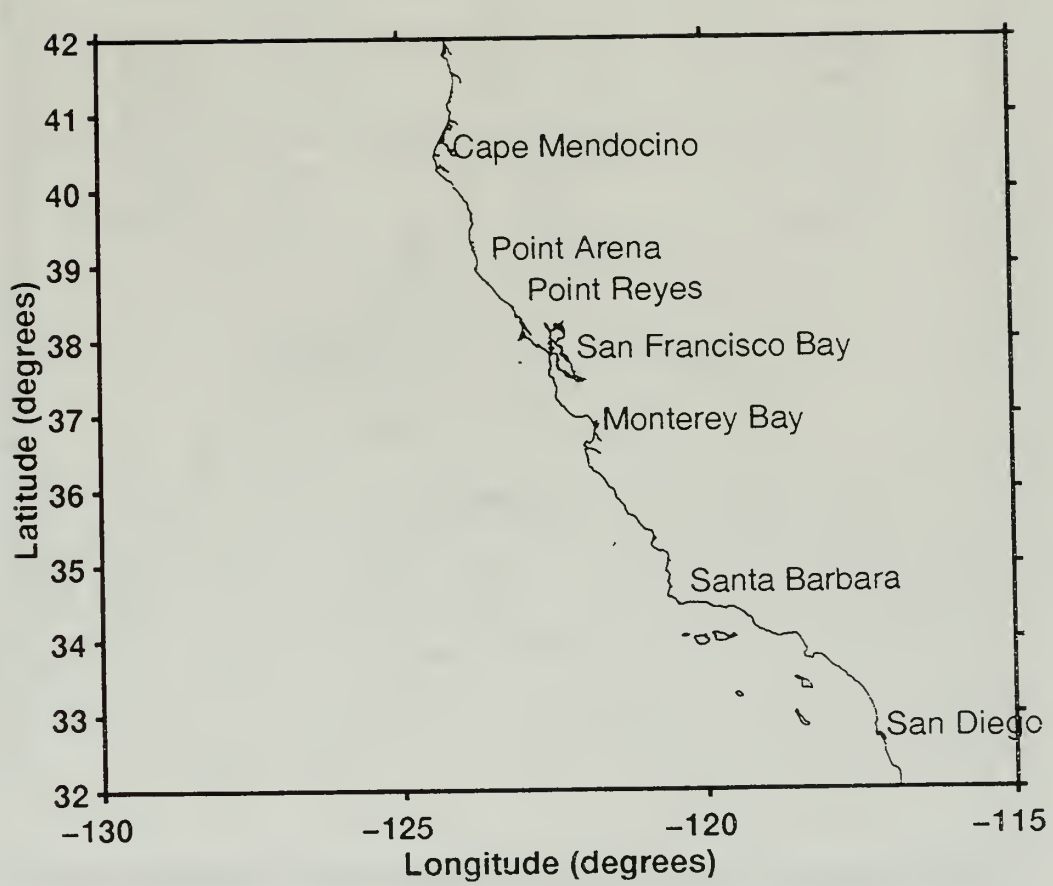


Figure 1.1 The Pacific Coast of California extending from the Oregon border in the north to the Mexican border in the south. Oceanographic features off the northern region from Cape Mendocino to San Francisco were the primary focus for the EBC program.

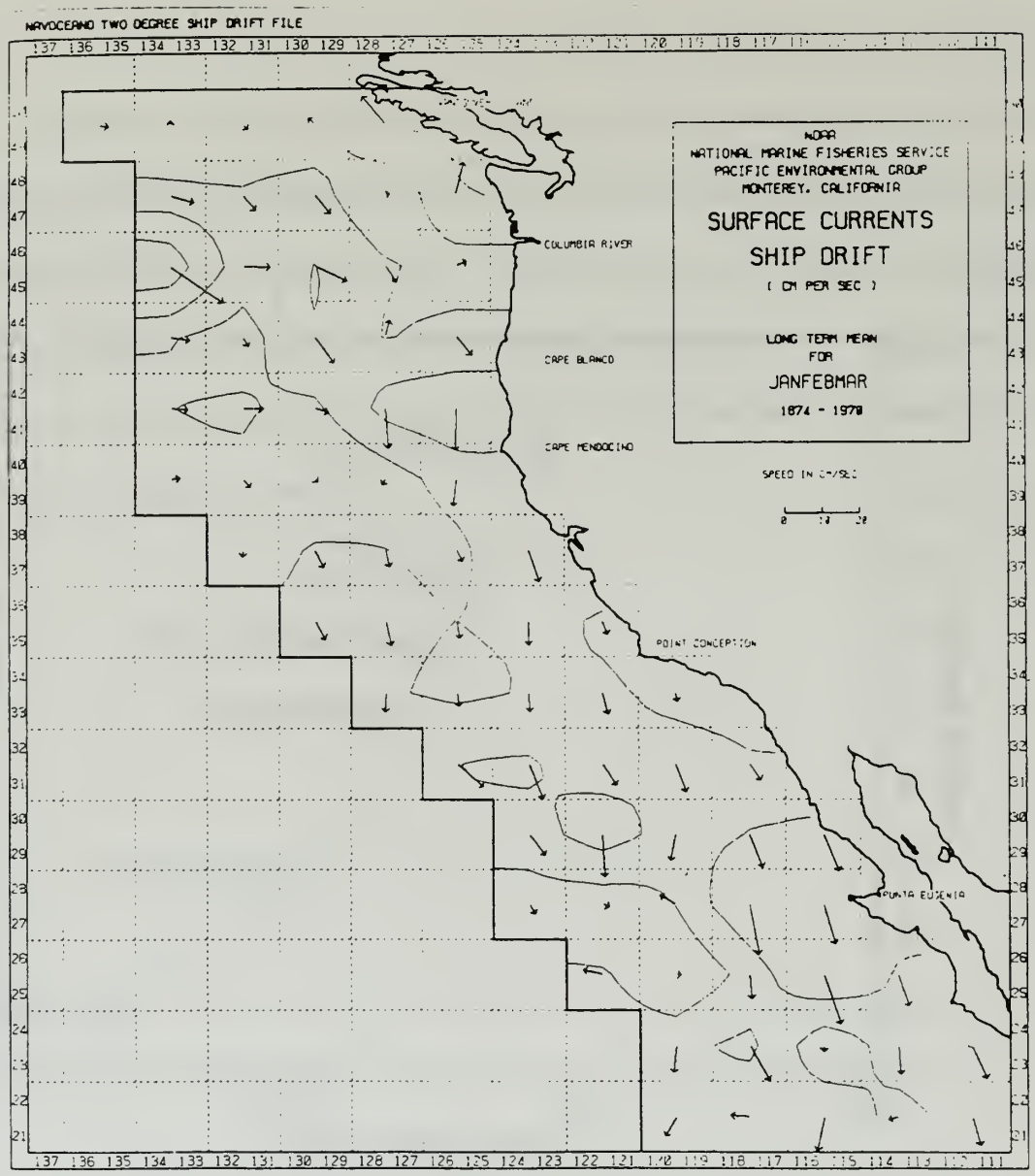


Figure 1.2 Long-term monthly mean distribution of surface ship drift for January-March. Mean vector magnitudes are contoured at intervals of 5 cm/s. Vector symbols are scaled according to the key in the figure. From Hickey (1979).

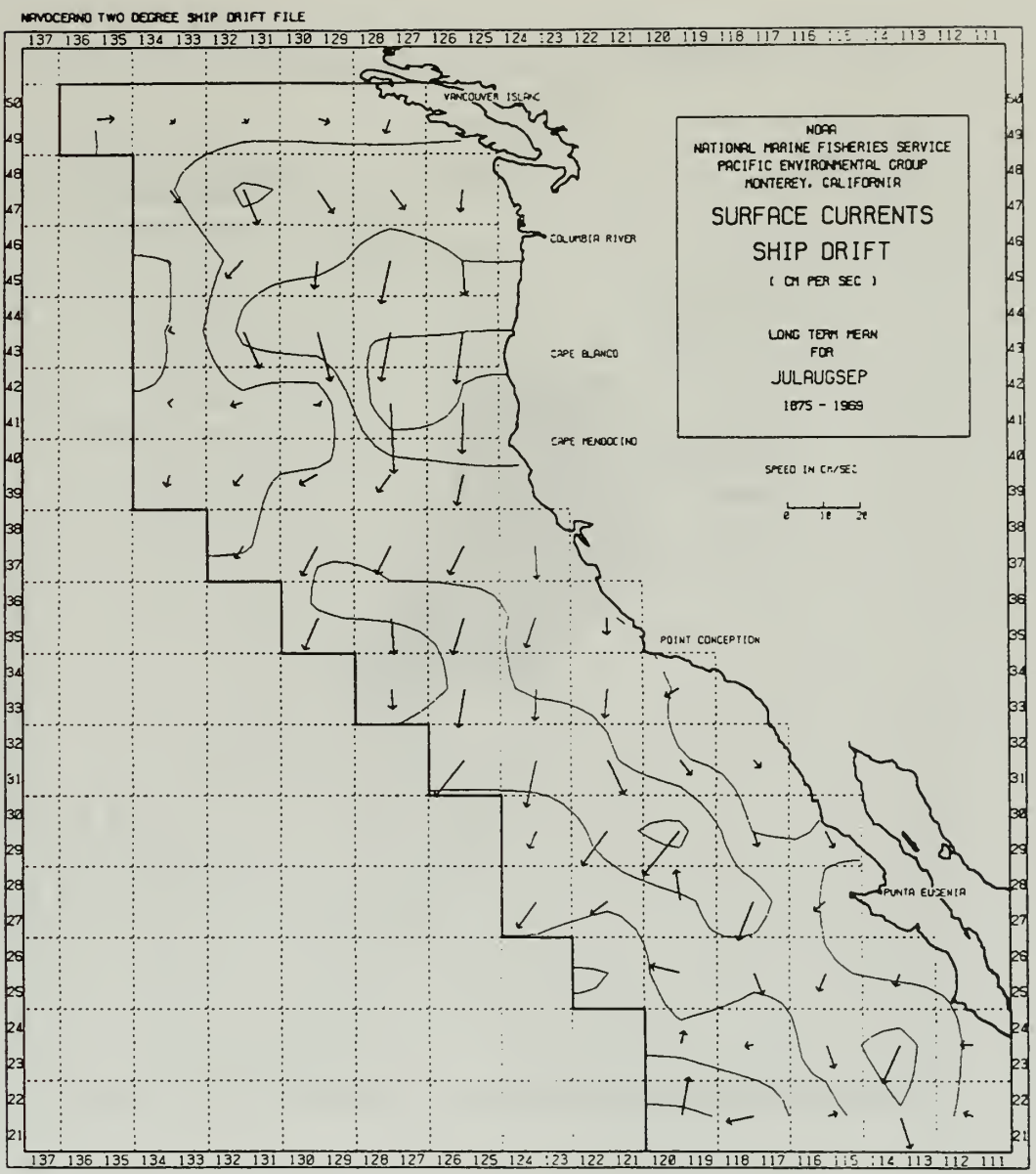


Figure 1.3 Long-term monthly mean distribution of surface ship drift for July-September. Mean vector magnitudes are contoured at intervals of 5 cm/s. Vector symbols are scaled according to the key in the figure. From Hickey (1979).

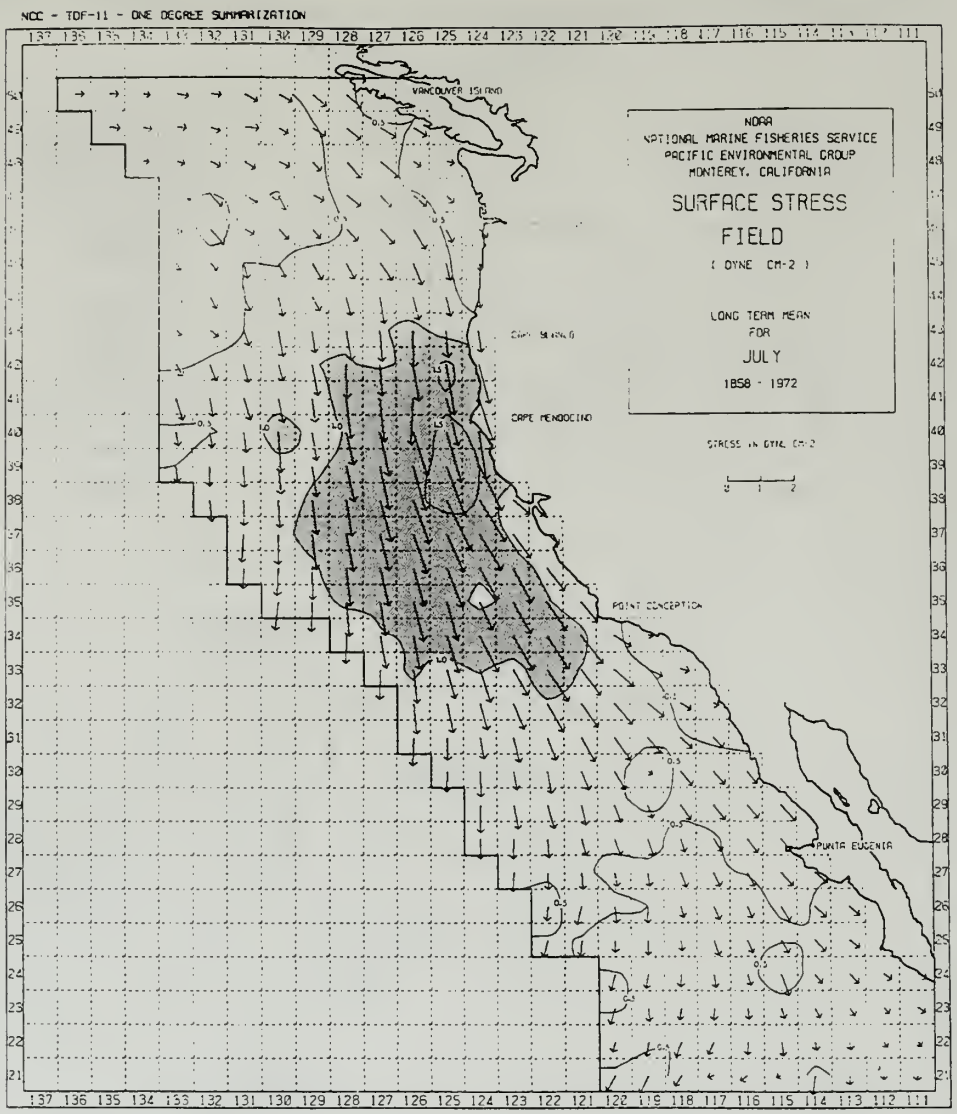


Figure 1.4 Long-term mean surface wind stress vectors for July. Shaded areas are regions of wind stress greater than 1 dyne/cm^2. From Nelson (1977).

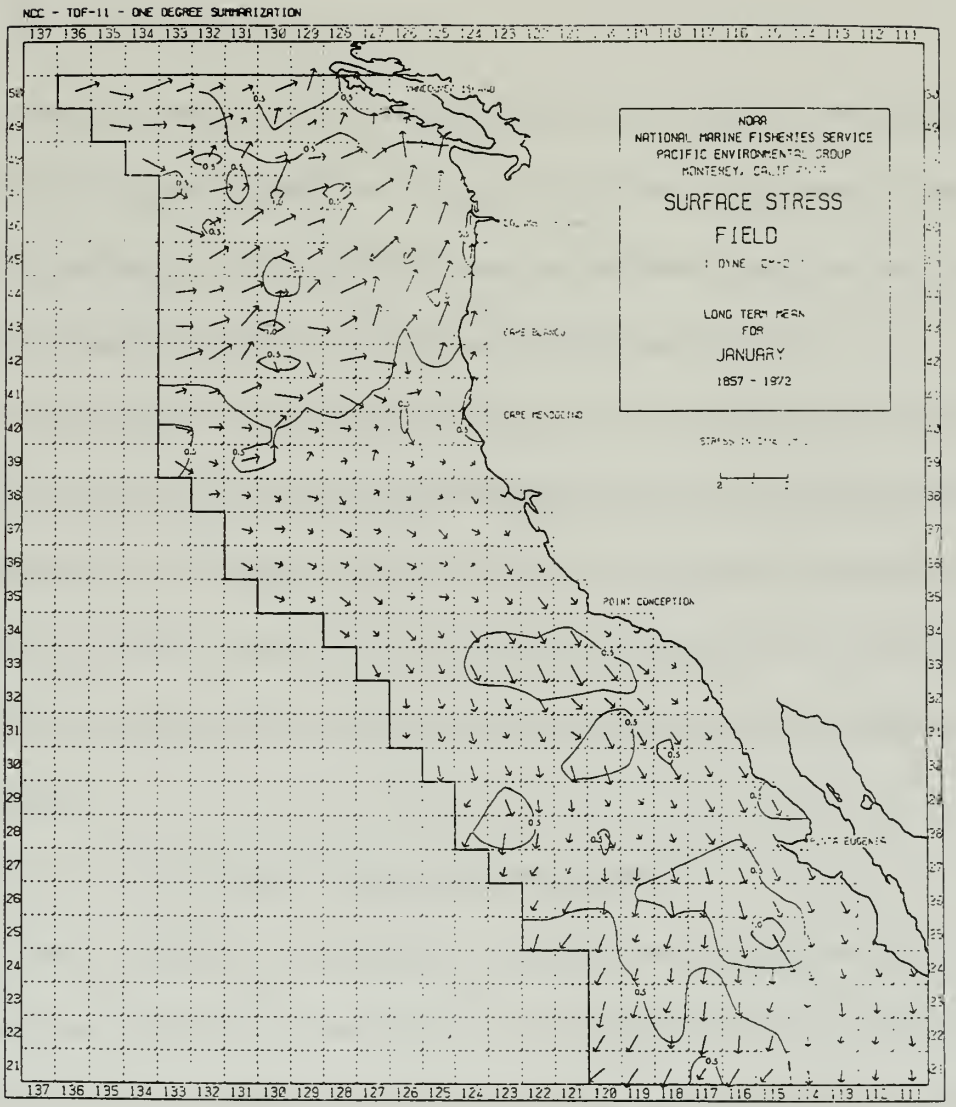


Figure 1.5 Long-term mean surface wind stress vectors for January. Shaded areas are regions of wind stress greater than 1 dyne/cm^2. From Nelson (1977).

# II. DESCRIPTION OF DATA

## A. DRIFTER OBSERVATIONS

Ninety-six drifting buoys were deployed in the EBC study region in 1993. WOCE/TOGA Lagrangian drifters were deployed by various institutions as a direct part of the EBC experiments. Additionally, data were obtained from drifters involved in the World Ocean Circulation Experiment (WOCE) that passed through the region.

NPS deployed twenty-three buoys during two coherent deployments in the summer of 1993. The buoy tracking was the responsibility of EBC researchers during the time period they remained in the CCS (approximately six months). In a data and cost-sharing agreement, the drifters were then turned over to the WOCE researchers who became responsible for tracking and reporting on the drifters but continued to make the data available to the EBC researchers.

### 1. WOCE/TOGA Lagrangian Drifting Buoy

The WOCE/TOGA Lagrangian drifting buoy was designed to follow vertically averaged water parcels approximately 15m below the surface (Niiler et al., 1987). The drifter is comprised of four significant parts, the surface float, the subsurface float, the tether and the drogue (Figure 2.1). In the surface float is the antenna, ARGOS transmitter, batteries, sea surface temperature (SST) and drogue presence sensors. The subsurface float, tethered 3 m below the surface, acts to dampen motions caused by breaking surface gravity waves, which would rapidly accelerate or jerk the drogue assembly (Poulain et al., 1996). Plastic-

impregnated wire rope tethers the surface float to the drogue. The drogue used is the holey-sock, which is approximately 1 m in diameter by 6.5 m in length.

Any drifting buoy that makes use of surface floatation is subject to errors from wind and wind-forced surface gravity waves. The WOCE/TOGA drifter is no exception. The key to minimizing this source of error is using the proper type of equipment. Niiler and Paduan (1995) show that differences in wind-driven currents can be attributed to the water following capabilities of the instrument used. Niiler et al. (1987,1995) list various slip-producing forces that can affect drifters and show that both the shape of the drogue and its drag area ratio (ratio of drag area of drogue to drag area of surface float and tether) are important. The WOCE/TOGA holey-sock drifters have been designed with drag area ratios of approximately 40, to keep the slip of the drogue below 1 cm/sec in 10 m/s windspeed (Niiler et al., 1991, 1995).

The WOCE/TOGA drifters used for EBC were tracked with the ARGOS sensor onboard NOAA polar orbiting satellites. The data was collected by Service Argos and forwarded on to the scientific investigators at Woods Hole Oceanographic Institute (WHOI) and the Naval Postgraduate School (NPS). Brown (1995) provides a detailed description of the ARGOS system of retrieval, processing and dissemination of drifter data. The drifting buoy's longitude and latitude were reported at uneven intervals between six and twelve times per day. These data were processed in three different ways: 1) the entire dataset was low-pass filtered using a technique designed by Limeburner at WHOI and subsampled every six hours, 2) selected trajectories in single eddies were spline-interpolated to one-tenth of a day intervals to preserve the high-frequency information and 3) the eddy trajectories were low-

pass-filtered separately by extracting a best-fit inertial signal each day and retaining the daily positions. Current direction and speed were obtained from the position data.

### 2. Other EBC Drifting Buoys

In addition to the WOCE/TOGA drifters used by NPS and WHOI, special instrumented drifters were deployed by Oregon State University (OSU) and Scripps Institution of Oceanography (SIO) in both the coherent and incoherent arrays. SIO deployed five barometric-pressure sensor buoys to study air pressure readings at the ocean surface. These buoys were deployed during the second coherent deployment in September 1993. Two of the buoys died upon deployment and were not observed by ARGOS.

OSU deployed a total of fifteen buoys during both coherent deployments and three of the four non-coherent (i.e., non-biased) deployments conducted by WHOI. These buoys were deployed with a small, downward-looking spectroradiometer in the surface float that was used to study upwelling radiance. These drifters were drogued with a 40 m holey sock that was approximately 40 cm in diameter with a 15 m tether line (M. Abbott, personal communication). The estimated drag area ratio of these drifters was approximately 40.

### 3. Spatial Coverage

The spatial coverage during 1993 is seen in Figures 2.2-2.5, showing the low-pass filtered tracks of all the drifters passing through the EBC study area. Of the 96 drifters present in the study area, 23 were the NPS deployed buoys and fourteen were SIO and OSU buoys placed in the two coherent deployments. Twenty-eight buoys were deployed by WHOI and six by OSU in four incoherent deployments (discussed in some detail below) and the

remainder happened to drift through the study area as part of the larger-scale WOCE experiment as stated above.

### *a. Coherent Deployments*

A total of 37 drifting buoys were deployed in two separate events to allow the detailed mapping of single eddy features. Original plans called for deploying 12 buoys into an eddy at the conclusion of two planned hydrographic surveys. Using both satellite imagery (discussed in the next section) and results from the hydrographic cruises, seven NPS and six OSU drifting buoys were deployed in a dog-leg track from the NE, through the center of a cyclonic eddy and exiting to the SE approximately 200 km from PT Arena, California in July 1993. Figure 2.6 shows the seasonal strengthening of upwelling-favorable winds at various sites in the EBC area. The July period winds were particularly strong in this area. Because of these winds and corresponding high seas (reaching in excess of 5 m), it was decided not to deploy the remaining buoys planned for this period (Paduan, personal communication). The winds quickly blew the NPS drifters out of the eddy and the drifters moved either northward across the Point Arena filament or southward along with the prevailing winds and currents. Figure 2.7 shows the trajectories of the buoys while still in the eddy superimposed on a satellite SST image of 07 July 93. Due to the limited time the buoys were in the eddy and the poor spacing of buoys around the eddy, only limited data about the eddy was obtained from drifter observations.

The second deployment of the remaining 16 NPS drifters, as well as 3 OSU and 5 SIO buoys, was conducted in mid-September 1993. Following a ten-day detailed hydrographic survey involving ADCP, SEASOAR and CTD measurements, the drifters were

deployed in a "radiator" cluster pattern approximately 60 km across (M. Kosro, personal communication). One OSU and two SIO buoys died upon launching, but the remaining buoys appeared to initially move within an anti-cyclonic eddy offshore of Point Reyes, California (Figure 2.8). As the drifters migrated out of the eddy over the course of the next month, most continued southward following the general flow of the prevailing current.

### *b. Incoherent Deployments*

Thirty-four drifting buoys were deployed in four incoherent deployments in May, June, August and November 1993. These incoherent deployments were notable among other things for the use of aircraft to deploy WOCE/TOGA drifters. Their most important attribute is that the deployments were not biased to particular features, or to a single season, as was the case for all prior drifter programs in the CCS.

Three incoherent deployments (first, second and fourth) took place roughly on a line at 39.5 N latitude from 125 W to 128 W (Figure 2. 9). The third deployment took place farther south at 39 N. A principal purpose of the incoherent drifter deployments was to confirm conclusively whether or not the eddy and filament view that Strub and James (1995) had developed for the flow of the CCS could be reproduced from drifter deployments.

## 4. Temporal Coverage

### *a. Coherent Deployments*

Figure 2.10 shows the temporal distribution of the 96 drifters present in 1993. The two coherent deployment periods were tied to the two hydrographic surveys that preceded the drifter deployments. The first survey, including the deployment of 13 drifting buoys was conducted in July 1993. Because of the wind conditions and high sea states

discussed above, the drifter data from the eddy (about one week) provided only a limited description of its kinematic properties.

The second survey and deployment in September 1993 proved somewhat more successful. Twenty-four drifter buoys were deployed in a cluster formation around the warm-core eddy. After five days, seven NPS drifters had migrated out of the eddy, three SIO buoys had failed as had two OSU buoys. The other twelve drifters remained in the eddy for various lengths of time, the longest time-series acquired being 28 days from one of the drifters.

### *b. Incoherent Deployment*

As stated above, the incoherent deployments were conducted in May, June, August and November 1993. The deployments were planned to correspond with the various periods of upwelling and relaxation in the CCS. It was hoped by spacing out these deployments that a nearly complete year-round picture of the CCS could be obtained from unbiased drifter data. The incoherent deployments continued in 1994 with spacing between the deployments set at three month intervals.

## B. SATELLITE OBSERVATIONS

One of the key research tools used by oceanographers during the EBC experiments was satellite observations of the oceanic environment. Satellite altimeter and infrared radiance measurements were made to study the velocity and SST fields in the CCS and to describe the variability of the CC. Velocity field measurements were obtained using the

dual-frequency altimeter onboard the TOPEX/Poseidon satellite. NOAA-11 and NOAA-12 Polar Orbiting Environmental Satellites (POES) provided the platform for the previously discussed ARGOS sensor and the Advanced Very High Resolution Radiometer (AVHRR).

### 1. AVHRR Imagery

The principal source of satellite data during EBC came from AVHRR imagery. Used in conjunction with other oceanographic tools (ADCP/SEASOAR, satellite altimetry and drifters among others), satellite SST imagery provided the necessary large-scale picture to help in deciphering the meaning of local in-situ measurements.

#### *a. Advanced Very High Resolution Radiometer (AVHRR)*

Located onboard the NOAA Polar Orbiter Satellites, the AVHRR was used to provide sea surface temperature (SST) fields to researchers. The AVHRR measures the infrared thermal radiation emitted by the ocean surface. After corrections for water vapor absorption and cloud contamination, SST fields are obtained from the measured radiances (P.-M. Poulain, personal communication). Reynolds (1988) and Brown (1995) describe in detail the AVHRR, types of measurements it can take and various data retrieval techniques.

Atmospheric attenuation due to clouds or water vapor can be a problem with AVHRR measurements. The CCS is an area of high cloud content, particularly in the summer months due to subsiding air from the Pacific High over cooler oceanic water. Winter months are often influenced by strong northern Pacific storms.

#### *b. EBC AVHRR Imagery*

AVHRR images for EBC were registered to cover the region 121.5W to 129W and 35N-41N. The image size was 512 by 512 pixels, and the spatial resolution was

1.1 km in the across and along-track directions near the satellite ground track. Images were obtained four times a day from the two NOAA satellites. The raw images were processed by OCEAN IMAGING which produced hard copy, gray-scale images twice a day for the study area during the field campaigns and registered the images to the EBC grid (P. Strub, personal communication).

Researchers had planned to use the real-time imagery for tracking of oceanic features in conjunction with the hydrographic surveys conducted prior to the two coherent drifter deployments. Figure 2.11 shows the days with good thermal images (defined as mostly clear over the EBC region defined above) that were available off the coast of California during 1993. Good images were available prior to the early July drifter deployment. The period prior to the September deployment, however, was cloud covered and few clear images were available.

### 2. TOPEX/Poseidon

Launched in summer 1992, the TOPEX/Poseidon satellite provides very accurate sea surface height measurements. It carries a dual-frequency altimeter used for the measurement of sea surface heights and a microwave radiometer that measures atmospheric water vapor content for correction of the altimeter measurements. Maps of dynamic topography (related to ocean geostrophic currents) and of significant wave height are the major products obtained from these observations.

During the EBC studies, the TOPEX/Poseidon altimeter was used to measure sea surface heights in the CCS. Investigators using the data hope to refine the description of Strub and James (1995) of the evolution of the seasonal jet off the Northern California Coast

originally put forth from GEOSAT altimeter data acquired during the aforementioned CTZ experiments. Kelly et al. (1997) have compared the drifter data described in this study with TOPEX/Poseidon observations.

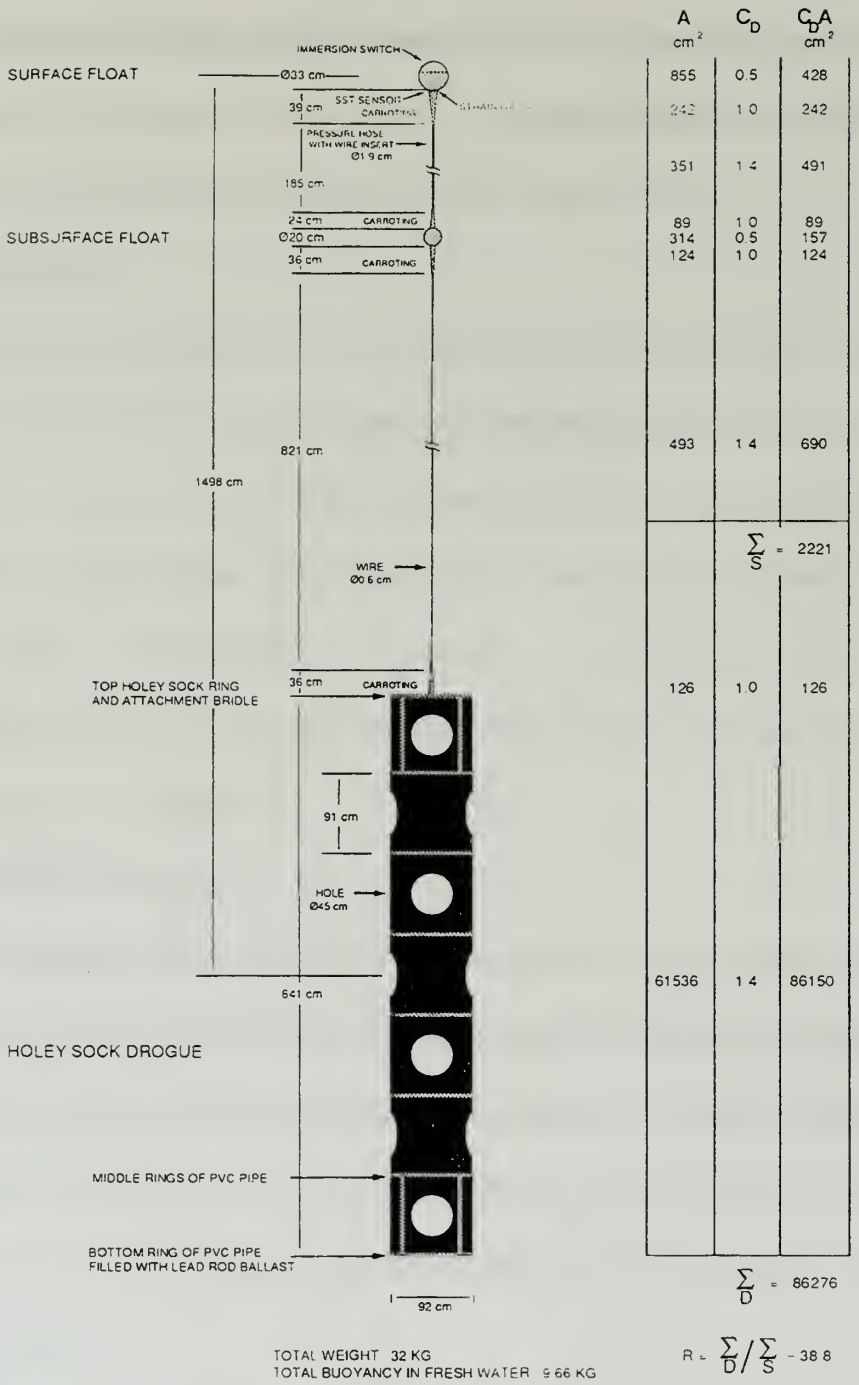


Figure 2.1 Scale drawing of the "holey sock" drifting buoy with a drag area ratio of 38.8. From Poulain et al. (1996).

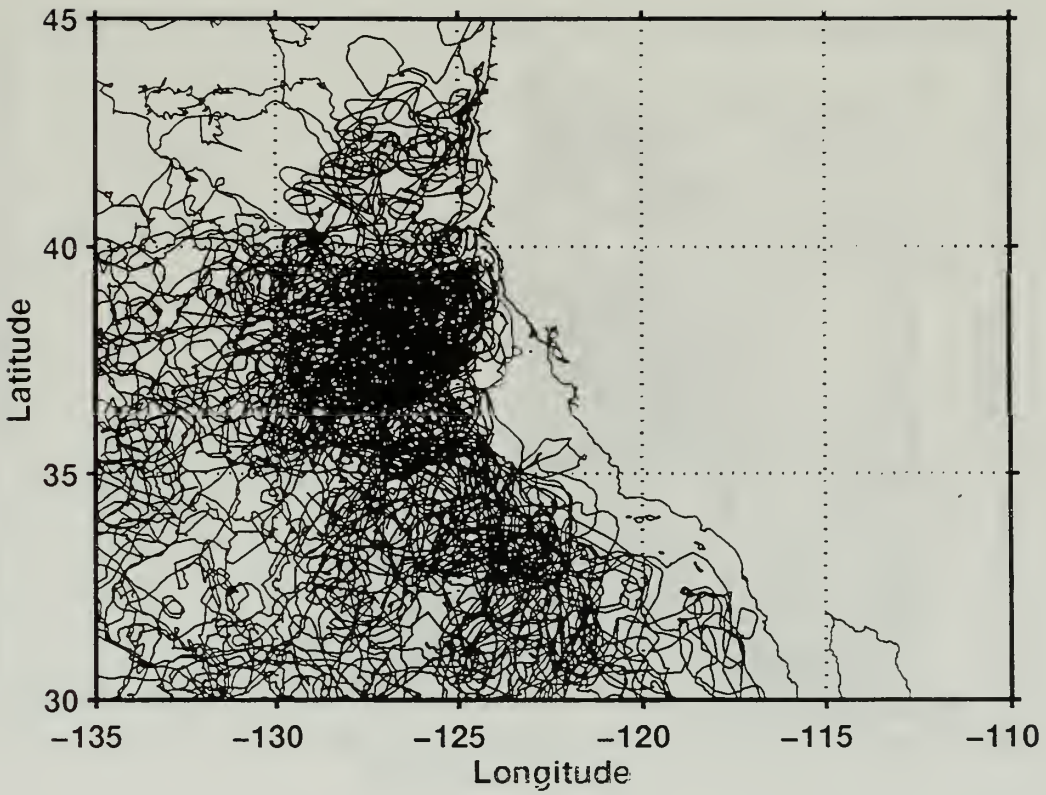


Figure 2.2 Trajectories of 96 surface (15 m) drifters that spent at least one day in the EBC study area in 1993.

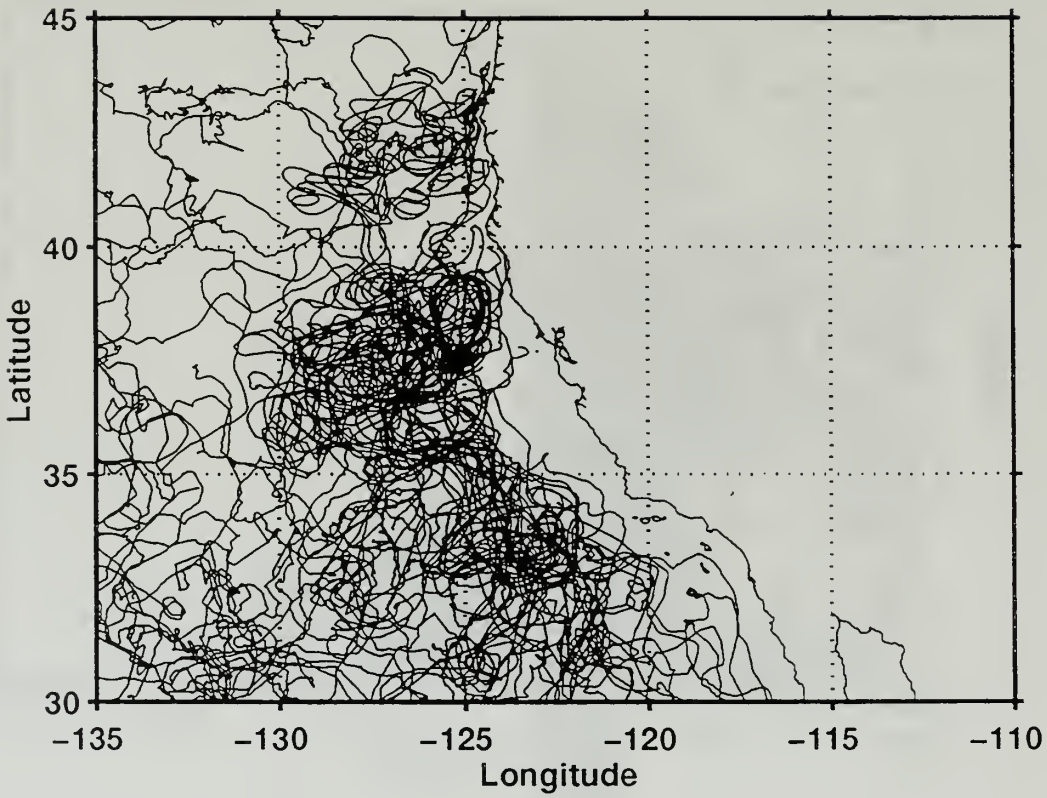


Figure 2.3 Subset of the data in Figure 2.2 showing trajectories of 68 surface (15 m) drifters from the WOCE program that spent at least one day in the EBC study area in 1993. Surface drifters from NPS and SIO are included in the WOCE dataset.

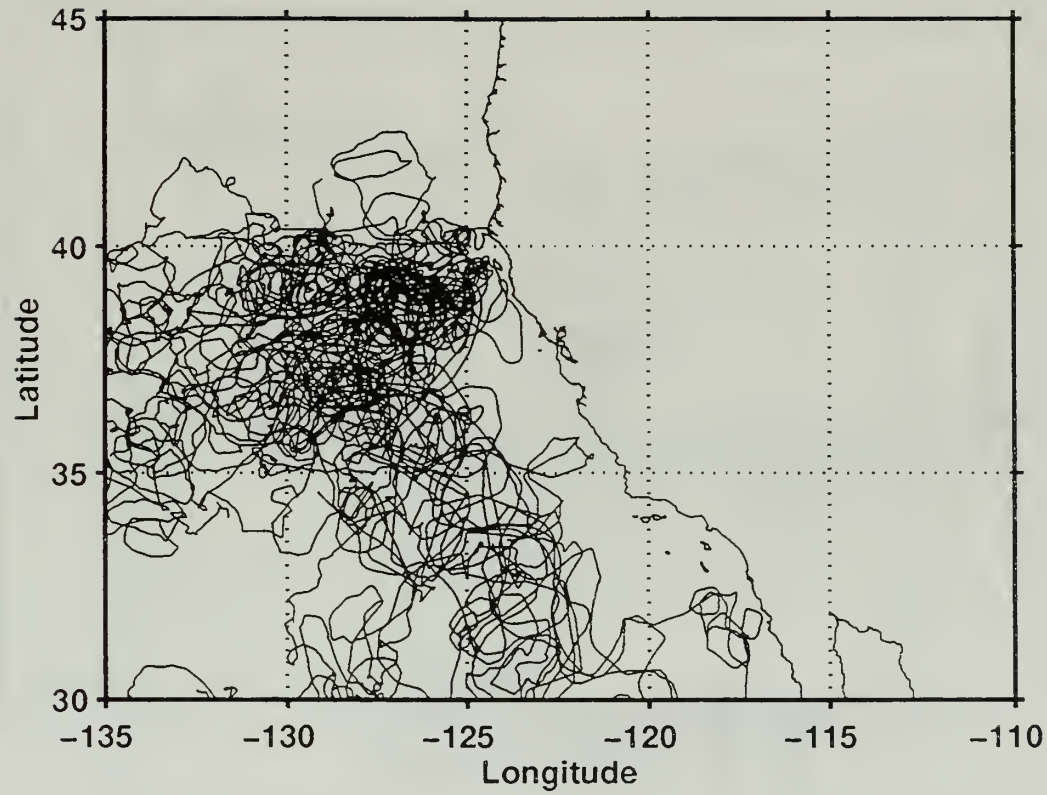


Figure 2.4 Subset of the data in Figure 2.2 showing trajectories of 28 surface (15 m) drifters deployed by WHOI for the four incoherent deployments in 1993 as a part of the EBC program.

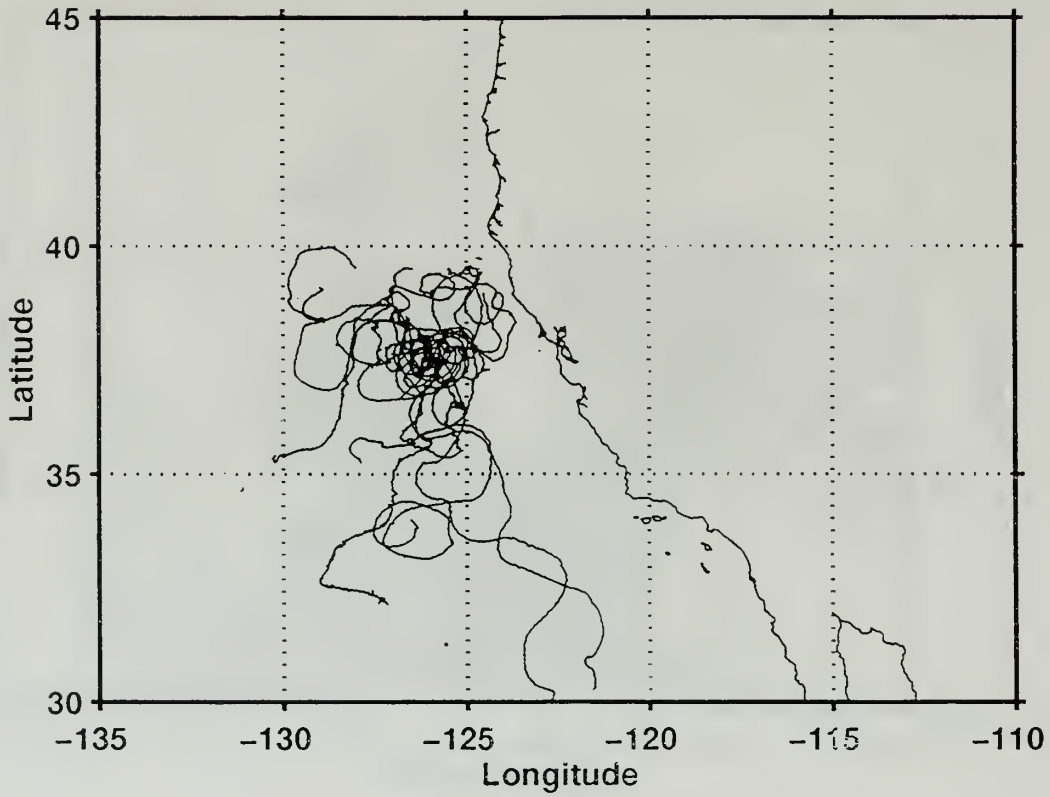


Figure 2.5 Subset of the data in Figure 2.2 showing trajectories of 14 surface (15 m) drifters deployed by OSU in 1993 as a part of the EBC program.

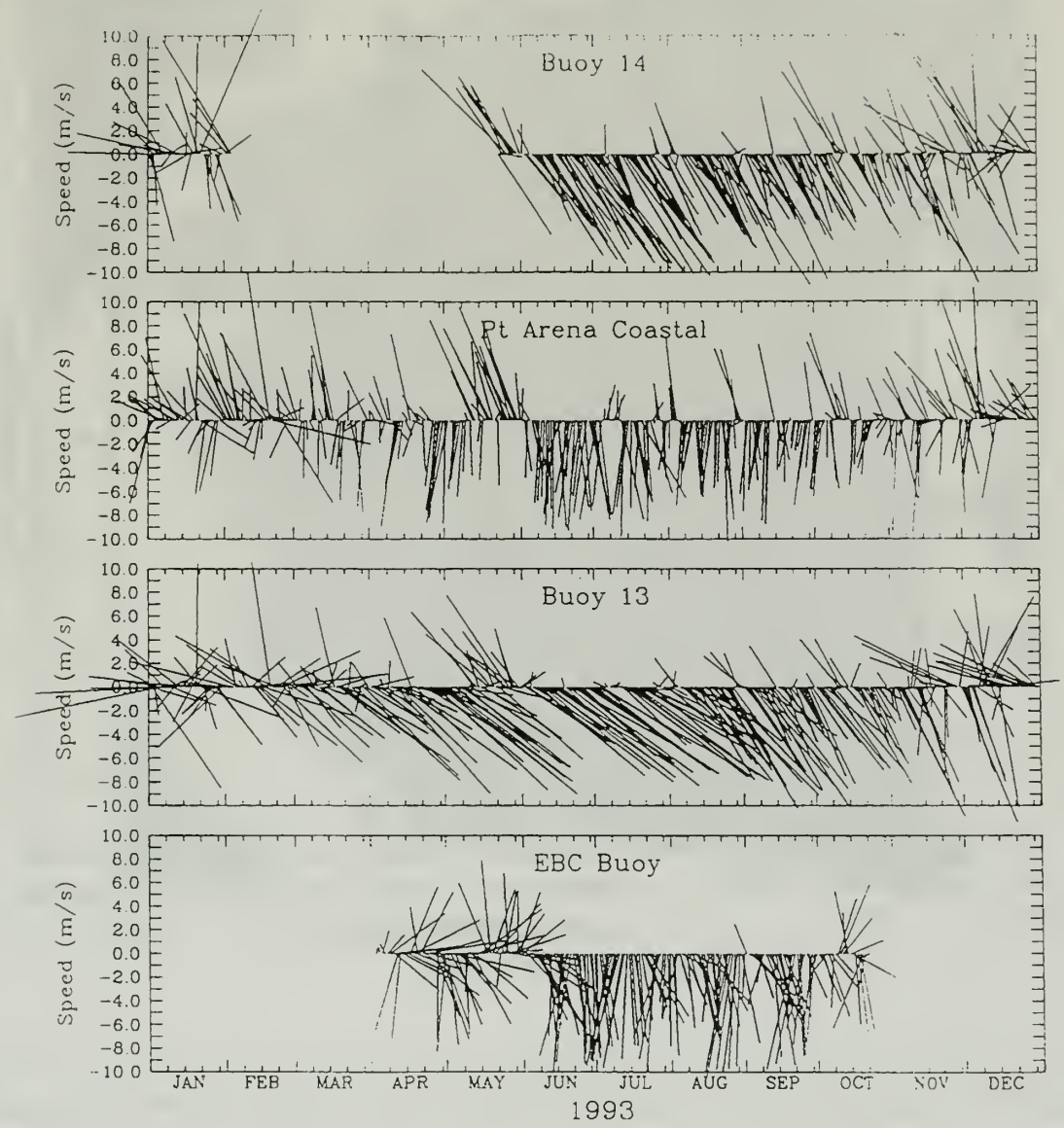


Figure 2.6 Time series of average daily wind velocities for 1993 in the EBC study area. NDBC stations offshore of Point Arena (Buoy 14) and Point Reyes (Buoy 13) and a coastal station at Point Arena are compared to an EBC program meteorlogical/oceanographic buoy west of the study region.

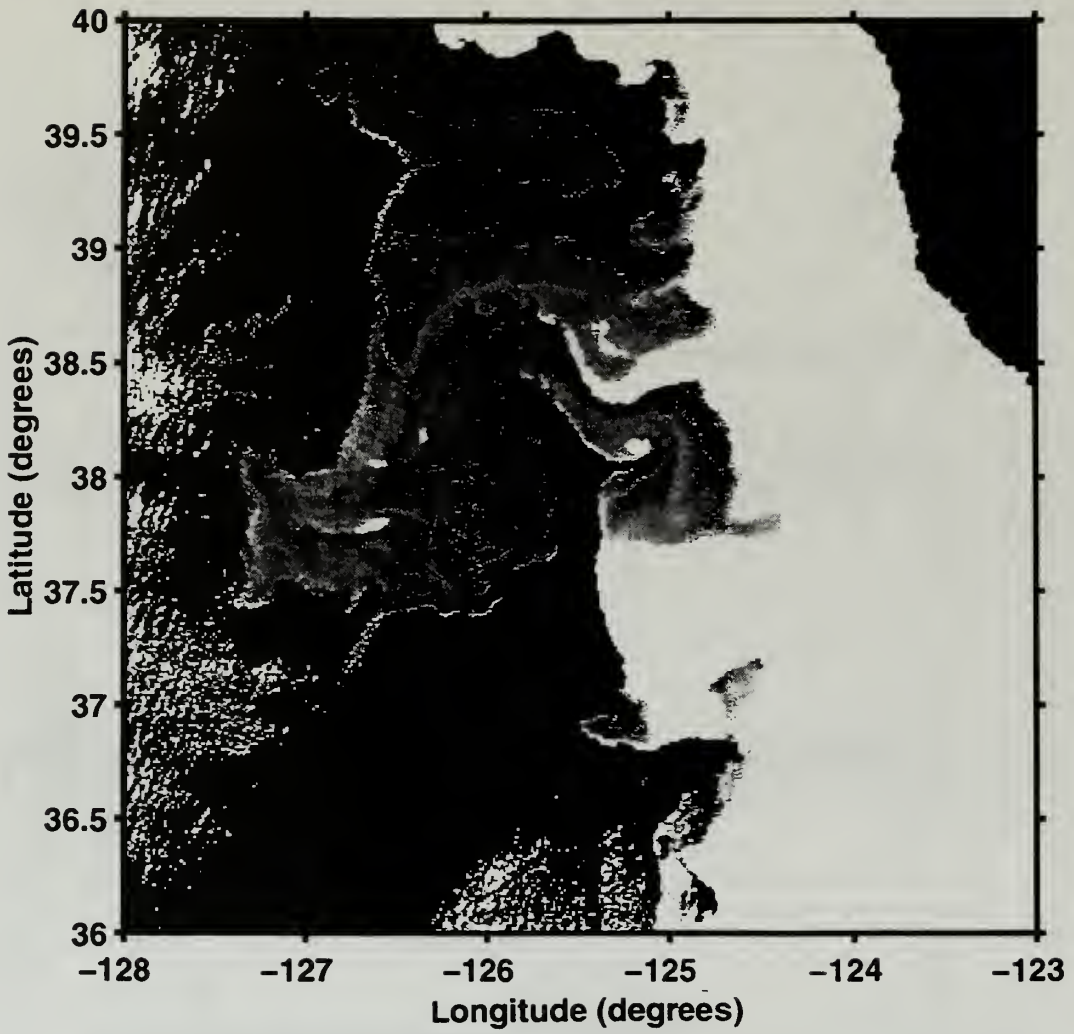


Figure 2.7 Surface (15 m) drifter tracks for July 9-16, 1993 (circles denote starting positions) overlaid on a satellite SST image from July 7, 1993. Lighter colors represent colder temperatures in the range 13.5 C - 16 C.

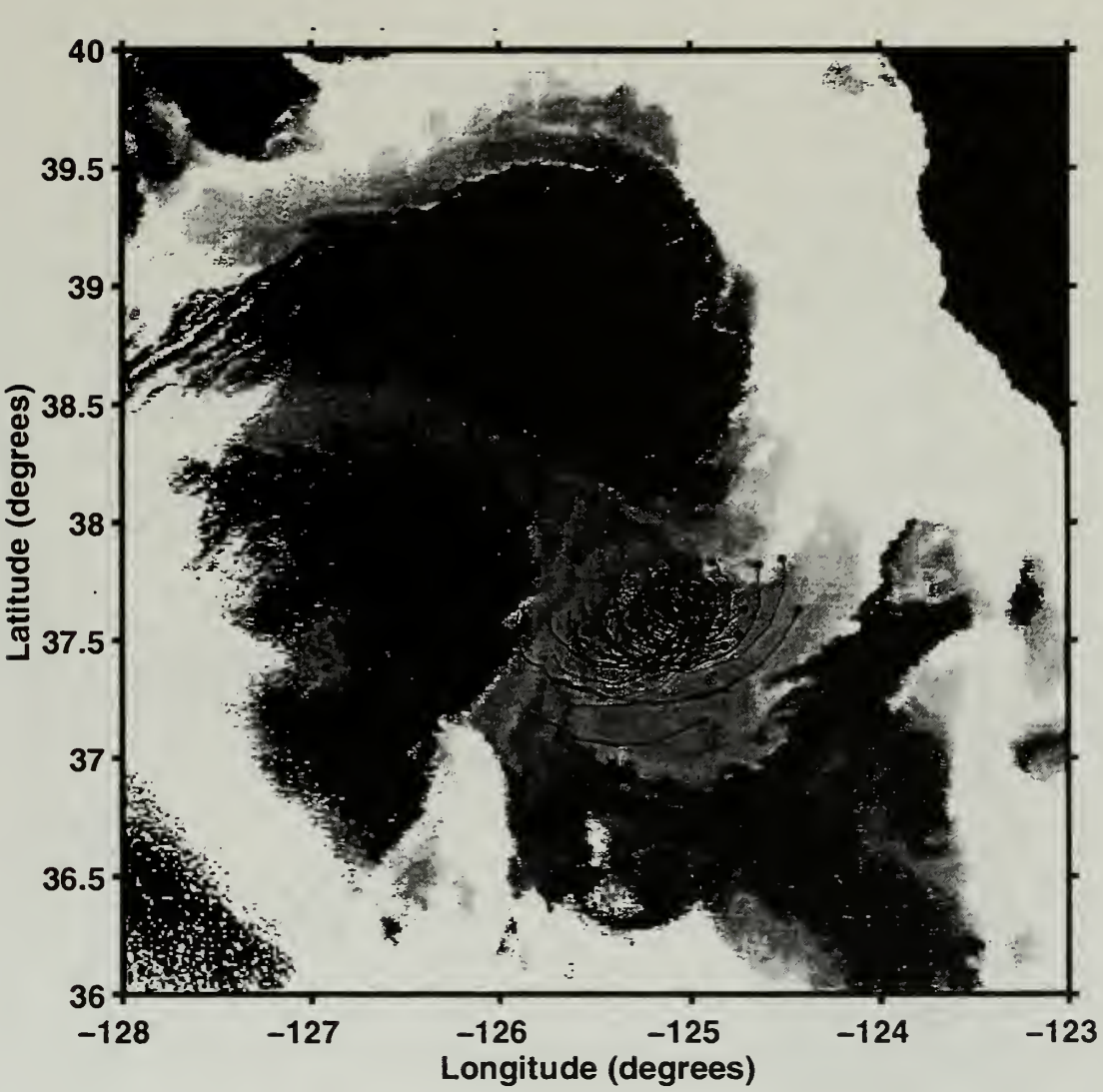


Figure 2.8 Surface (15 m) drifter tracks for September 19-30, 1993 (circles denote starting positions) overlaid on a satellite SST image from September 26, 1993. Lighter colors represent colder temperatures in the range 12 C - 16 C.

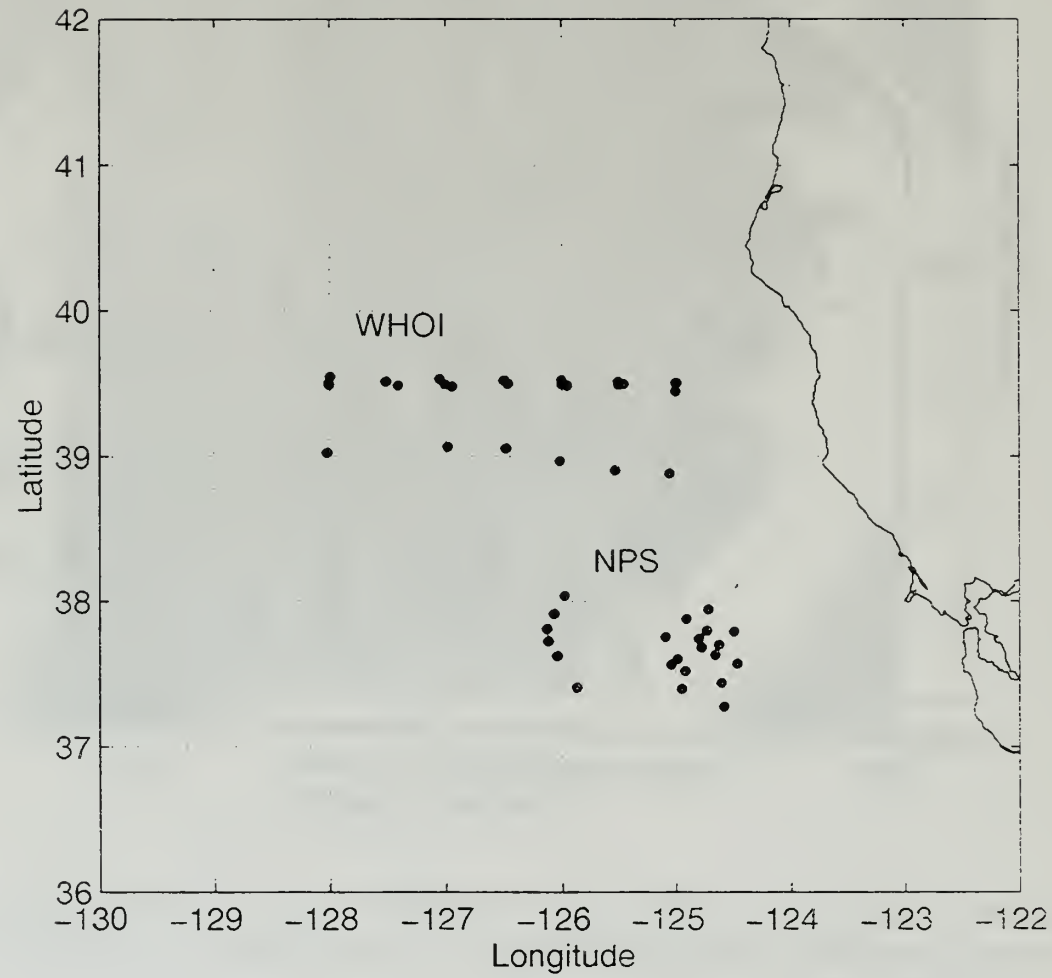


Figure 2.9 Initial deployment positions of surface (15 m) drifters used in the four incoherent deployments (WHOI) and two coherent deployments (NPS) during the EBC program in 1993.

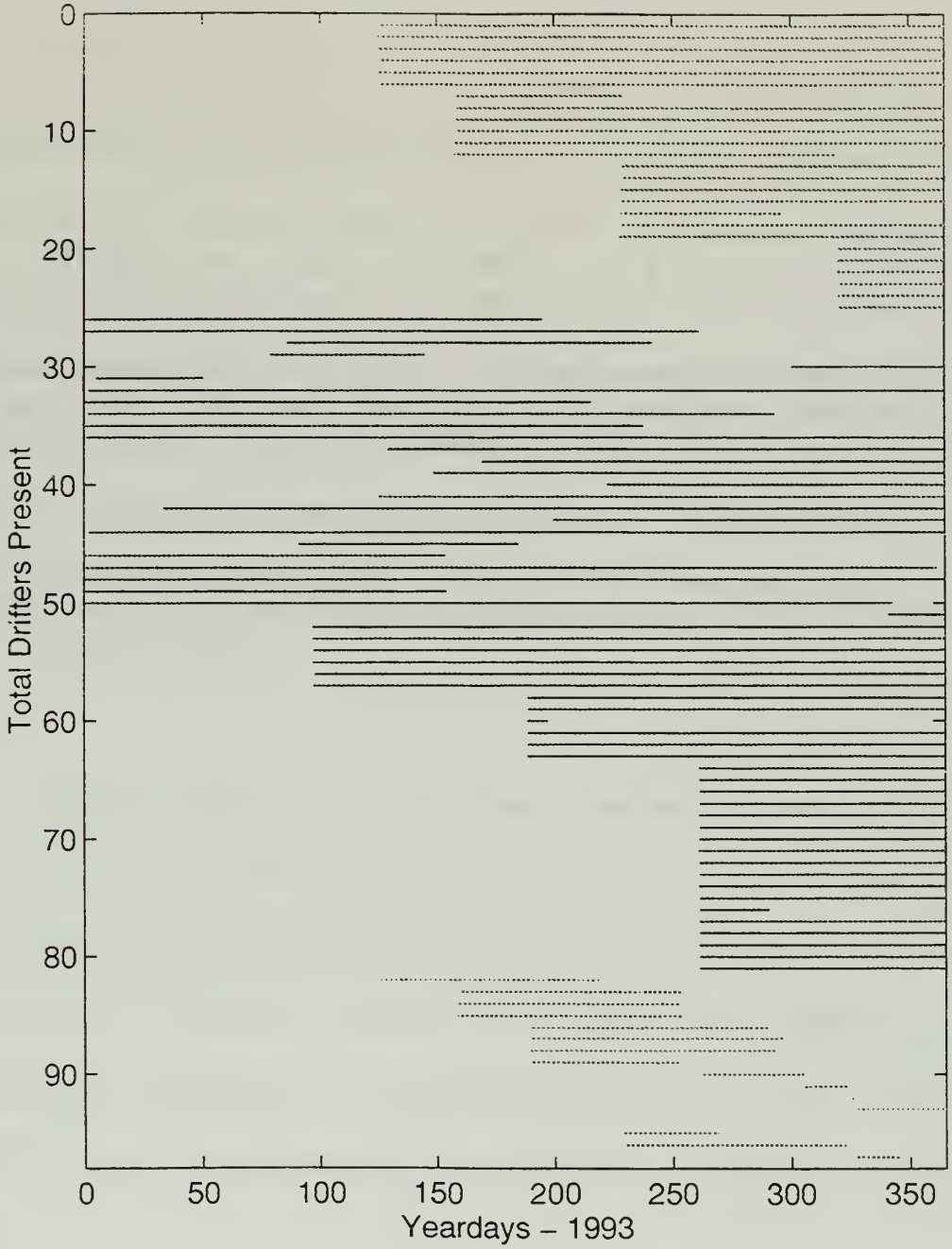


Figure 2.10 Time line of surface (15 m) drifter reporting periods for instruments operating in the EBC region during 1993.

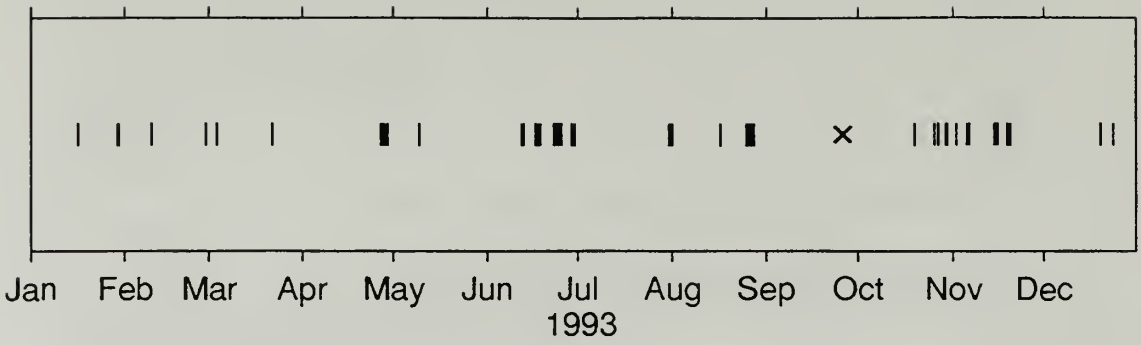


Figure 2.11 Times of clear satellite SST images of the EBC region (vertical bars) from the AVHRR sensor. The time of a partially clear image (x) used in this study is also shown.

# III. DESCRIPTIONS OF CCS FEATURES FROM SATELLITE IMAGERY AND DRIFTER TRAJECTORIES

To achieve the objectives of EBC, a number of techniques and methods were employed. This thesis focuses on two. First, satellite imagery from the NOAA AVHRR is used to provide a large-scale overview of the CCS and its mesoscale field and, second, WOCE-type drifting buoys are used to study the surface currents associated with SST mesoscale patterns. Two isolated eddies with relatively dense drifter observation are given special consideration. These observations, when compared with earlier studies, help to improve our understanding of the dynamical processes and interactions present in the CCS.

## A. ANNUAL CYCLE

AVHRR imagery, from the EBC period, is used here as a means of providing a general overview of the CCS, and the evolution of the mesoscale field over the course of a year. Figures 3.1-3.10 show the evolution of the SST mesoscale field and the current flow. The images are produced in gray shades, with darker colors representing warmer temperatures. Surface drifters that were in the EBC study area, as well as WOCE/TOGA drifters that passed through the area from the same periods, are superimposed on the satellite images.

### 1. Winter and Spring Transition

Hickey (1979) presented the traditional view of the CCS. Since then CALCOFI, CODE, OPTOMA and CTZ have led to a revised description, as described by Batteen (1997). The CCS in winter (Figures 3.1 and 3.2) is marked by relatively uncomplicated mesoscale patterns in SST off of Northern/Central California. The most important feature present in SST during winter is the surfacing of the CU to form the Davidson Current from roughly late October through February. This poleward-flowing, relatively warm water is clearly visible in the images from January (Figure 3.1) and March (Figure 3.2).

The reason for the relatively uncomplicated patterns in the winter months in the CCS is due to the seasonal variations in the wind field. These variations are governed by the position of the North Pacific subtropical high, the Aleutian Low and the thermal low over southwestern North America (Halliwell and Allen, 1987; Reinecker and Mooers, 1989a). During the fall and winter months, the Aleutian Low dominates the general circulation pattern. Winds in the winter (Figure 1.5) over the CCS are driven by the passages of storms and can fluctuate in speed and direction depending on the characteristics of each storm system (Halliwell and Allen, 1987). These storms can cause abrupt short-term changes to occur in the windfield.

The winter wind field data during EBC (Figure 2.6) did not differ from this climatalogical view. As a result, the January and March images show little eddy activity in the study area and no filament development along the coast. In both images, the warmer waters of the Davidson Current can be seen flowing poleward along the continential slope with colder water against the northern California coast. Interestingly, mesoscale instabilities

are visible along the edges of the warm current, but their scale is small compared with the filaments and eddies that develop during the upwelling season. The only drifters present during this winter period were those of the WOCE program that were passing through the southern edge of the study area. (WHOI incoherent winter deployments did not occur until 1994.)

By the time of the April image (Figure 3.3), the Spring Transition had occurred. The Spring Transition at nearshore locations is marked by abrupt decreases in the sea surface temperatures and reductions or reversals in the poleward flow (Huyer et al., 1979; Lynn and Simpson, 1987). Activity in the CCS is marked by more mesoscale activity following this transition. Figure 3.3 shows this marked change. Along the coast, colder water from both entrainment from the north and from early season upwelling is seen. Filament activity is seen in its earliest stages forming along coastal points and capes, as suggested by Paduan and Niiler (1990), Strub et al. (1991) and Hickey (1996).

The April image also shows the drifter tracks present in the study area. Drifters from the WOCE program are present in the southern half of the study area. To the north, at 39.5 N, trajectories from the WHOI buoys and one OSU buoy from the first incoherent deployment are visible.

### 2. Summer

The CCS in the summer is a highly dynamic, mesoscale rich, equatorward flow. Previous studies, such as OPTOMA and CTZ, have stated that the major difference between seasons is the existence of intensive, nearshore current filaments associated with the summer upwelling (Reinecker and Mooers, 1989b; Strub et al., 1991).

The atmospheric changes over the CCS region are equally dramatic. Beginning with the spring transition, the Aleutian Low gives way to the north Pacific subtropical high and the southwestern United States thermal low. The continuous existence of a strong inversion layer in the coastal marine boundary layer along with the two pressure system's positions and relative strengths dominate the wind field (Figure 1.4), which drives the upwelling and current flow (Halliwell and Allen, 1987).

The June satellite image (Figure 3.5 ) shows a flow that matches the OPTOMA and CTZ observations. Relatively cold water dominates the inshore regime where strong coastal upwelling is occurring. Drifter trajectories from the second incoherent deployment highlight the quickly strengthening filament off Point Arena (39 N). The early formation of eddies both to the north and south of the Point Arena filament, as previous described by Strub et al. (1991), are present.

By July (Figure 3.6) the filament off Point Arena has grown further in length and intensity and now dominates the flow field some 300 km from shore. The eddy pair seen in June has grown in size and intensity, as evidenced by drifter trajectories from the first coherent deployment. Upwelling has continued along the coast and the band of cold water has grown further in size. Drifters traveling in strong narrow currents appear to reinforce previous studies that flow in the CC becomes sharper and of smaller horizontal scale in the summer months (Strub and James, 1995).

The August imagery (Figure 3.7) shows the flow field just prior to the second coherent drifter deployment. To the north, the filament off Cape Mendocino (40 N) is starting to intensify, lagging the Point Arena filament by about a month. To the north of the

Cape Mendocino filament, the first indications of an anti-cyclonic eddy are present, and to the southwestern edge, the possibility of a cyclonic eddy forming is seen.

A large anti-cyclonic eddy dominates the flow field to the north of the Point Arena filament. WHOI drifters deployed as a part of the third incoherent deployment are caught up in this eddy. To the south of the filament, an eddy pair is visible, with the eddy further to the west showing cyclonic rotation and the eddy to the east showing anti-cyclonic rotation. This anti-cyclonic eddy is the focus of the second coherent drifter deployment and the second of the hydrographic surveys that proceeded the drifter deployments.

### 3. Fall Transition andWinter

From the end of August until the end of October, there are only few good cloud-free images available (Figure 2.11). Figure 3.8 provides a limited view of the EBC focus area in September. The center of the area was relatively cloudless, allowing for the only clear post-deployment view of the anti-cyclone studied during the second coherent deployment. WOCE (NPS) drifter trajectories mark the position of the eddy on 19 September when the buoys were deployed. Figure 3.8 shows that the eddy has translated to the southwest since the deployment. Drifters that exited the eddy to the west were advected northward as much as 150 km into the large anti-cyclone north of the Point Arena filament. Farther north the Cape Mendocino filament has become elongated and now extends to its maximum length of nearly 300 km, arcing toward the southwest.

By October (Figure 3.9), the Cape Mendocino filament has already reached its maximum strength and has started to recede. The Point Arena filament has also grown weaker in intensity, becoming elongated and now flowing in a southwestward direction

nearly 500 km from shore. Neither imagery nor drifter trajectories show conclusive evidence of eddy activity. Coastal upwelling has either ended or greatly reduced in intensity, resulting in a warming of the SST. However, the processing of this image differed from the others as can be seen by the fact that land temperatures were not masked out. As a result, this image's sensitivity to ocean features is reduced, possibly concealing mesoscale features still present along the sides of the visible Point Arena filament.

By December (Figure 3.10), atmospheric cyclonic activity is increasing in intensity, resulting in increased clouds over the regions. Imagery from this period is similar to that of the preceding January. Filaments off Cape Mendocino and Point Arena have dissipated due to the lack of upwelling favorable winds. Warmer water, probably from the Davidson Current, is moving into coastal areas as far north as Cape Mendocino. Drifter trajectories show none of the coherent flows present during the summer months.

## B. SUMMERTIME MESOSCALE FIELD

In this section, a more detailed investigation of the translation characteristics of mesoscale eddies is presented using two-week segments of drifter trajectories from the summer period. Obvious translation of looping features in the trajectories, combined with fortuitous eddy positions from hydrographic surveys, is used to estimate the translation velocities of three different mesoscale features.

### 1. Overview of Mesoscale Field

Figures 3.11-3.17 present a general overview of the EBC concentration area in the CCS from drifter trajectories. The CCS in 1993 appeared similar to that observed during CTZ in 1988 (Strub et al., 1991). The first fifteen days of June (Figure 3.11) marked the beginning of the summertime mesoscale activity in the CCS. Drifter trajectories during this period show an anticyclone similar to the one revealed by CTZ to the north of the Point Arena filament. That filament is highlighted by a drifter which appears to travel to its western edge before moving south with the general flow of the CC.

The buoy closest to the coast appears to initially be following the southward flow until being advected northward in a small filament (see Figure 3.5) and eventually into a cyclonic eddy at the terminal end of the Point Arena filament (Figure 3.12). The buoy makes two rotations around the eddy before becoming absorbed into the Point Arena filament and then exiting to the south.

By the first two weeks of July (Figure 3.13), drifter trajectories show the clockwise rotation of the large anticyclone to the north of the filament. To the south of the filament, buoys from the first coherent deployment mark the center of the cyclonic eddy. Although some buoys appear to exit the eddy to both the north and south by mid-July, others continue to mark the cyclone's position during the second half of July (Figure 3.14). Buoys that exited the cyclone to the north were advected across the filament and into the clockwise rotation of the large anticyclone to the north of the filament (Figure 3.15).

To the south of the filament, an eddy pair is visible. By the end of August (Figure 3.16), the cyclone has weakened sufficiently enough to lose its surface expression, resulting

in the remaining buoy still tracking it becoming stalled. The anticyclone to the east has remained strong and is translating to the southwest, as discussed below.

To the north of the eddy pair, the Point Arena filament is transited by five buoys, clearly marking its northern and southern extremes. To the north of the filament, the large anticyclone becomes clearly marked as the buoys of the third incoherent deployment almost entirely become trapped in the clockwise rotation of the large eddy. This eddy clearly dominates the flow field north of the filament. By mid-September (Figure 3.17), drifter trajectories still clearly mark the location of the anticyclone to the north of the filament, although these trajectories are becoming more elliptical in nature. South of the filament, the other anticyclone continues to move off to the southwest, as evidenced by the trajectory of one buoy remaining in it.

### 2. Estimated Eddy Translation Rates

Three eddies were sampled in the summertime study area. Estimated translation rates for each of the eddies are presented in Table 3.1. These estimates are based upon computed center positions from both hydrographic/ADCP surveys and from drifter cluster centroids. Although by assuming that the cluster centroid is also the eddy center can lead to erroneous estimates of the kinematic properties (Kirwan, 1988), for the purpose of providing a first-guess estimate of eddy translation rates, the errors should be minimal.

The cyclonic eddy was originally observed from a hydrographic/ADCP survey conducted in May 1993 (Chumbinho, 1994). The survey results (Figure 3.18) showed a cyclonic eddy centered at 38.62 N, 124.25 W. A total of 32 CTD casts were made in and around the eddy with continuous ADCP measurements (P. Jessen, personal communication).

A larger-scale survey in mid-June 1993 indicated that the eddy had moved to a new center position of 38.3 N, 125.25 W (Figure 3.19). The eddy had moved at an average translation rate of 3.08 cm/s to the southwest. By the time of the coherent deployment in July (July 9-10, 1993) the eddy center was estimated to be at 37.73 N 126.17 W, indicating an average translation rate of almost 6 cm/s. For the remainder of the month, however, little movement was seen in the eddy. Until almost the middle of August, estimated translation rates were near 1.5 cm/s, almost entirely to the west. In the last days of August, a second large scale survey was conducted (Figure 3.20). By this time, the eddy had shifted considerably to the north, with an average translation speed of a little more than 4 cm/s. The mean translation of the eddy over the sampling period was 3.7 cm/s to the southwest.

Table 3.1 Translation rates (cm/s) for the three eddies in the Eastern Boundary Current study area during summer 1993. Roman numerals represent the cyclonic eddy from the first coherent deployment (I), the anticyclonic eddy from the second coherent deployment(II), and the anticyclonic eddy north of the Point Arena filament (III).

| EDDY | PERIOD | U | V | SPEED |
|---|---|---|---|---|
| I | May 22-Jun 19 | -2.8 | -1.4 | 3.1 |
| I | Jun 19-Jul 09 | -4.8 | -3.4 | 5.9 |
| I | Jul 09-Aug 09 | -1.3 | -0.8 | 1.5 |
| I | Aug 09-Aug23 | -0.5 | +4.1 | 4.2 |
| AVG | | -2.3 | -0.4 | 3.7 |
| I (7 Day Fit) | | -3.2 | -1.1 | 3.4 |
| II | Aug 01-Aug23 | -4.7 | 0.0 | 4.7 |
| II | Aug 23-Sep 08 | -1.7 | -3.3 | 3.8 |
| AVG | | -3.2 | -1.7 | 4.2 |
| II (12 Day Fit) | | -4.0 | -1.9 | 4.5 |
| III | Aug 23-Sep 08 | -1.2 | -0.9 | 1.5 |

The anticyclone that became the focus of the second coherent deployment was originally seen forming as part of the eddy pair located south of the Point Arena filament (Figure 3.15). From an initial center position of 37.5 N, 125.25 W the eddy translated to the west at about 4.5 cm/s. During the second large-scale hydrographic survey observations showed that the eddy had moved SW at 3.8 cm/s from a center position of 37.5 N, 126.2 W to 37.11 N, 126.45 W by the middle of September in time for the second coherent deployment. The average translation rate for this anticyclone was 4.2 cm/s to the southwest.

The third eddy considered was the large anticyclone to the north of the Point Arena filament. This eddy was not the focus of either of the coherent deployments, although the third incoherent deployment drifters became embedded in the eddy for nearly a month. On 23 August (Figure 3.16), the eddy was observed to be centered at approximately 39 N, 126.2 W. Over the next 15 days, the eddy was observed to translate at almost 1.5 cm/s to the southwest to a center position of 38.86 N, 126.3 W on 8 September (Figure 3.17).

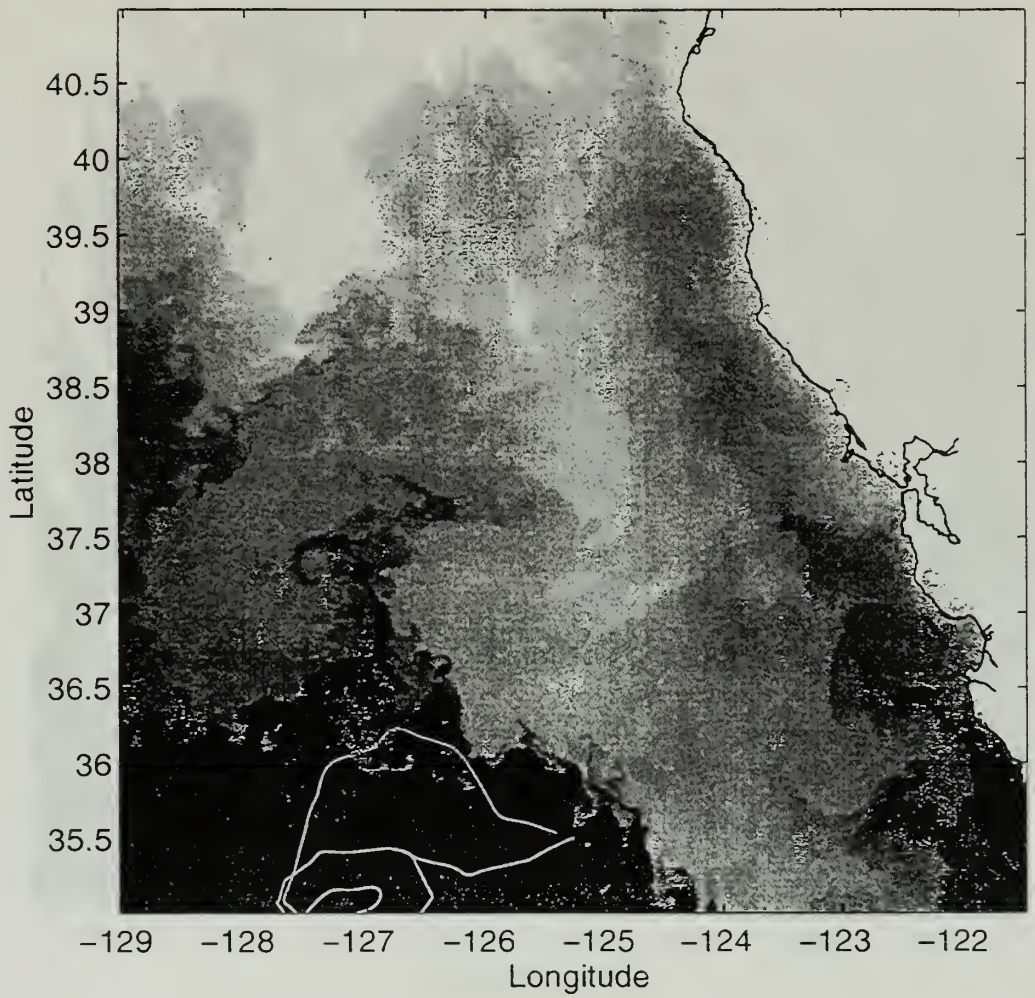


Figure 3.1 Surface (15 m) drifter tracks for the period January 15 - February 14, 1993 overlaid on the satellite SST image from January 30, 1993. Lighter gray shades represent colder temperatures in the range 8.5 C - 13 C.

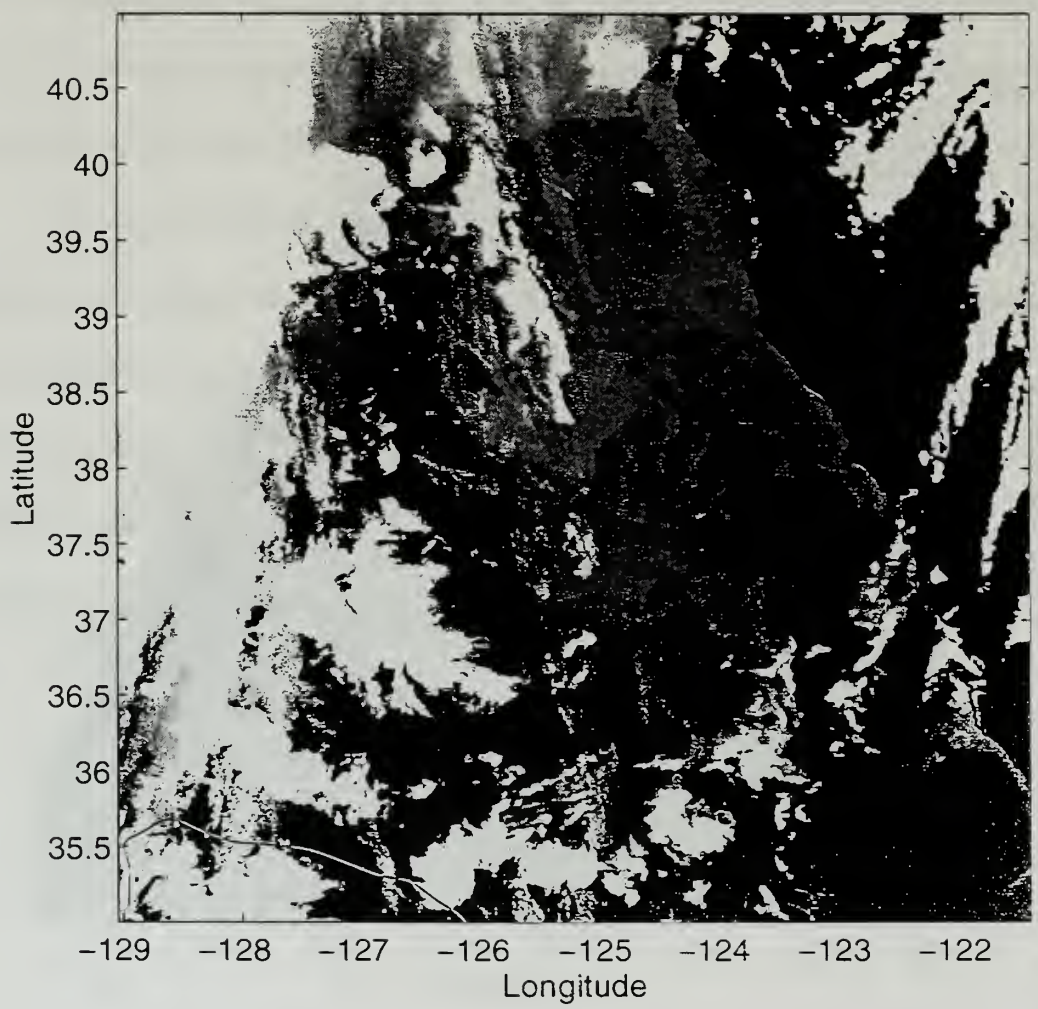


Figure 3.2 Surface (15 m) drifter tracks for the period March 6 - April 5, 1993 overlaid on the satellite SST image from March 21, 1993. Lighter gray shades represent colder temperatures in the range 8.5 C - 13 C.

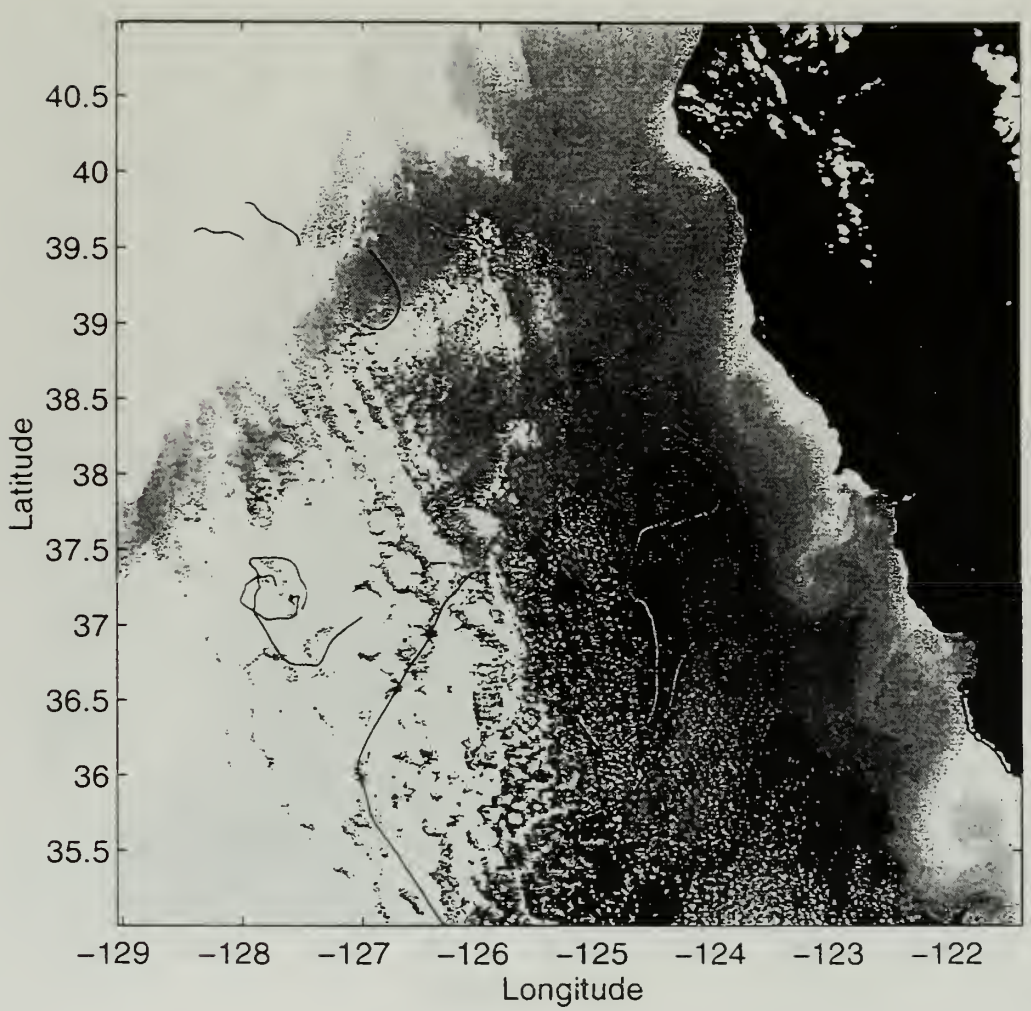


Figure 3.3 Surface (15 m) drifter tracks for the period April 12 - May 11, 1993 overlaid on the satellite SST image from April 27, 1993. Lighter gray shades represent colder temperatures in the range 9.5 C - 14 C.

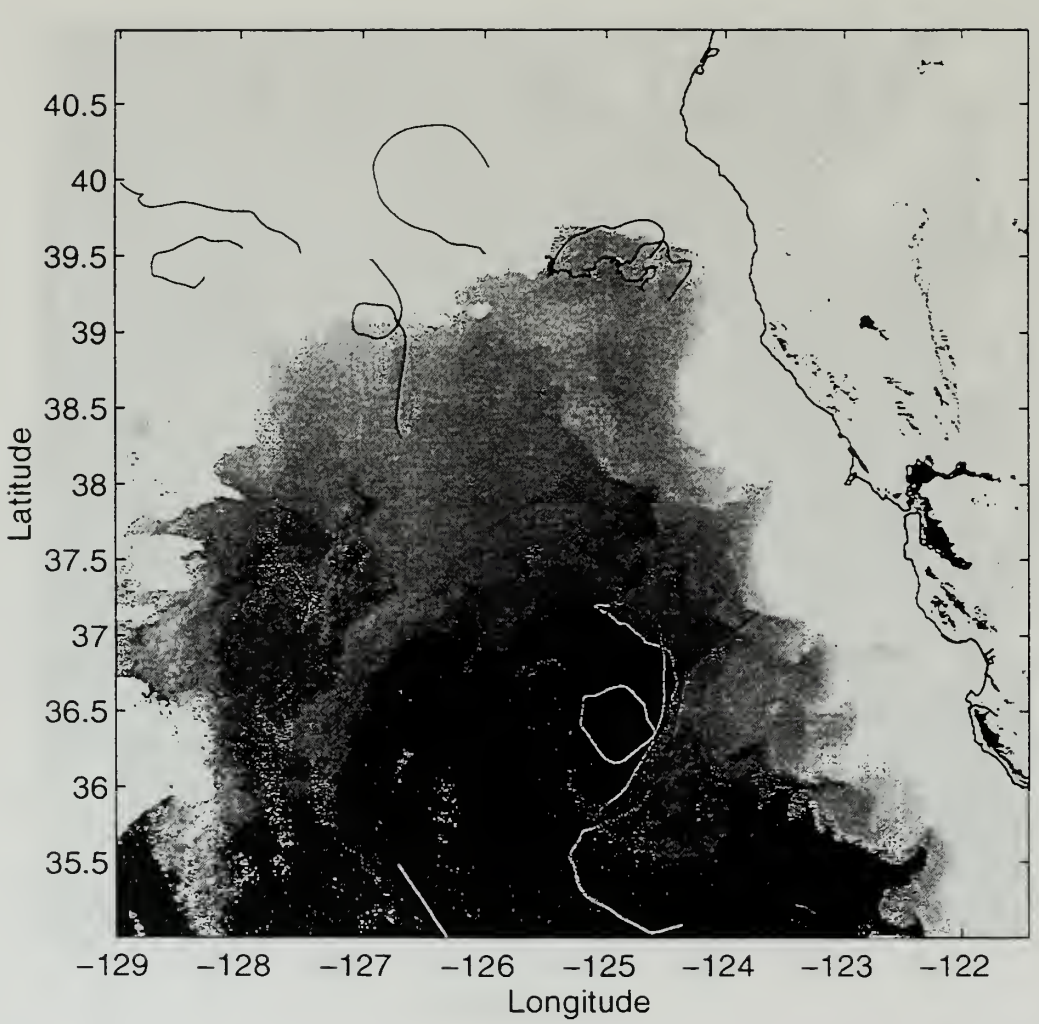


Figure 3.4 Surface (15 m) drifter tracks for the period April 25 - May 24, 1993 overlaid on the satellite SST image from May 9, 1993. Lighter gray shades represent colder temperatures in the range 11 C - 14.5 C.

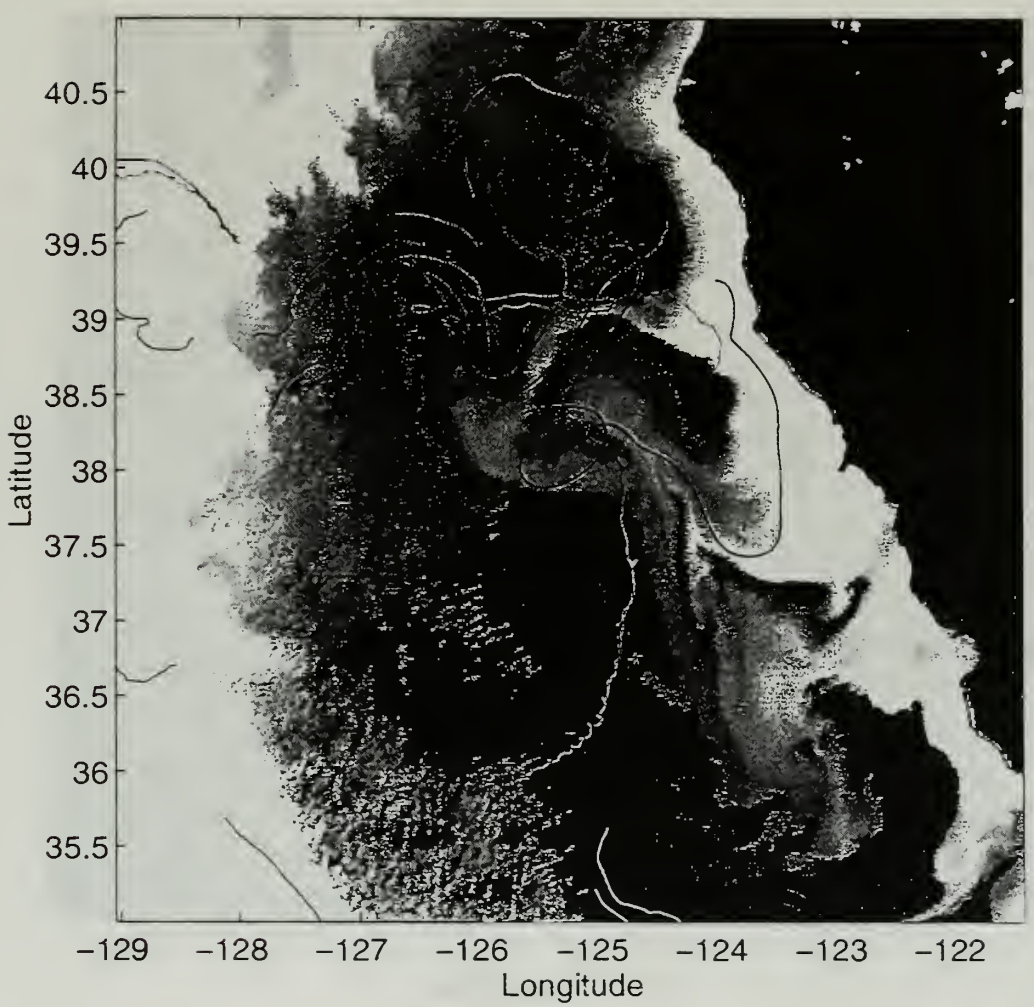


Figure 3.5 Surface (15 m) drifter tracks for the period June 1 - July 1, 1993 overlaid on the satellite SST image from June 16, 1993. Lighter gray shades represent colder temperatures in the range 12 C - 15 C.

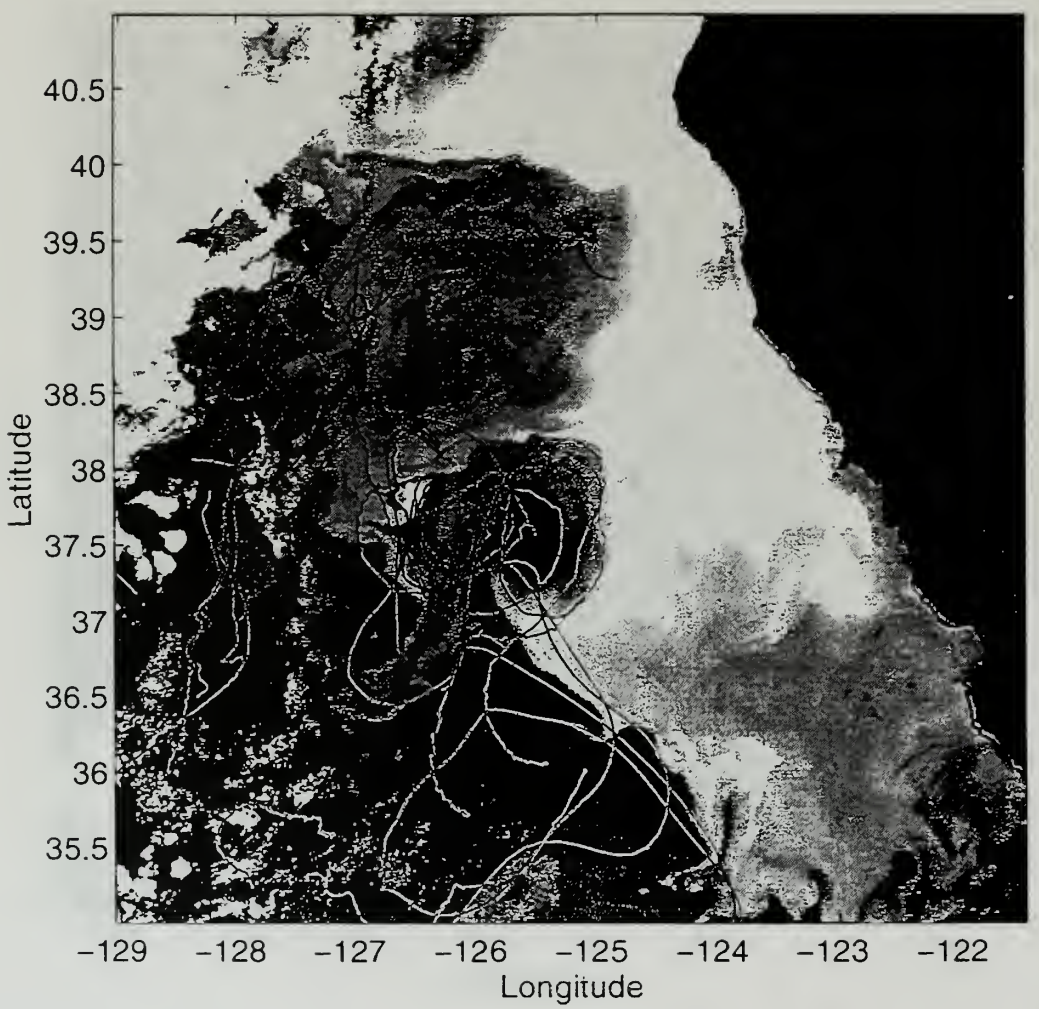


Figure 3.6 Surface (15 m) drifter tracks for the period July 16 - August 15, 1993 overlaid on the satellite SST image from July 31, 1993. Lighter gray shades represent colder temperatures in the range 13.5 C - 16 C.

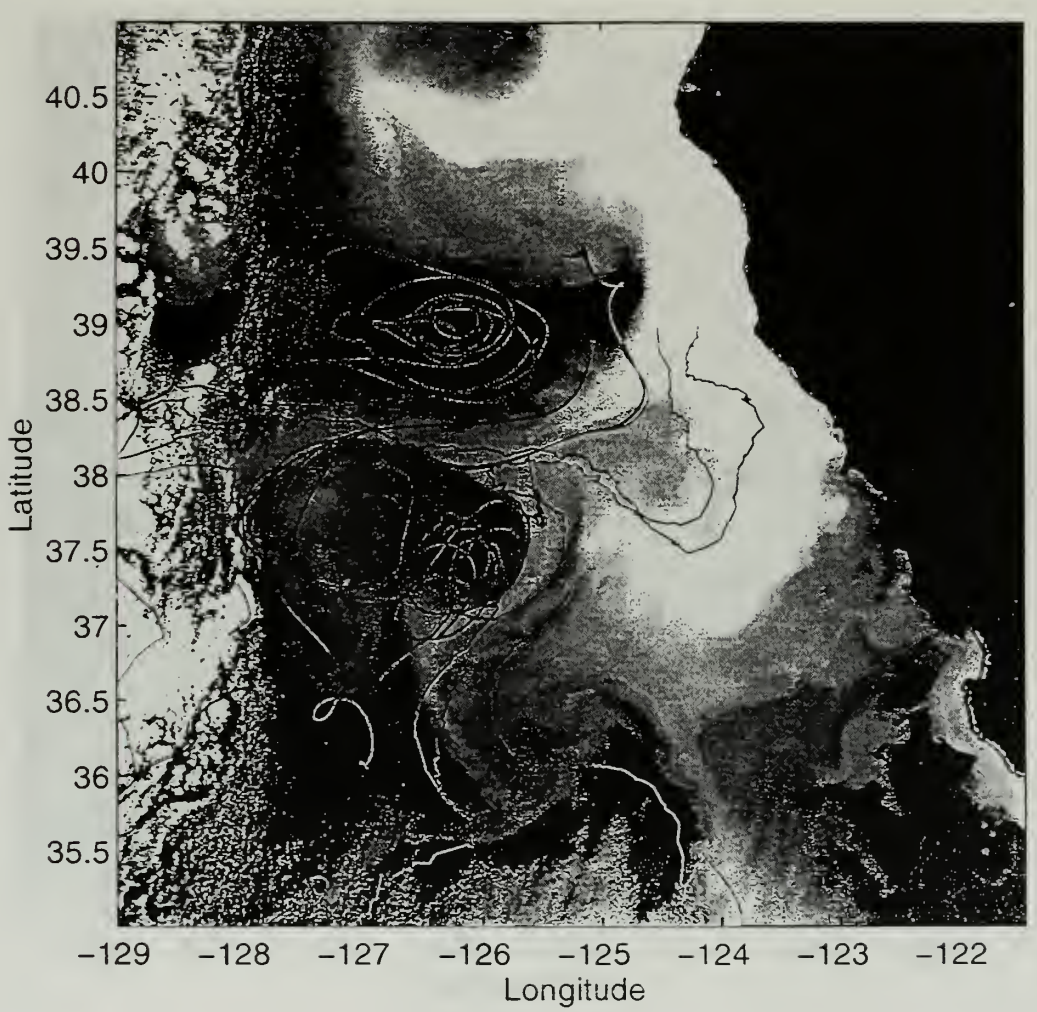


Figure 3.7 Surface (15 m) drifter tracks for the period August 11 - September 10, 1993 overlaid on the satellite SST image from August 26, 1993. Lighter gray shades represent colder temperatures in the range 12.5 C - 17 C.

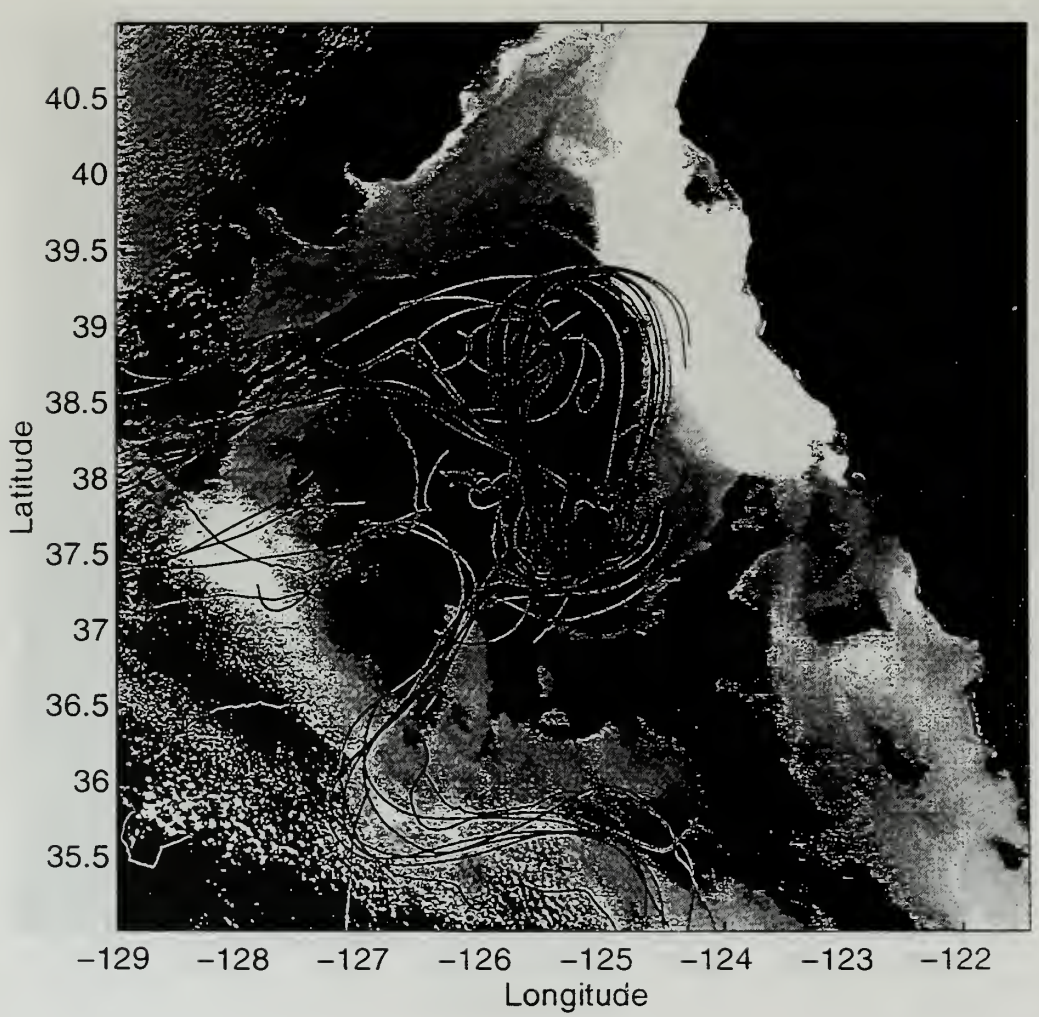


Figure 3.8 Surface (15 m) drifter tracks for the period September 11 - October 11, 1993 overlaid on the satellite SST image from September 26, 1993. Lighter gray shades represent colder temperatures in the range 12 C - 16 C.

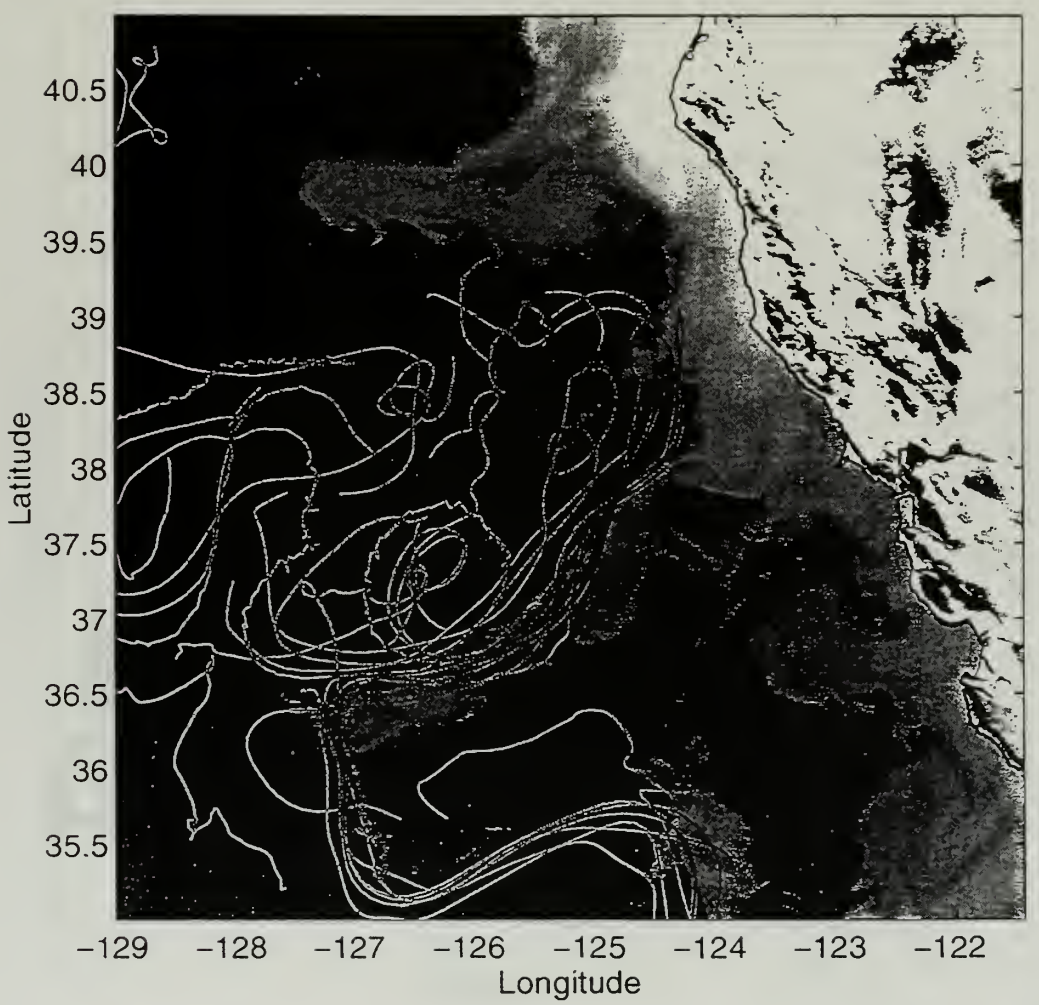


Figure 3.9 Surface (15 m) drifter tracks for the period October 10 - November 9, 1993 overlaid on the satellite SST image from October 25, 1993. Lighter gray shades represent colder temperatures in the range 11.5 C - 16 C.

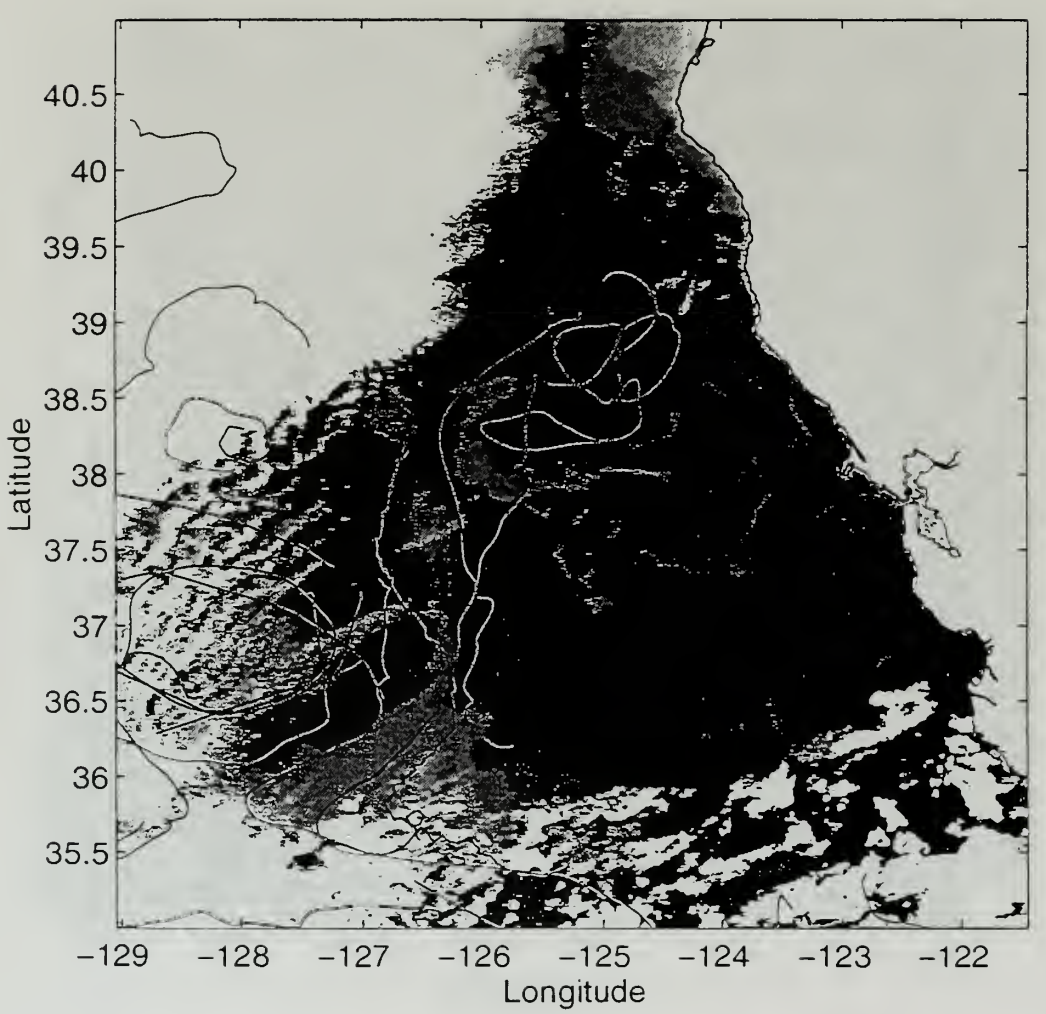


Figure 3.10 Surface (15 m) drifter tracks for the period December 1 - December 31, 1993 overlaid on the satellite SST image from December 19, 1993. Lighter gray shades represent colder temperatures in the range 8.5 C - 11.5 C.

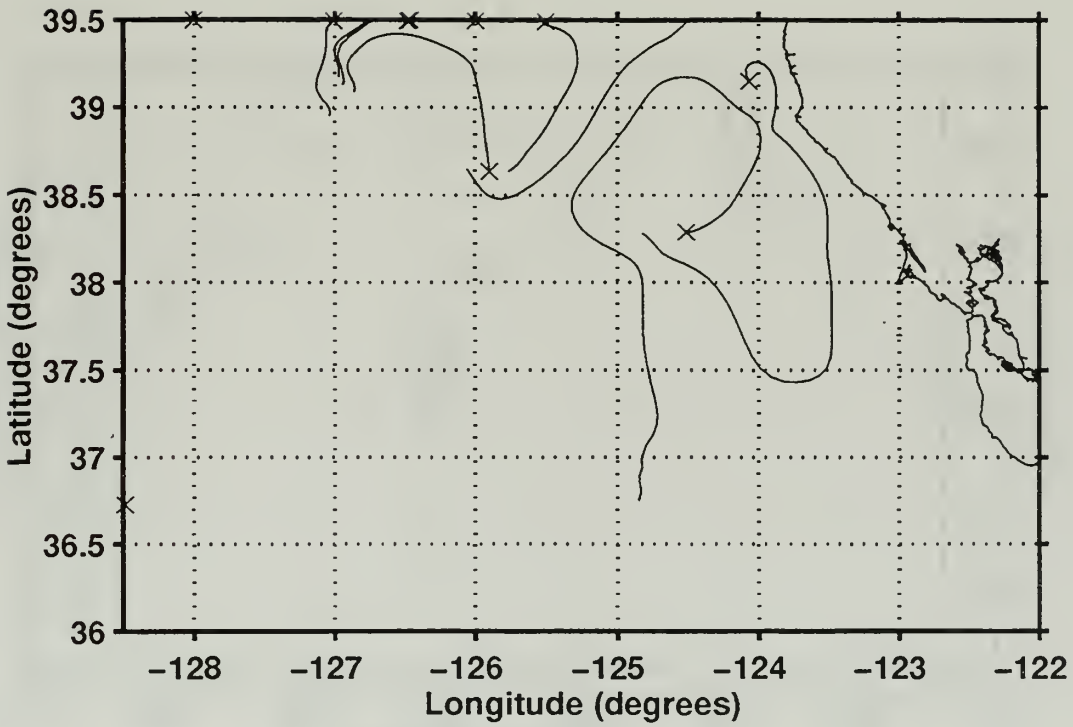


Figure 3.11 Surface (15 m) drifter trajectories for June 1-15, 1993. Starting locations (x) are also shown.

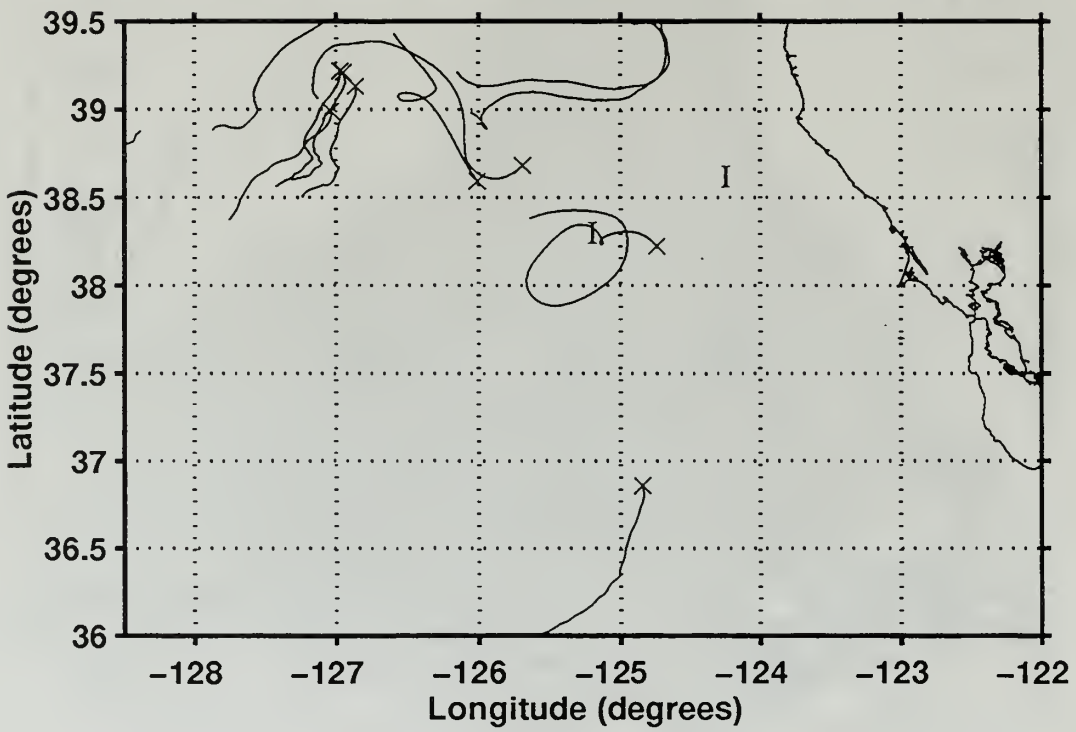


Figure 3.12 Surface (15 m) drifter trajectories for June 16-31, 1993. Starting locations (x) are also shown. The Roman numerals represent previous known positions of the cyclonic eddy from hydrographic/ADCP surveys.

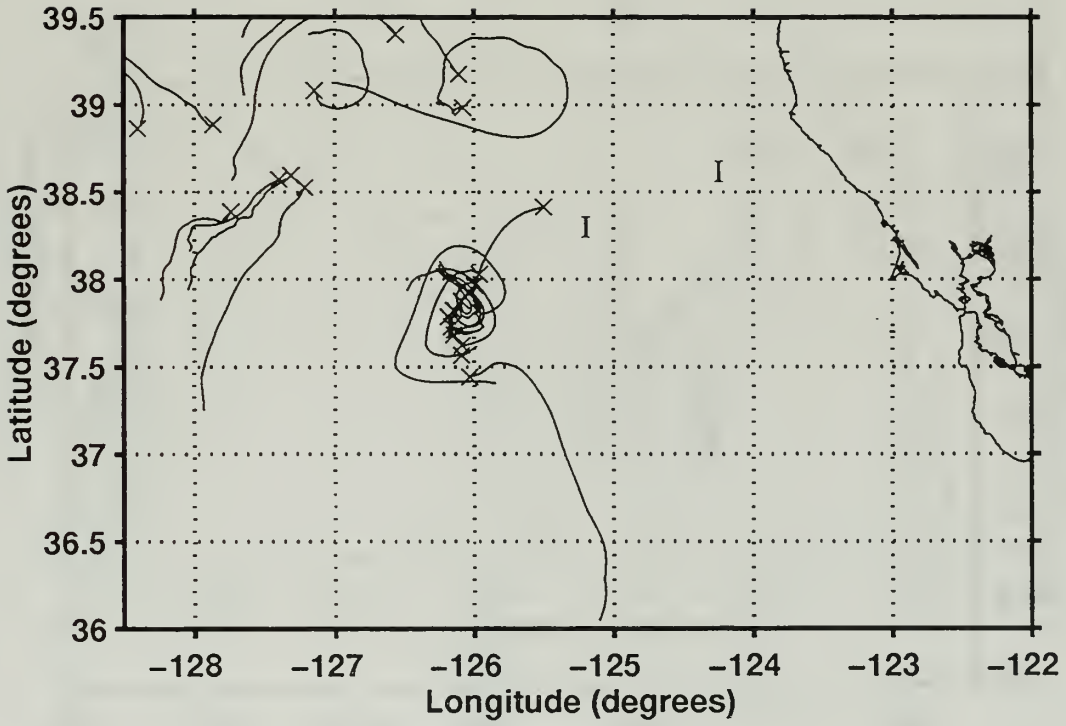


Figure 3.13 Surface (15 m) drifter trajectories for July 1-15, 1993. Starting locations (x) are also shown. The Roman numerals represent previous known positions of the cyclonic eddy from hydrographic/ADCP surveys.

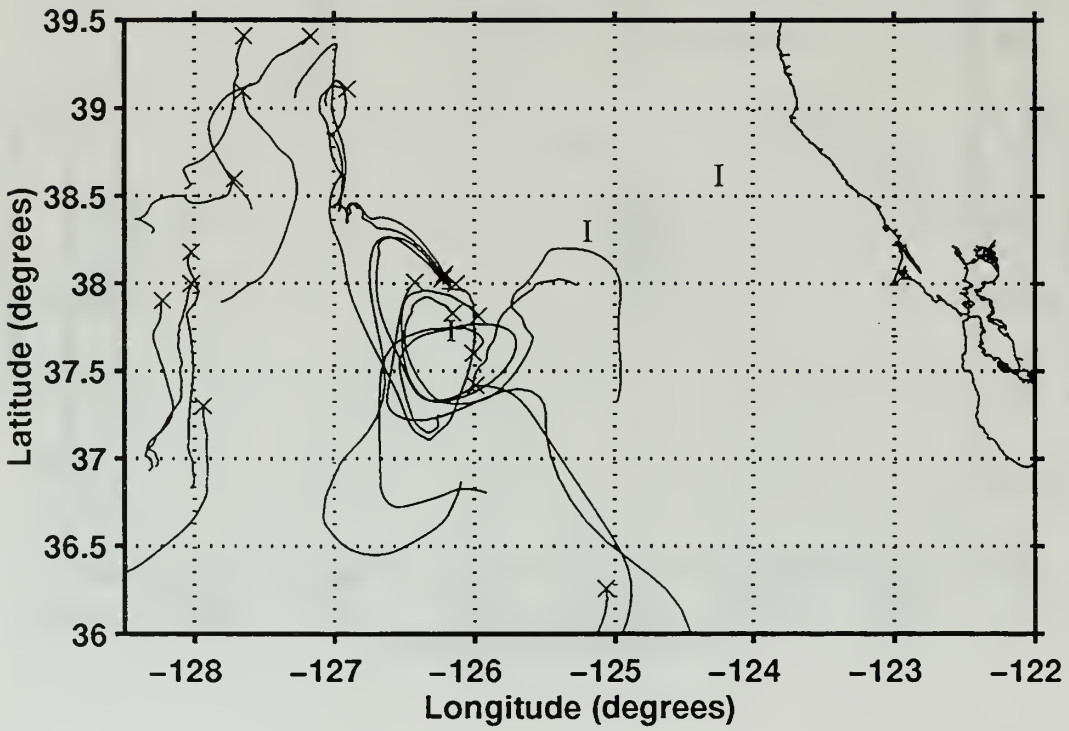


Figure 3.14 Surface (15 m) drifter trajectories for July 16-31, 1993. Starting locations (x) are also shown. The Roman numerals represent previous known positions of the cyclonic eddy from hydrographic/ADCP surveys and surface drifter derived positions.

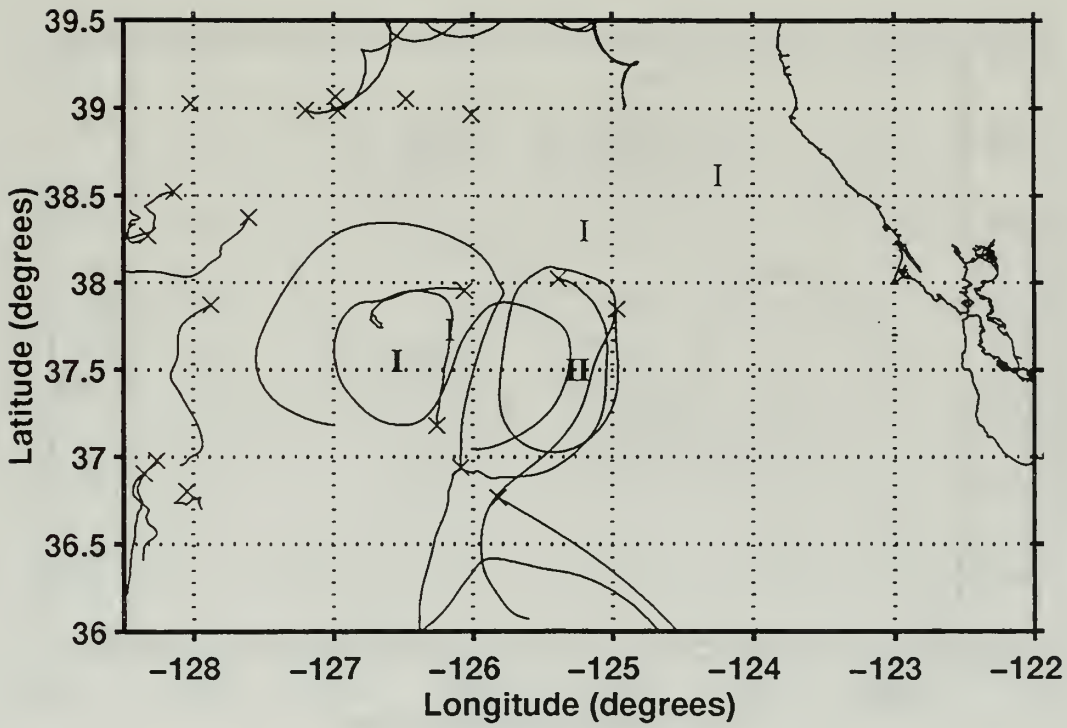


Figure 3.15 Surface (15 m) drifter trajectories for August 1-15, 1993. Starting locations (x) are also shown. Roman numerals represent present (bold) and previous known positions of the cyclonic (I) and anticyclonic (II) eddies from hydrographic/ADCP surveys and surface drifter derived positions.

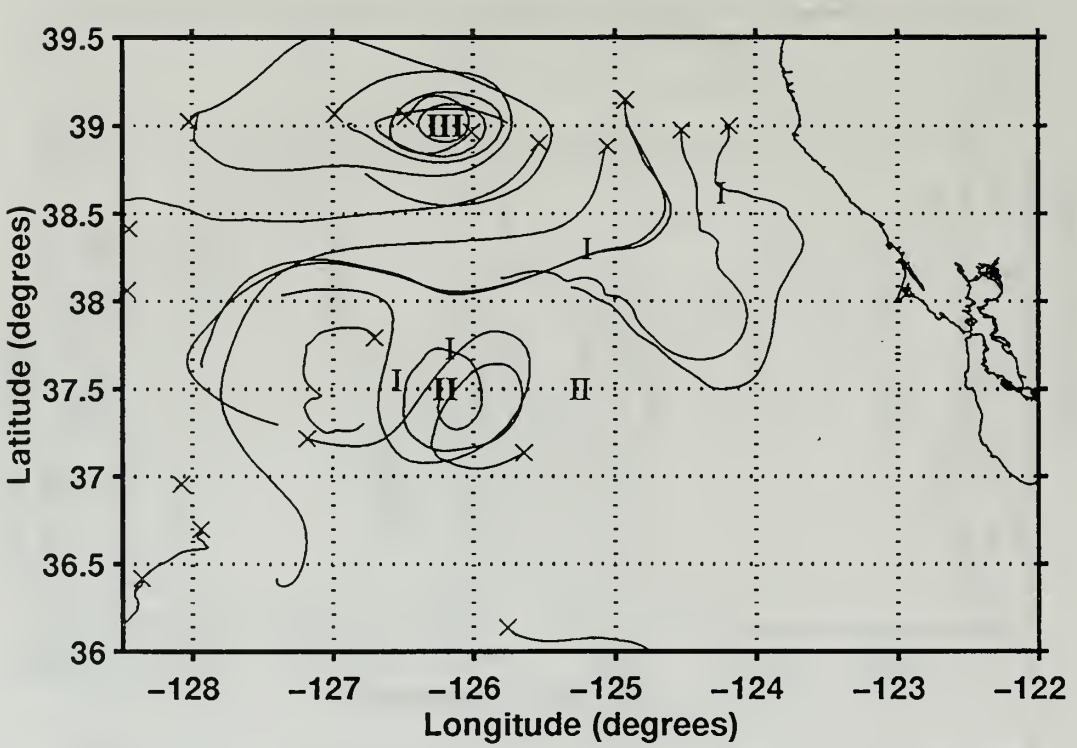


Figure 3.16 Surface (15 m) drifter trajectories for August 16-31, 1993. Starting locations (x) are also shown. Roman numerals represent present (bold) and previous known positions of the cyclonic (I) and anticyclonic (II, III) eddies from hydrographic/ADCP surveys and surface drifter derived positions.

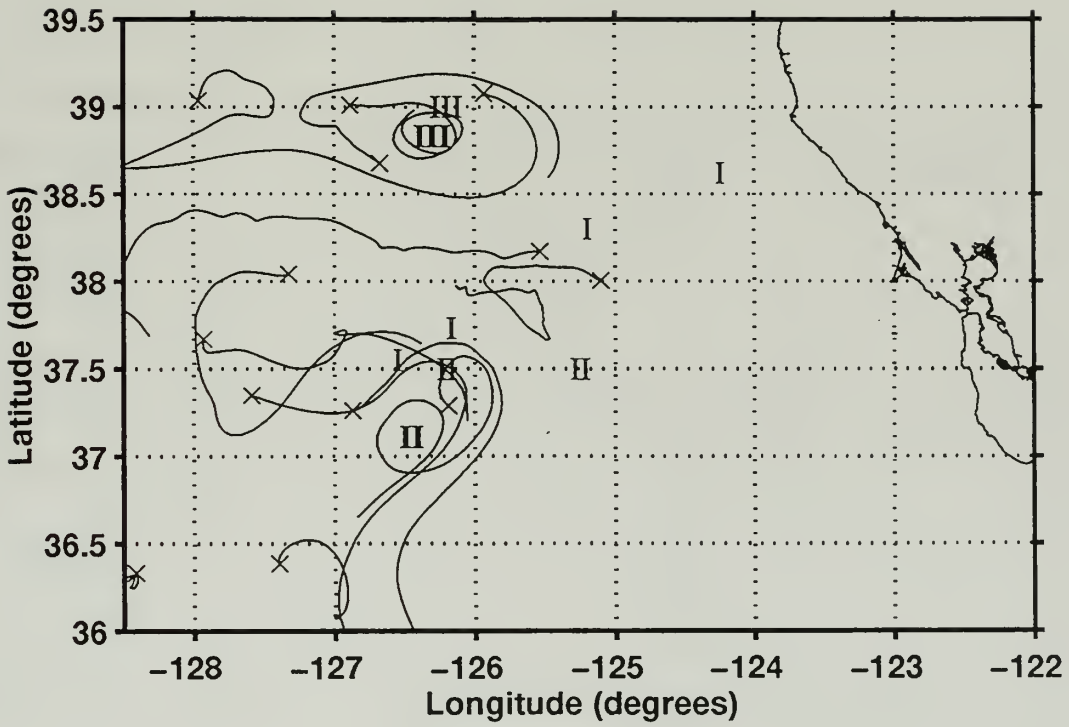


Figure 3.17 Surface (15 m) drifter trajectories for September 1-15, 1993. Starting locations (x) are also shown. Roman numerals represent present (bold) and previous known positions of the cyclonic (I) and anticyclonic (II, III) eddies from hydrographic/ADCP surveys and surface drifter derived positions.

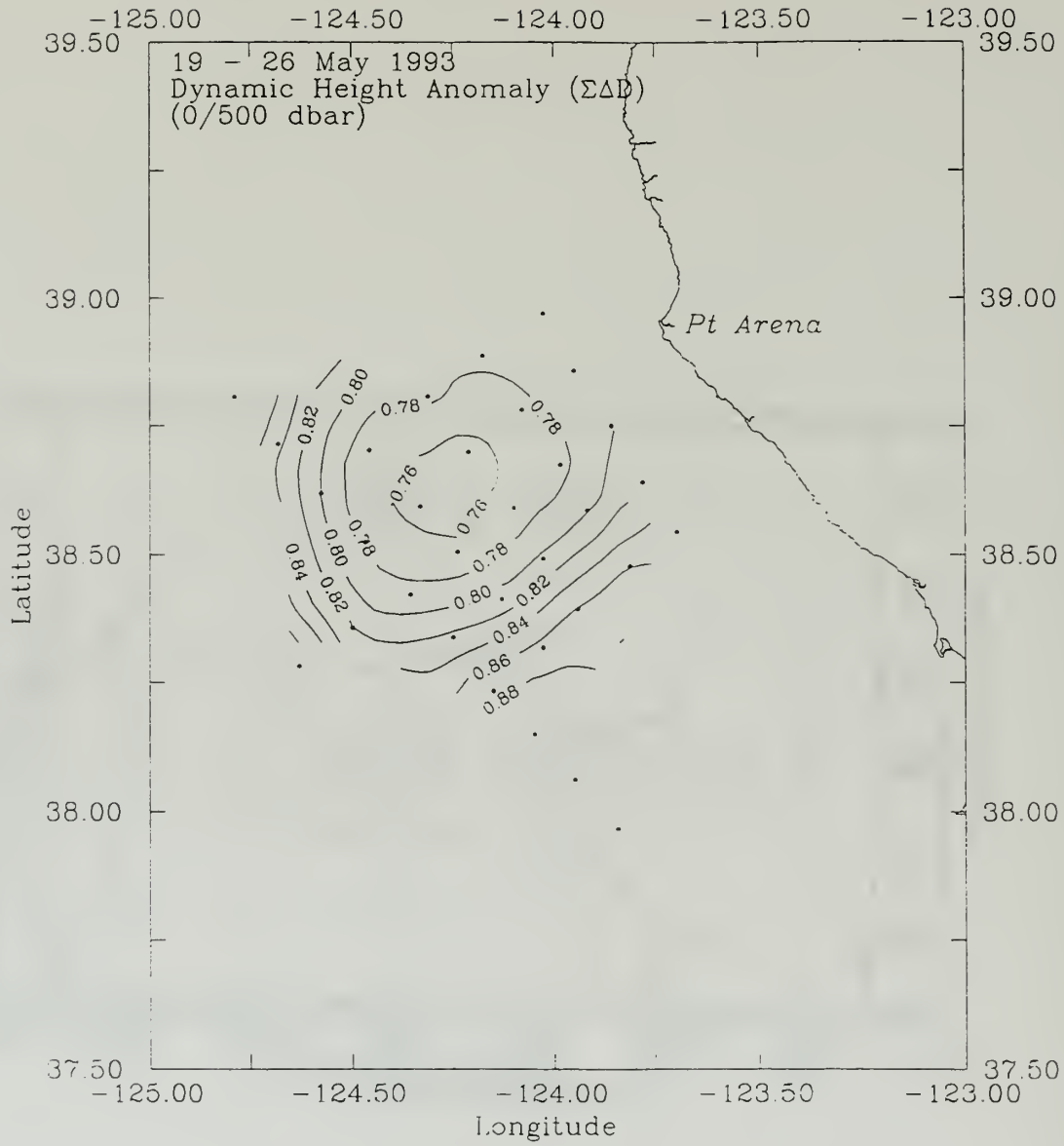


Figure 3.18 The dynamic height anomaly field at the surface relative to 500 dbar for the survey conducted May 19-26, 1993

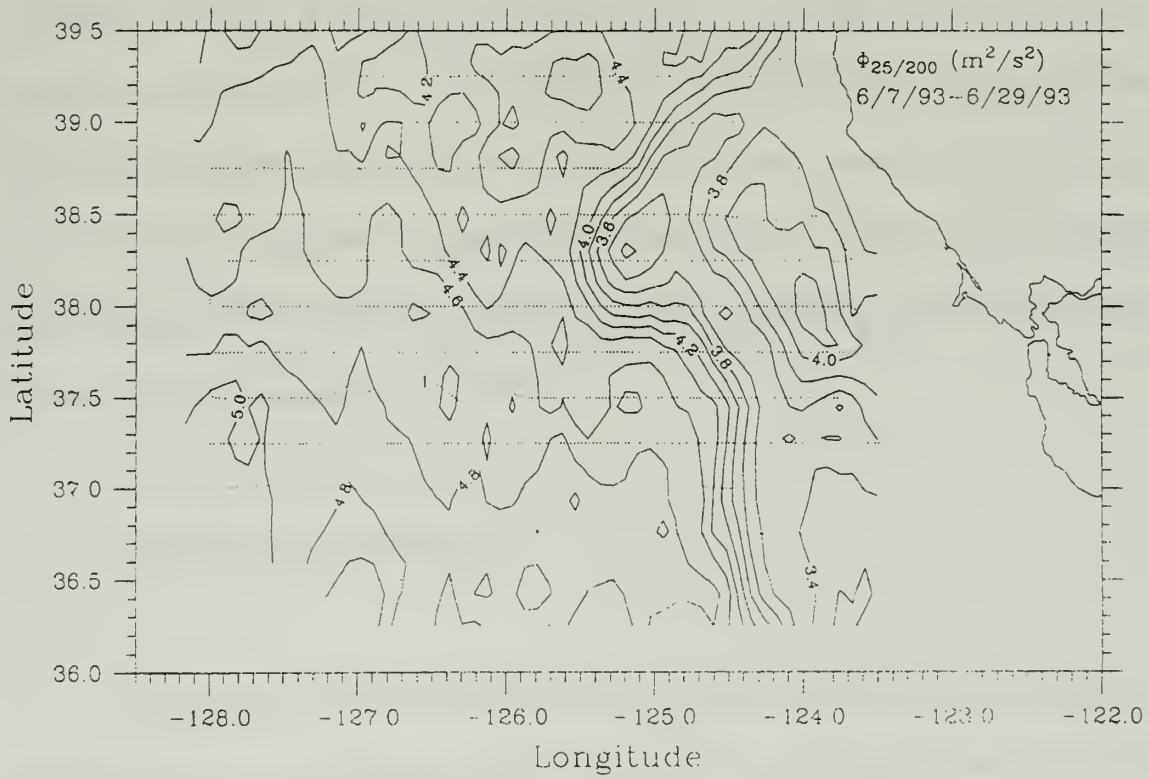


Figure 3.19 The dynamic height field at 25 m relative to 200 dbar for the survey conducted June 7-29, 1993. For comparison, plotting scales are the same as in Figures 3.11-3.17.

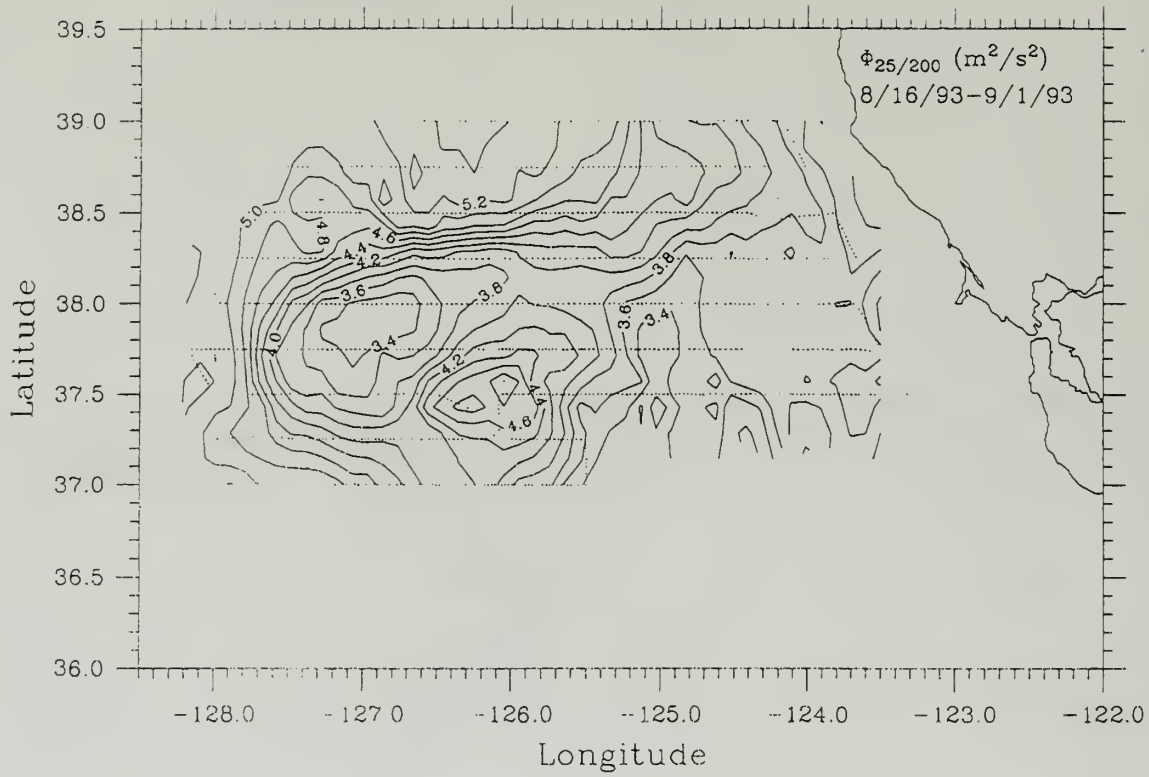


Figure 3.20 The dynamic height field at 25 m relative to 200 dbar for the survey conducted August 16-September 1, 1993. For comparison, plotting scales are the same as in Figures 3.11-3.17.

# IV. DRIFTER ANALYSIS AND RESULTS

The July and September coherent deployment drifter data were evaluated to determine eddy translation rates and the DKP of the surface flow field. Both sets of data were spline interpolated to one-tenth of a day intervals as discussed previously. In addition, the September eddy trajectories were low-pass filtered to remove higher frequency motions, such as inertial currents. Comparison of results based on the filtered and unfiltered trajectories was used to describe the effects of higher frequency motions on the eddy parameters. Three datasets, the July and September one-tenth of a day datasets (unfiltered data), and the September daily low-passed dataset (filtered data) were then used in the linear regression technique originally designed by Halide and Sanderson (1993) and improved upon by Sanderson (1995). The improved analysis presented by Sanderson (1995) will be refered to as the Sanderson technique.

## A. SANDERSON TECHNIQUE

The original method for calculating DKP, velocity and positions of a flow field was developed by Kirwan and Molinari (1975). As stated in the introduction, Kirwan relied upon the paradigm that the flow field center corresponded to the cluster center (Kirwan et al., 1984). He later realized the problems associated with this assumption (Kirwan, 1988). Kirwan et al. (1988, 1990) provided solutions that alleviate these problems involving estimating time derivatives to fourth order. Halide and Sanderson (1993) first developed a

two-stage linear regression technique to obtain results similar to Kirwan et al. (1988, 1990), but without the need to estimate these higher order derivatives. Sanderson (1995) improved on the two-stage technique by explicitly regressing over time and space, allowing for all the variables to be solved for in a single regression. The remainder of this section provides a brief description of the Sanderson technique (Sanderson, 1995).

The Sanderson technique makes two important assumptions. The first is that the eddy has spatially uniform velocity gradients that are independent of time. The divergence, vorticity, stretching and shearing deformation terms are all functions of these velocity gradients:

$$divergence = \frac{du}{dx} + \frac{dv}{dy} \quad (1)$$

$$vorticity = \frac{dv}{dx} - \frac{du}{dy} \quad (2)$$

$$streching = \frac{du}{dx} - \frac{dv}{dy} \quad (3)$$

$$shearing = \frac{dv}{dx} + \frac{du}{dy} \quad (4)$$

The second assumption is that the eddy flow center moves at a constant velocity. With distance from the eddy center, the total flow has an additional component due to the velocity gradients. This assumption is the key to the Sanderson technique. The model is set up to take snapshot looks at the flow field that are averaged over a set length of time, known as the fit length. The individual drifter velocities are assumed to follow the linear Taylor expansion:

$$u_i(t_k) = U + \frac{du}{dx}[x_i(t_k) - X_o - U\,t_k] + \frac{du}{dy}[y_i(t_k) - Y_o - V\,t_k] + u'_i(t_k) \quad \textbf{(5)}$$

$$v_i(t_k) = V + \frac{dv}{dx}[x_i(t_k) - X_o - U\,t_k] + \frac{dv}{dy}[y_i(t_k) - Y_o - V\,t_k] + v'_i(t_k) \quad \textbf{(6)}$$

where $x_i$ (t) and $y_i$ (t) are the position of drifter i at the time t. The last terms of each equation, $u'_i(t_k)$ and $v'_i(t_k)$, are the residual velocities. Equations (5) and (6) contain a total of eight unknown parameters, the four velocity gradients plus the mean translation velocity components U and V and the eddy center locations $X_0$ and $Y_0$ . Therefore, velocity observations from a minimum of four drifters (or one drifter at four different locations) are required to solve this system of equations. Where more observations are available, the overdetermined system can be solved in the least squares sense.

Writing out equations (5) and (6) into a linear polynomial in $t_k$ and $x_i(t_k)$ and $y_i(t_k)$ results in the following:

$$u_i(t_k) = a + a_1 t_k + \frac{du}{dx} x_i(t_k) + \frac{du}{dy} y_i(t_k) + u'_i(t_k) \qquad (7)$$

$$v_i(t_k) = b + b_1 t_k + \frac{dv}{dx} x_i(t_k) + \frac{dv}{dy} y_i(t_k) + v'_i(t_k) \qquad (8)$$

where the coefficients a, $a_1$, b and $b_1$ are:

$$a = U - \frac{du}{dx} X_0 - \frac{du}{dy} Y_0 \qquad (9)$$

$$b = V - \frac{dv}{dx} X_0 - \frac{dv}{dy} Y_0 \qquad (10)$$

$$a_1 = - \frac{du}{dx} U - \frac{du}{dy} V \qquad (11)$$

$$b_1 = - \frac{dv}{dx} U - \frac{dv}{dy} V \qquad (12)$$

Equations (7) and (8) can be written in matrix form as :

$$A = GP + R \qquad (13)$$

where A is the data, G is the data kernal, P represents the unknown and R is the residual data. Standard linear regression (e.g., Menke, 1984) yields the solutions for P (a, $a_1$, b, $b_1$, du/dx, du/dy, dv/dx and dv/dy) and for R. The eddy center location and mean translation rates are then solved for by substitution:

$$U = \frac{\frac{dv}{dy}a_1 - \frac{du}{dy}b_1}{\frac{du}{dy}\frac{dv}{dx} - \frac{du}{dx}\frac{dv}{dy}} \quad (14)$$

$$V = \frac{\frac{du}{dx}b_1 - \frac{dv}{dx}a_1}{\frac{du}{dy}\frac{dv}{dx} - \frac{du}{dx}\frac{dv}{dy}} \quad (15)$$

$$X_0 = \frac{\frac{dv}{dy}(a - U) - \frac{du}{dy}(b - V)}{\frac{du}{dy}\frac{dv}{dx} - \frac{du}{dx}\frac{dv}{dy}} \quad (16)$$

$$Y_0 = \frac{\frac{du}{dx}(b - V) - \frac{dv}{dx}(a - U)}{\frac{du}{dy}\frac{dv}{dx} - \frac{du}{dx}\frac{dv}{dy}} \quad (17)$$

The Sanderson technique suffers from two shortcomings. First, it requires at least four velocity observations. These should be evenly spaced from each other and the flow center. A relatively small error in drifter positioning can result in a large error in the spatial velocity derivatives (Halide and Sanderson, 1993). Because the regression is both spatial and temporal, when drifter spacing is small the model becomes much more sensitive to noise and generally will not depict an accurate account of eddy properties or motion. This problem becomes even more magnified over a short, sparcely sampled time series.

The second shortcoming is of a more theoretical nature. It assumes that kinematic properties are constant within fit intervals. Halide and Sanderson (1993) show that drifters may be affected by more than one singularity in the flow field. Under such cases, errors in computation of the DKP occur.

The Sanderson technique was used to analyze data obtained from both coherent drifter deployments. Estimates of vorticity, divergence and translation rates are discussed below for the two unfiltered datasets. The low-pass filtered dataset from September was also used as a mean of assessing high frequency noise effects, such as inertial currents.

Fit lengths of various sizes were used. The size of the fit length for each period was chosen so as to minimize unwanted noise from the data, but not too high to smooth out small temporal changes in eddy properties. A fit length of one day for the July data and two days for the September data (unfiltered and filtered) is discussed below. Fit lengths with intervals between 0.5 and 4.0 days did not appreciatively change the model results. Using these short windows, we attempted to calculate a time evolution of eddy parameters over the periods with relatively dense drifter coverages. Using long windows of 7 or 12 days, we obtained best-fit eddy parameters using all available drifter data.

## B. FIRST COHERENT (JULY) DEPLOYMENT

The drifters released during the July coherent deployment, on 8-9 July 1993, sampled a cyclonic eddy located at approximately 37.85 N, 126 N. The previous hydrographic/ADCP survey (discussed above) showed the eddy to have a mean translation rate of 3.7 cm/s to the

southwest (Table 3.1). Seven-day time series gathered from drifter trajectories were used in the Sanderson technique. Results showed the eddy had a mean vorticity of $1.2 \times 10^{-5}$ $s^{-1}$, divergence of $8.13 \times 10^{-8} s^{-1}$, shearing deformation rate of $2.13 \times 10^{-6}$ $s^{-1}$ and streching deformation rate of $-2.91 \times 10^{-7} s^{-1}$.

The eddy's mean translation using the 7-day fit length (U= -3.2 cm/s, V= -1.1 cm/s) indicates a movement to the southwest consistent with the prior estimates in Table 3.1 Translation estimates from shorter, 1-day fit lengths (Figure 4.1) are not stable. Rapid changes in direction and speed (in excess of 100 cm/s) are unrealistic and thus not reflective of the true eddy translation. The resulting mean of the 1-day fits is about zero. Results of the 1-day model fits for the eddy center (Figure 4.1) also show little or no mean translation with large short-term excursions.

Plots of the vorticity , rotation periods and divergence from the 1-day fits (Figure 4.2) all indicate some event occured between days 192 and 193 to effect the eddy. Prior to this period, vorticity estimates ranged from 0.18 f to 0.20 f, indicating a relatively strong cyclonic circulation. (The inertial frequency, f, is $8.85 \times 10^{-5}$ $s^{-1}$). The sharp increase in vorticity seen on day 191 is considered a model artifact, discussed below. After day 192, vorticity decreases by 60 % in a three day period, dropping to 0.08 f. The mean vorticity decay rate is 55%.

Once the eddy parameters have been estimated for a fit period, it is possible to reconstruct a two-dimensional "model" view of the eddy. Plots of drifter positions and velocities along with the model results, and in particular, the estimated eddy center (Figures 4.3-4.9), help provide a graphic description of the rotation rates. From Day 190.5 (Figure

4.3) to Day 192.5 (Figure 4.5), trajectories show buoy rotations of about 90 degrees around the eddy, indicating an 8-9 day rotation rate. By Day 196.5 (Figure 4.9), however, the drifters have moved only another 45 degrees around the estimated center, evidence of the rapid slow down noted in the vorticity estimates. Figure 4.2 indicates that by the end of the period, rotation rates have settled out at 19 days, which is have double to the initial value.

For the first two days of observations, model results for divergence (Figure 4.2) indicated a mean divergence estimate of -0.02 f, slightly convergent as expected in a cyclonic eddy. After day 192, divergence estimates increased to +0.06 f in a twenty-four hour period. After three days, divergence estimates decrease at almost the same rate to approximately -0.01 f, close to the divergence rates at the beginning of the observation period.

A number of factors could be responsible for this sudden change in eddy parameters. A strong temperature gradient between the eddy and the surrounding warmer water and frictional effects as the eddy translates acts to slowly decay an eddy, but not at the rapid rates noted above. Changes of this magnitude are more in line with those of Gulf Stream rings when interacting with the Gulf Stream.

Similar movements of a cyclonic eddy at the terminal end of a filament were seen in both the OPTOMA 21 (Reinecker and Mooers, 1989b) and CTZ (Huyer et al., 1991; Strub et al., 1991). In the CTZ experiment off Cape Mendocino, Huyer et al. (1991) concentrated more on the filament response when it interacted with the eddy, rather than what happened to the eddy itself. Strub et al. (1991) noted in the CTZ filament that the terminal cyclonic eddy in 1988 moved offshore past the filament at 3 cm/s. Our observations, however, show no evidence of the eddy passing through the filament.

As stated above, a shortcoming of the Sanderson technique is that it requires at least four observations, evenly spaced from both the eddy center and from one another. Due to limited buoy spacing across the eddy (buoy geometry),measurements from one quadrant of the eddy had a greater weight on model results than it should. Sanderson (1995) had attempted to solve this problem; however, results of our study indicate this problem remains.

Figure 4.10 shows the percent of variance explained by our statistical model versus time for the 1-day fits. A high level of variance explained (i.e., 80% or greater) indicates that the model performs well in resolving the observed velocity fluctuations. The results in Figure 4.10 indicate the model only accounts for approximately 50% of the energy in both directions. The fluctuations in variance explained for the east-west and north-south directions are out of phase and appear to follow the variations in relative positions of the drifters.

Figures (4.3-4.9) show drifter positions around the eddy center during the seven days of observations. Figure 4.3 shows that the drifter positions on day 190.5 were initially in a north-south line through the estimated eddy center. This arrangement of drifters allows for a good measure of the energy in the east-west direction as the drifters continue to translate across the eddy, but poorer estimates of north-south motion, as evidenced by the results of Figure 4.10. By Day 192.5 (Figure 4.5), the drifters had become almost aligned in the east-west direction across the eddy, with almost all of the drifters in the eastern quadrant. Correspondingly, Figure 4.10 shows the explained variances have flipped, with explained variances in the north-south direction explained by the model approaching 90% while east-west variances decreased to less than 20% by day 193. By the end of the observation period

on day 196.5 (Figure 4.9), the drifters had become fairly well spaced out across two-thirds of the eddy, although the variances explained in Figure 4.10 are still well below that expected in a well-sampled eddy.

## C. SECOND COHERENT (SEPTEMBER) DEPLOYMENT

Following the September coherent deployment, conducted on 19-20 September 1993, drifters sampled an anticyclonic eddy located at approximately 37.9 N, 124.9 W. Results of a hydrographic/ADCP survey conducted prior to the deployment and trajectories from drifters deployed earlier in the year had determined that the eddy was translating to the southwest at 4.2 cm/s (Table 3.1). Twelve-day time series gathered from drifter trajectories were used in the Sanderson technique. The results indicate a strongly anticyclonic eddy with a mean vorticity of $-1.57 \times 10^{-5} s^{-1}$, divergence of $1.12 \times 10^{-6} s^{-1}$, stretching deformation rate of $-3.28 \times 10^{-6} s^{-1}$ and shearing deformation rate of $9.90 \times 10^{-7} s^{-1}$. Mean translation velocities for the eddy from the 12-day fit (U=-4.0 cm/s, V=-1.9 cm/s) indicate continued movement to the southwest, using shorter, 2-day fit lengths, an initial translation rate of 14 cm/s over the first three days of observations was observed (Figure 4.11). However, translation speeds quickly return to the more expected values of approximately 4 cm/s, with small variations in the direction of the eddy noted until the end of the time series. Estimated eddy center positions (Figure 4.11) also portray this initial rapid movement.

In contrast to the July cyclonic eddy, there are no indications of either strengthening or decay in the September anticyclone (Figure 4.12). Vorticity estimates range from a

minimum of almost -0.14 f to a maximum of -0.28 f, fluctuating around a mean of -0.20 f. Interestingly, values at the start of the observation period are almost identical to those at the end. The changes in vorticity during the time series are either the result of some submesoscale event or the result of poor data distribution around the eddy. Drifter rotation periods mirror vorticity. The max rotation period is on day 266 (11.34 days) and the minimum occurs only three days later (6.12 days) on day 269. Estimates of divergence (Figure 4.12) remain relatively constant throughout the observation period around the slightly divergent mean value. This is expected for the surface flow in an anticyclone.

Unlike the July eddy, poor buoy geometry does not appear to be the principle reason for the inaccuracies noted above. Figures 4.13-4.23 show drifter positioning around the estimated eddy center. Initially (Figure 4.13) buoy spacing in the eddy is limited to one quadrant of the eddy, a condition that may have biased some initial results as in the July time series. A look at the percentage of variances explained by the statistical model (Figure 4.24), however, indicates this may not be the case. Variances explained for the initial period are almost 80% for both u and v. The initial drop in explained variances occurs on day 266/267. Drifter trajectories for these days (Figures 4.16-4.17) show what appears to be a well-sampled eddy, particularly close to the eddy center. A closer look at these figures shows that the actual rotation is not around the center estimated by the model, but around a point slightly south and east of that point. Because of this error in estimating the center, the model now has an overly weighted quadrant of data, possibly biasing the results of model output seen in the vorticity plot (Figure 4.12) during this time period. Not until day 269 (Figure 4.19) do the center position and the cluster centroid again correspond.

A compounding problem for this data distribution error is the reduction in the number of observations over the first six days (Figure 4.24). An initial increase of 60% over one day is immediately followed by a sharp decrease of 54% over a five-day period. The last day of the record is marked by an additional 13% decrease from the day before, perhaps explaining the decrease in divergence on the last day (Figure 4.12).

## D. ASSESSMENT OF HIGH FREQUENCY EFFECTS

The Sanderson technique was also applied to the low-pass filtered September dataset to determine whether temporal distortion was present in the unfiltered data, and how the Sanderson technique responded to it. A stated advantage of the Sanderson technique over previously existing studies was the ability to separate the inertial and mesoscale (eddy) components of the circulation (Sanderson, 1995). The inertial period for 37.5N, the approximate latitude of the eddy center at drifter deployment, is 19.6 hours. Any oscillations at the inertial period then would be seen over almost a one day period.

Comparing model output from both the filtered and unfiltered datasets, Sanderson's technique appears to have effectively filtered the inertial currents. The filtered data yields vorticity estimates of -0.1674 f, or a mean vorticity of $-1.48 \times 10^{-5} s^{-1}$, only slightly less than with the unfiltered data. Similarly, mean divergence rates and rotation periods are very close to the unfiltered data results. Figure 4.12, however, shows that the filtered data provides consistently lower estimates of vorticity than the unfiltered data. This bias indicates there is some high-frequency movements that are not a part of the eddy motions that make their

way into the least square fit estimates. In this case, clockwise inertial rotation may have added, erroneous, to the estimated clockwise eddy rotation in the unfiltered case, which suggests that horizontial scales of the inertial currents may have been comparable to those of the mesoscale eddy.

Figure 4.25 shows the difference in x and y drifter positions between the unfiltered and filtered datasets. RMS values of the differences in x and y (1.66 cm/s and 1.58 cm/s, respectively) are two orders of magnitude less than the eddy diameter, indicating these high frequecny motions are second order effects. The effects of inertial currents appear to have been effectively filtered by the Sanderson technique, with the exception of the vorticity bias noted above.

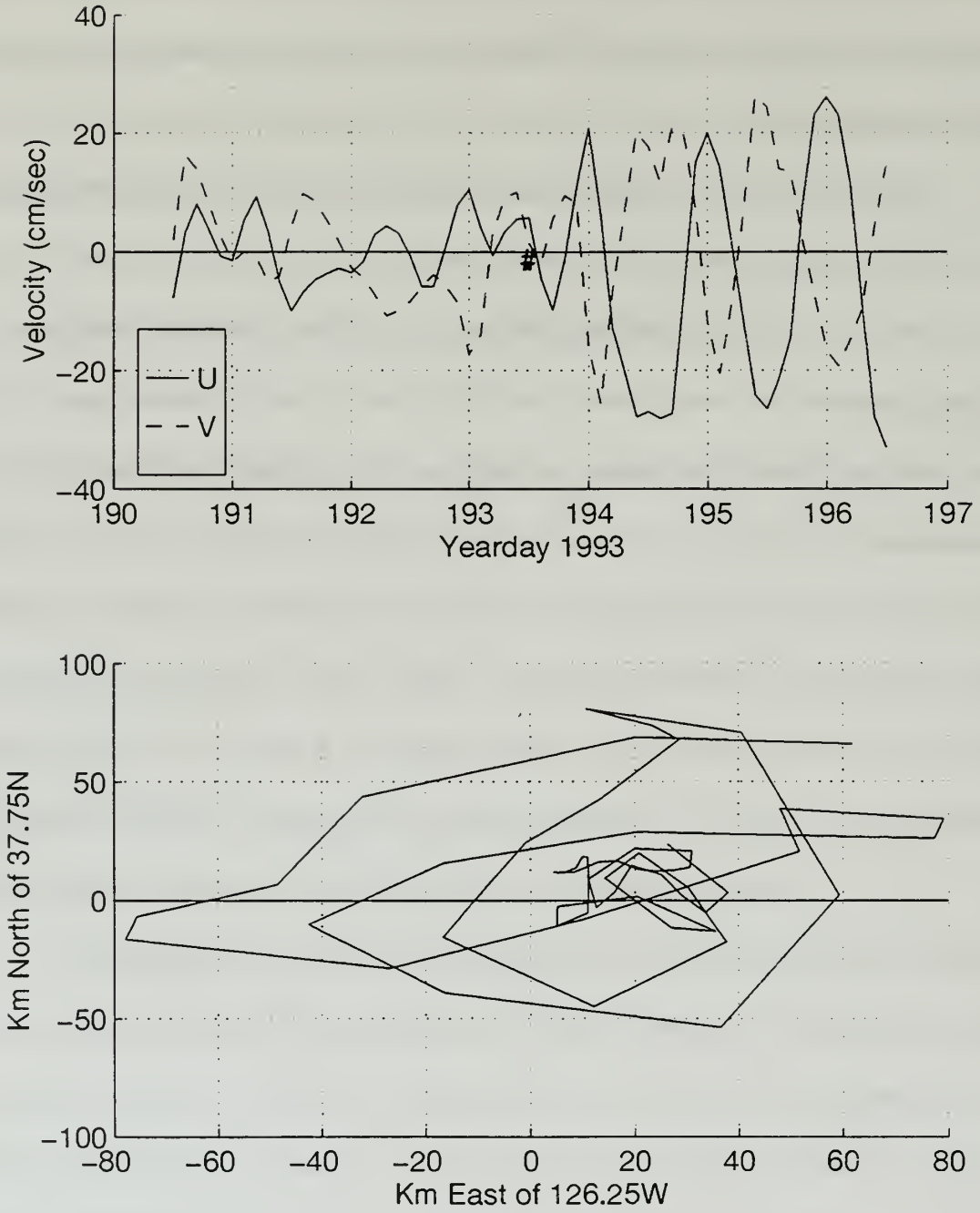


Figure 4.1 Sanderson technique estimates of eddy mean translation (top) and best-fit eddy center (bottom) using 1-day fit lengths for the cyclonic eddy studied during the first coherent deployment in July 1993. Symbols denote u(*) and v(#) averages from single, 7-day fit.

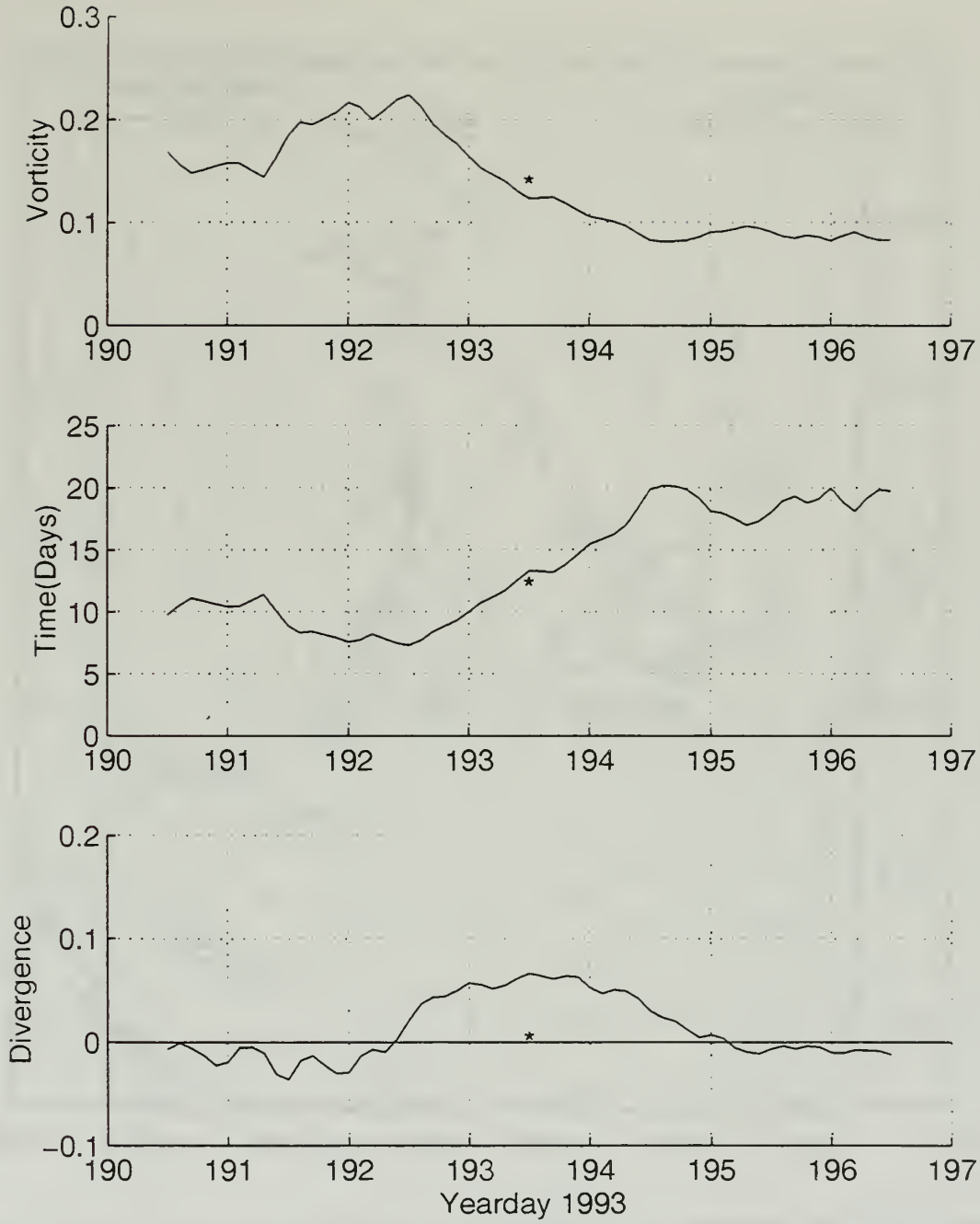


Figure 4.2 Estimates of vorticity (top), rotation rates around the eddy (middle) and divergence (bottom) using 1-day fit lengths for the cyclonic eddy studied during the first coherent deployment in July 1993. Symbols (*) denote averages from single, 7-day fit.

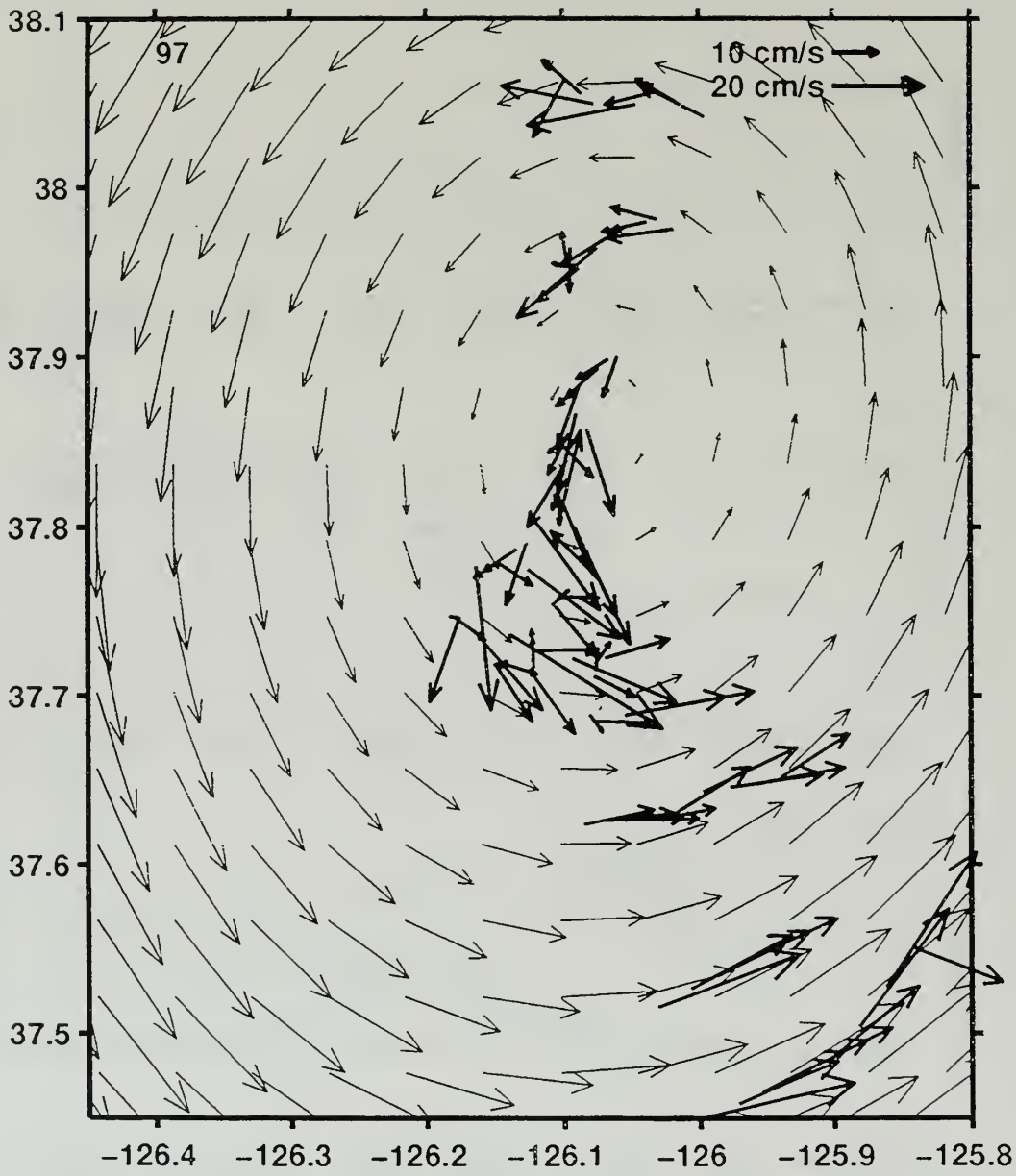


Figure 4.3 Drifter observations interpolated to one-tenth of a day overlaid on Sanderson technique's predicted eddy for Day 190.5.

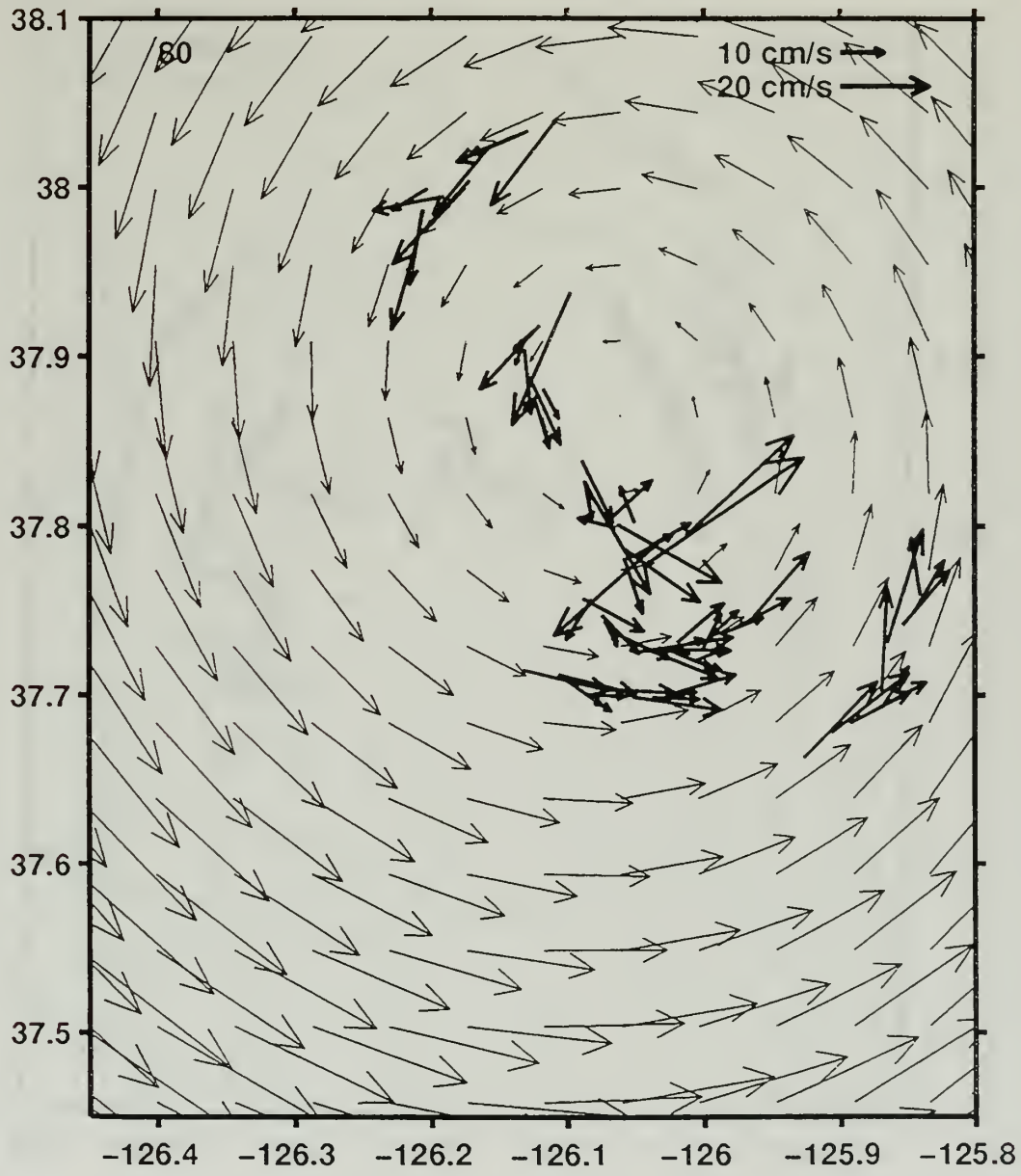


Figure 4.4 Drifter observations interpolated to one-tenth of a day overlaid on Sanderson technique's predicted eddy for Day 191.5.

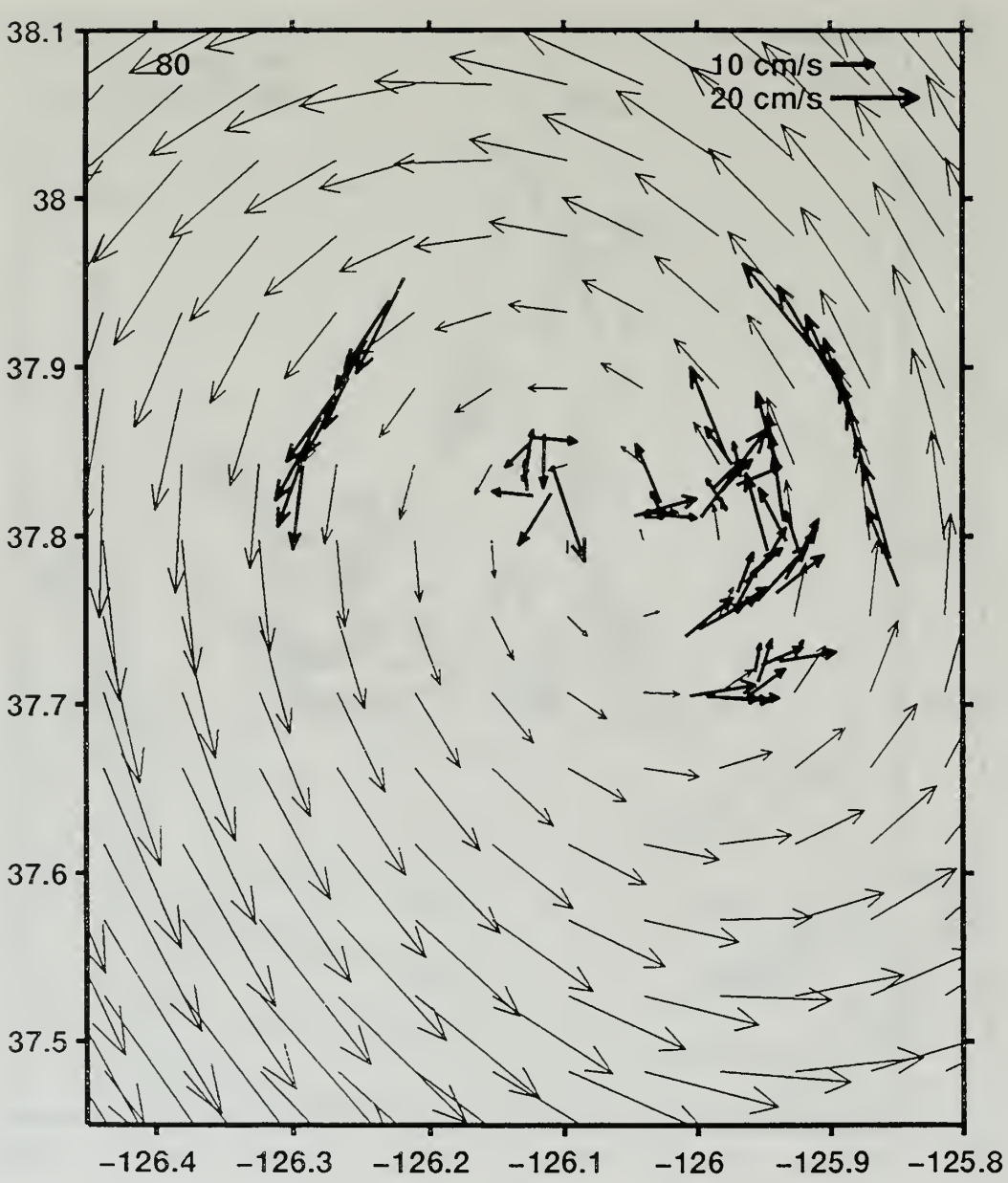


Figure 4.5 Drifter observations interpolated to one-tenth of a day overlaid on Sanderson technique's predicted eddy for Day 192.5.

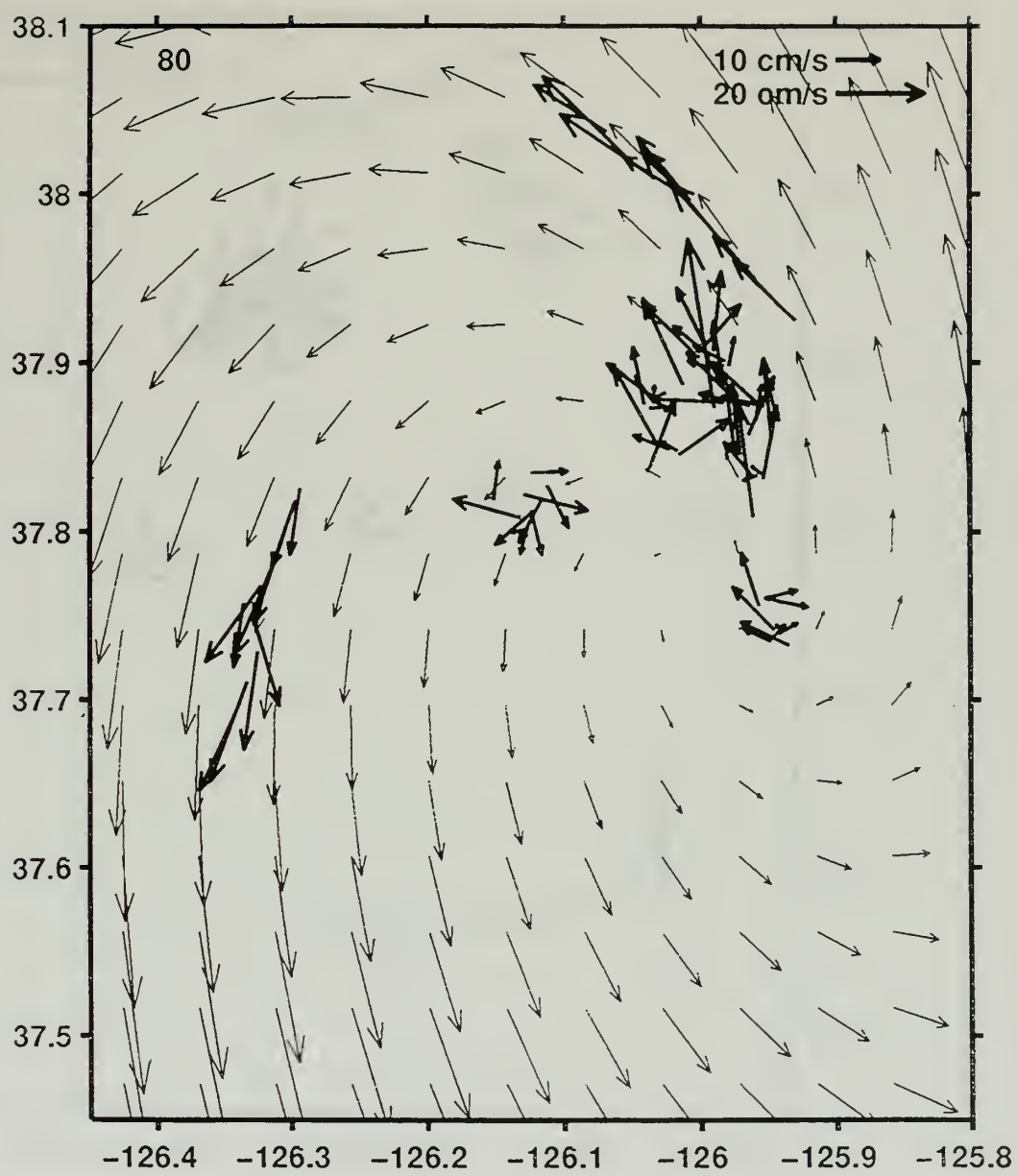


Figure 4.6 Drifter observations interpolated to one-tenth of a day overlaid on Sanderson technique's predicted eddy for Day 193.5.

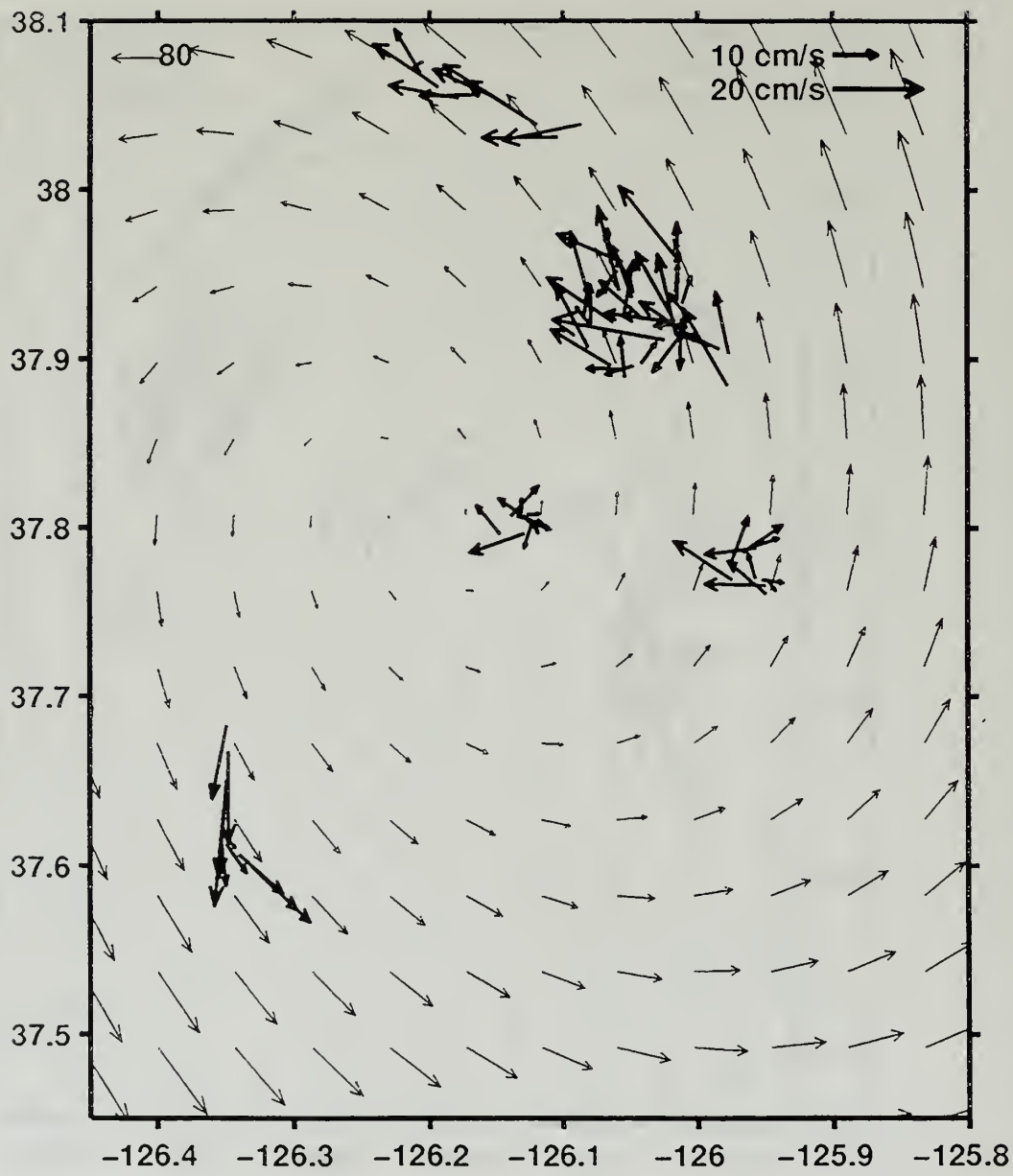


Figure 4.7 Drifter observations interpolated to one-tenth of a day overlaid on Sanderson technique's predicted eddy for Day 194.5.

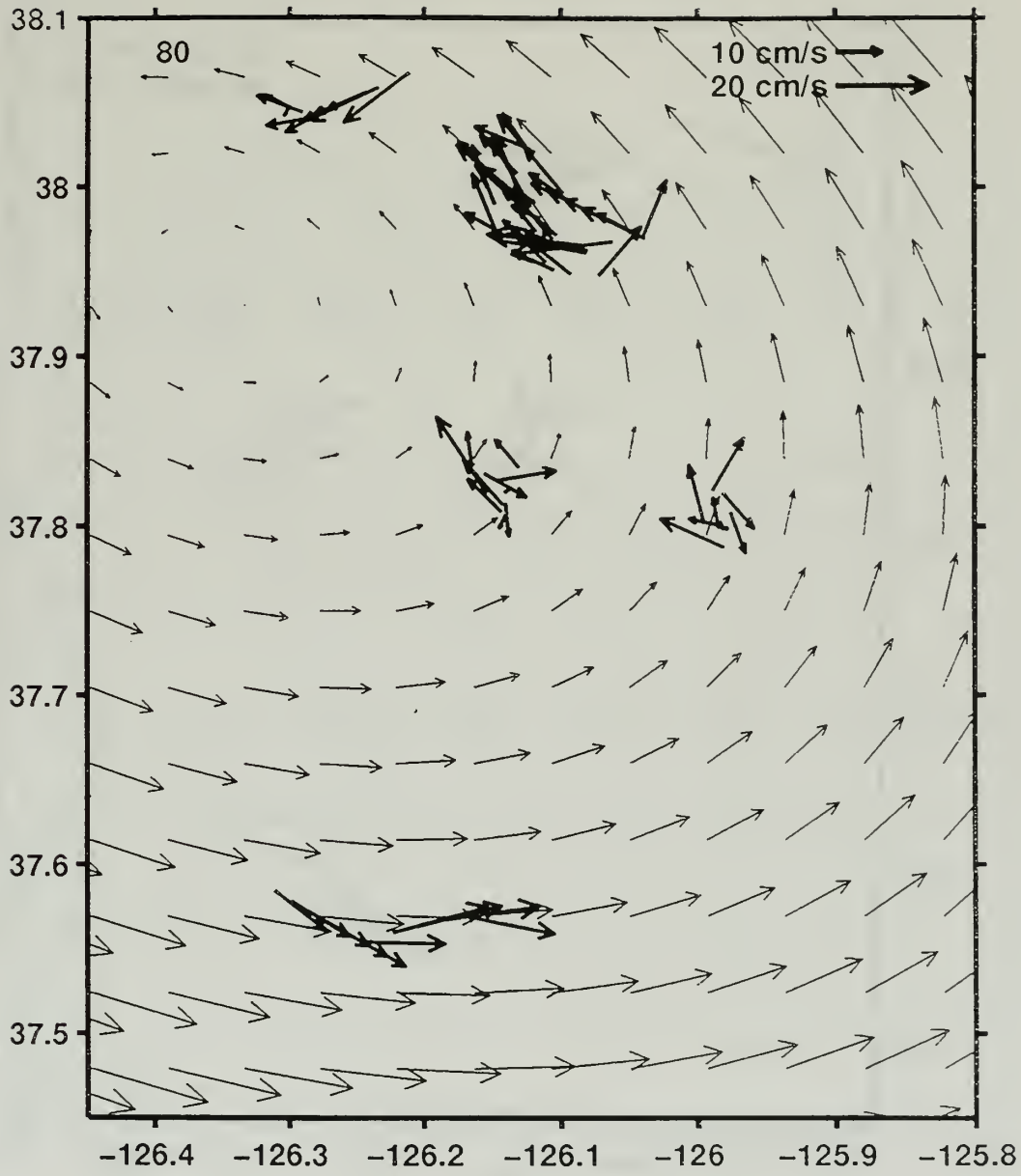


Figure 4.8 Drifter observations interpolated to one-tenth of a day overlaid on Sanderson technique's predicted eddy for Day 195.5.

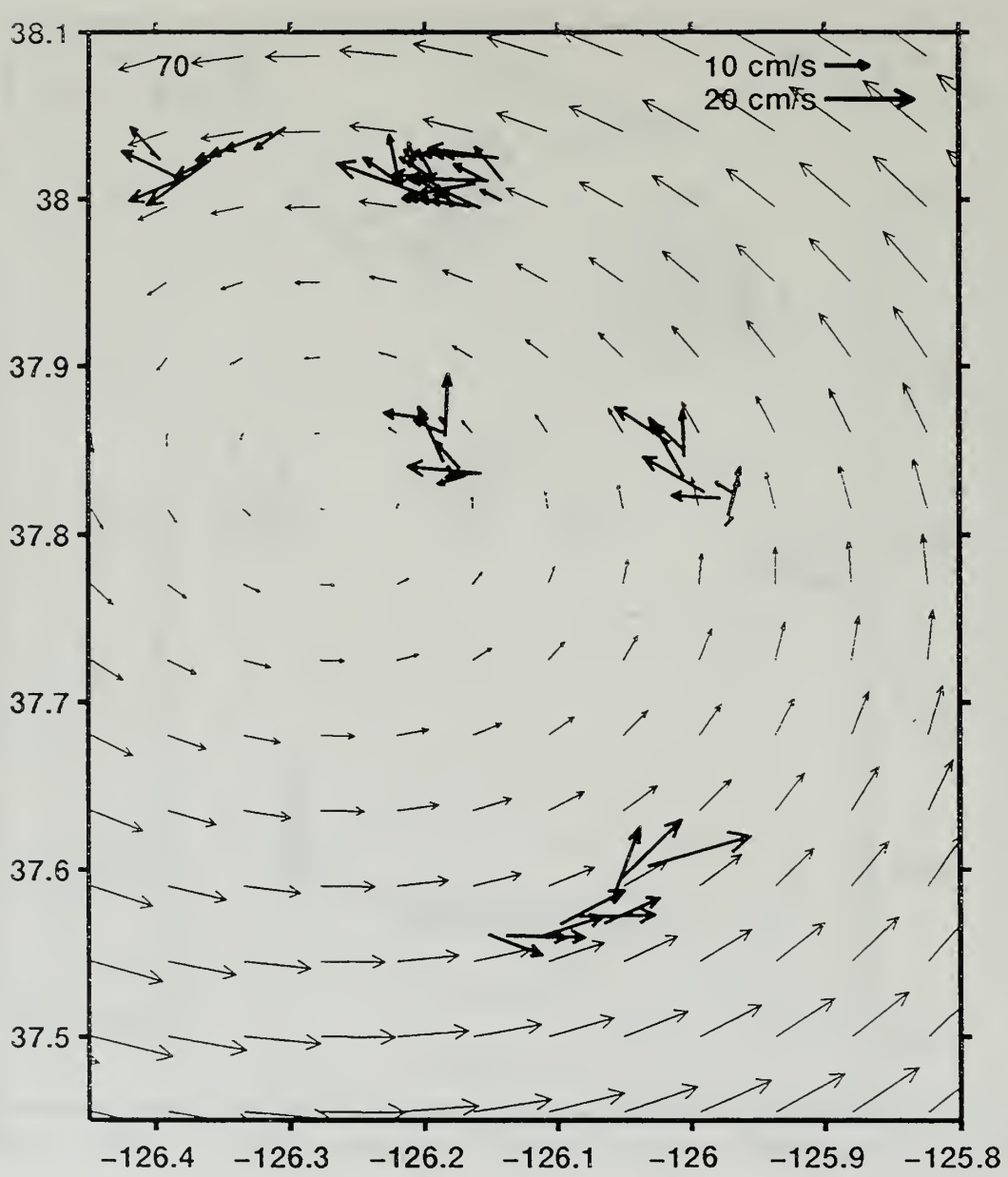


Figure 4.9 Drifter observations interpolated to one-tenth of a day overlaid on Sanderson technique's predicted eddy for Day 196.5.

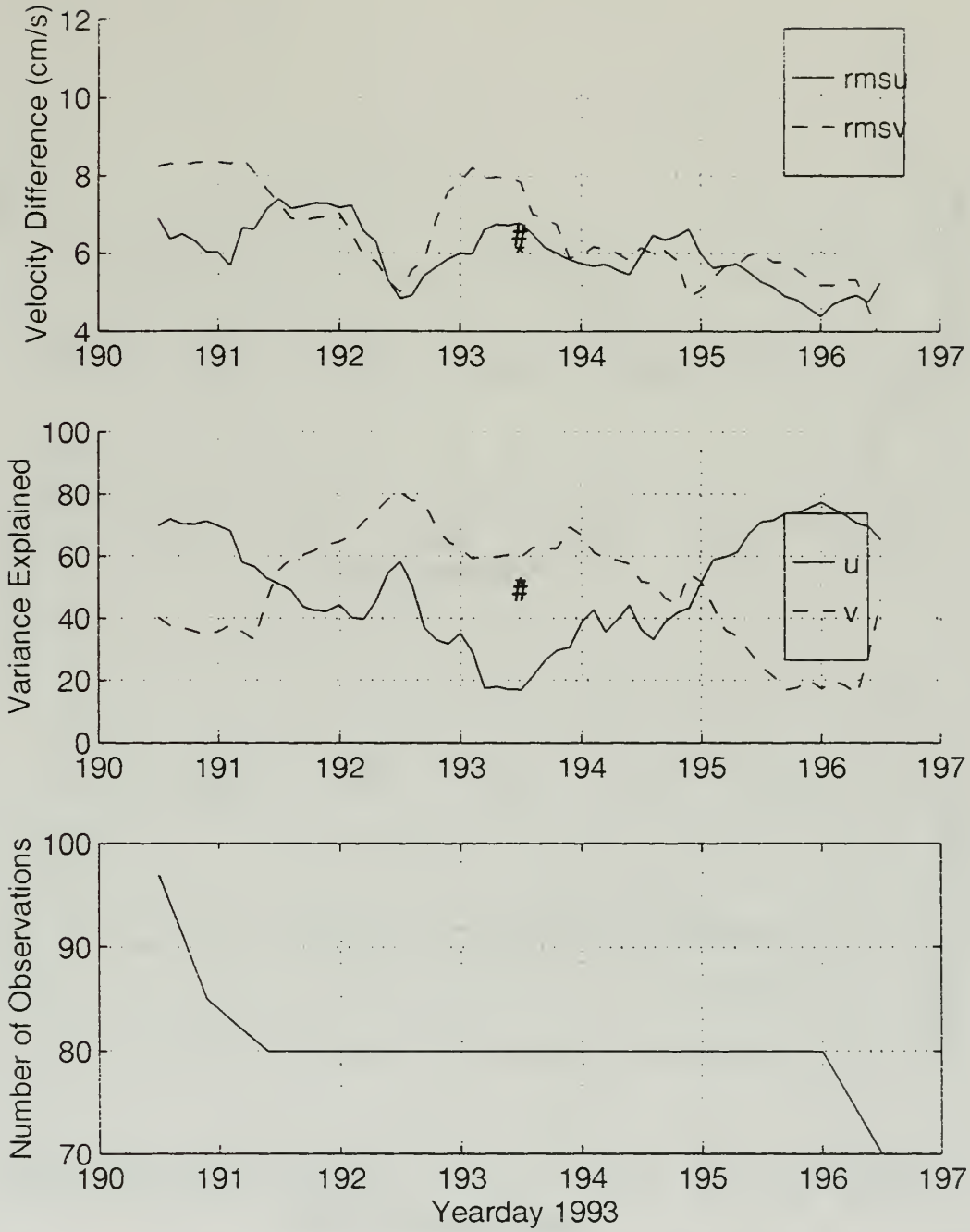


Figure 4.10 Rms velocity differences between actual observations and Sanderson-technique velocities (top), percent variance explained by the model velocities (middle), and the number of observations per day over the seven day time series (bottom) using 1-day fit lengths for the cyclonic eddy. Symbols denote east-west (*) and north-south(#) averages from single, 7-day fit.

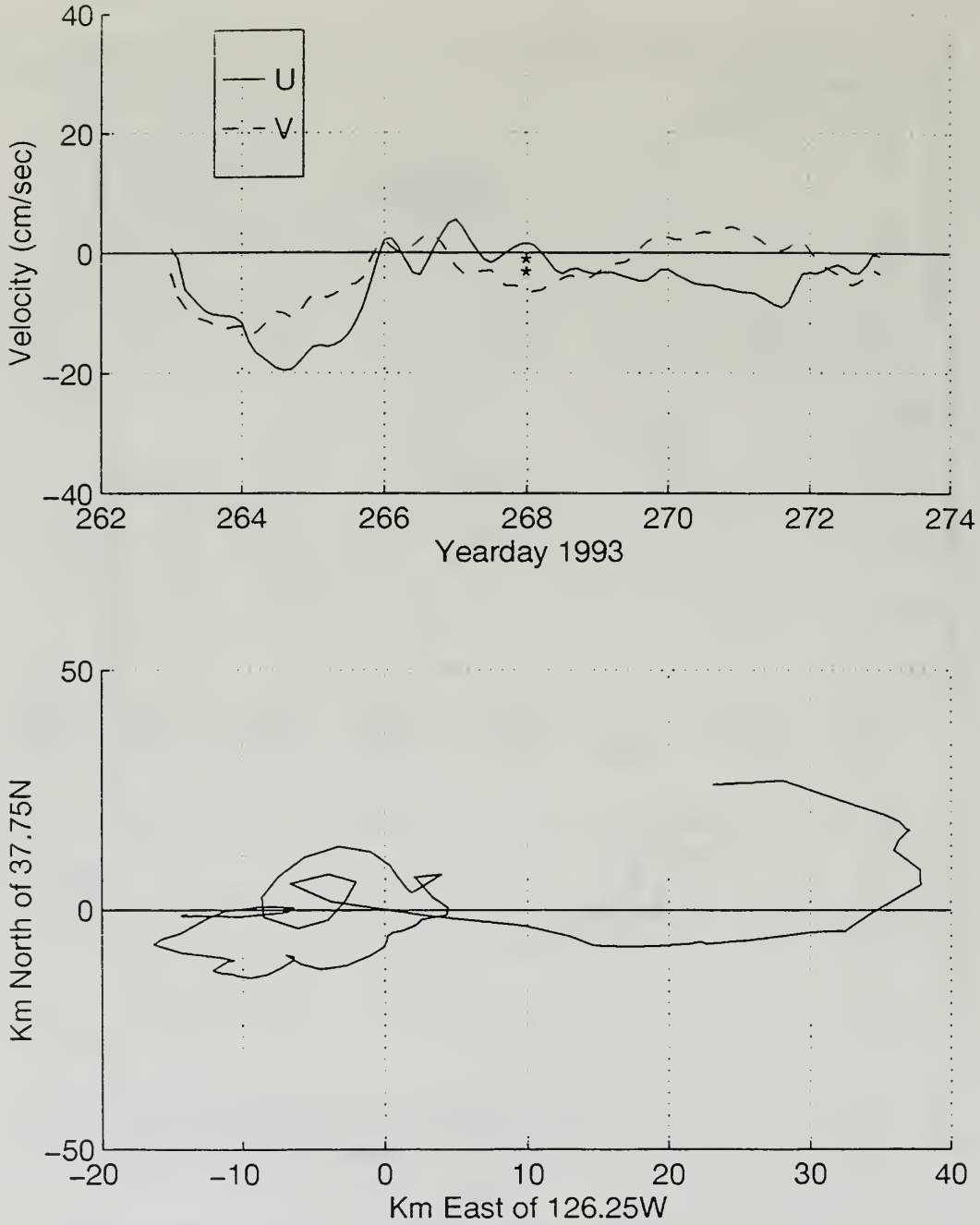


Figure 4.11 Sanderson technique estimates of eddy mean translation (top) and best-fit eddy center (bottom) using 2-day fit lengths for the anticyclonic eddy studied during the second coherent deployment in September 1993. Symbols denote u(*) and v(#) averages from single, 12-day fit.

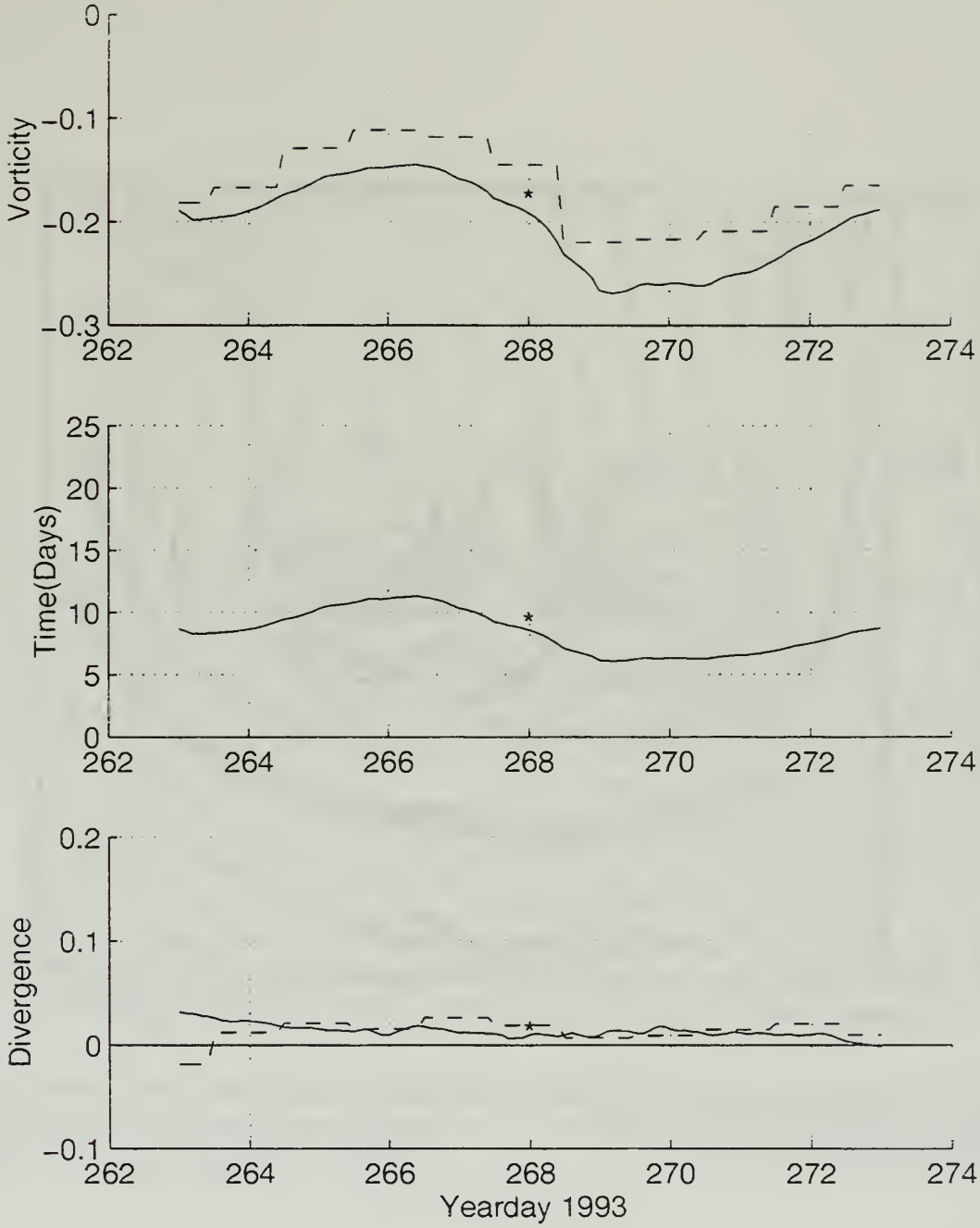


Figure 4.12 Estimates of vorticity (top), rotation rates around the eddy (middle) and divergence (bottom) using 2-day fit lengths for the anticyclonic eddy studied during the second coherent deployment in September 1993. Symbols (*) denote averages from single, 12-day fit. Vorticity and divergence estimates from the filtered dataset (dashed) are also shown.

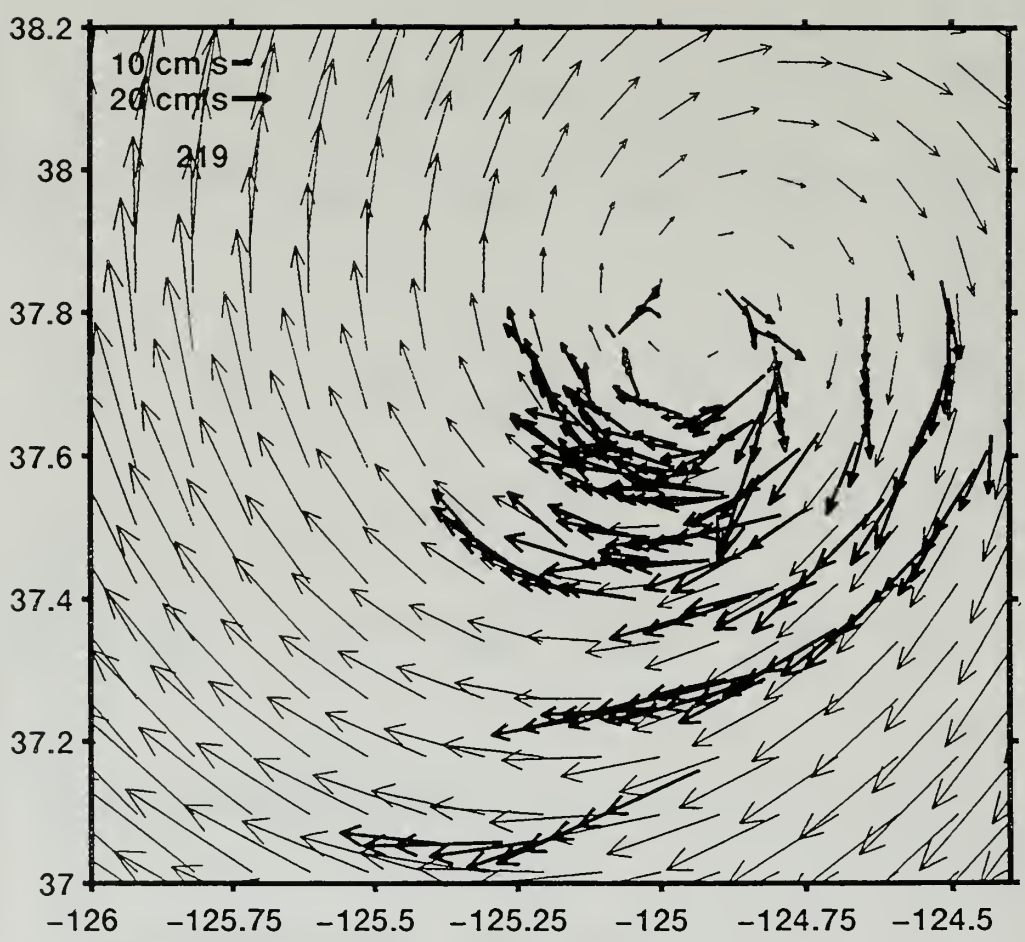


Figure 4.13 Drifter observations interpolated to one-tenth of a day overlaid on Sanderson technique's predicted eddy for Day 263.

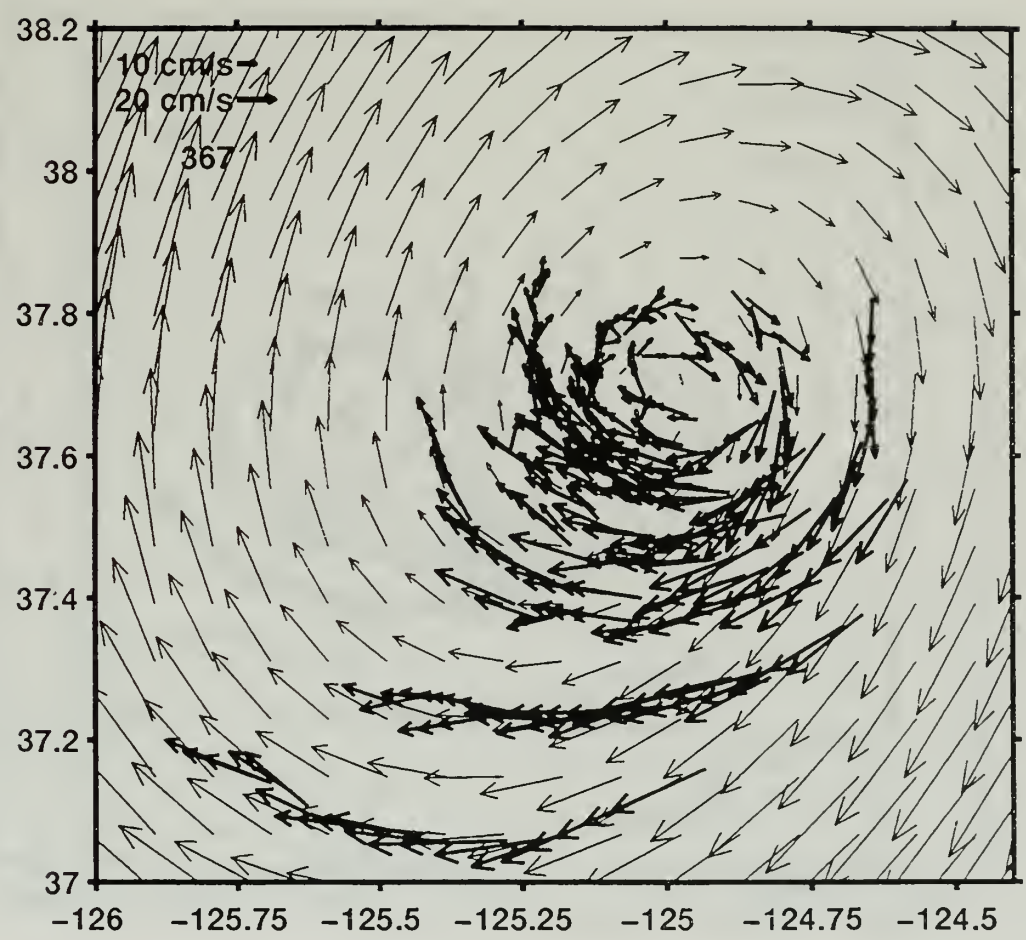


Figure 4.14 Drifter observations interpolated to one-tenth of a day overlaid on Sanderson technique's predicted eddy for Day 264.

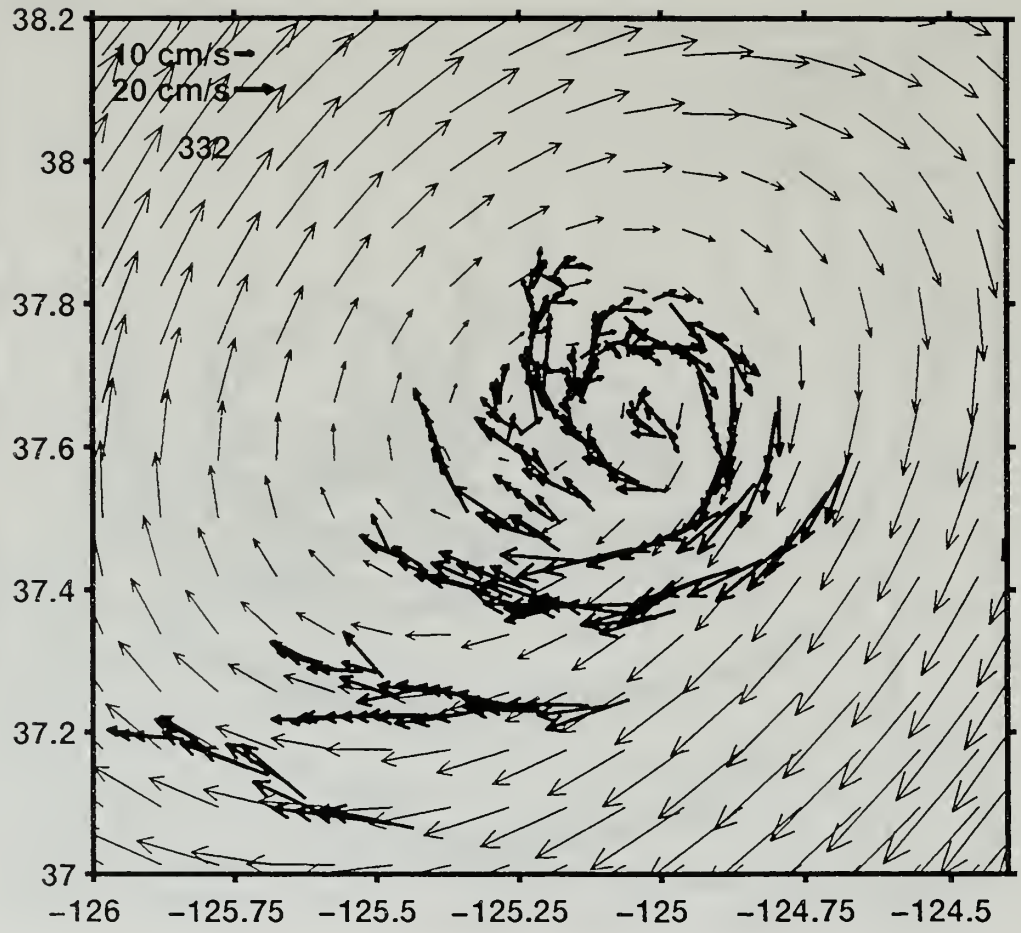


Figure 4.15 Drifter observations interpolated to one-tenth of a day overlaid on Sanderson technique's predicted eddy for Day 265.

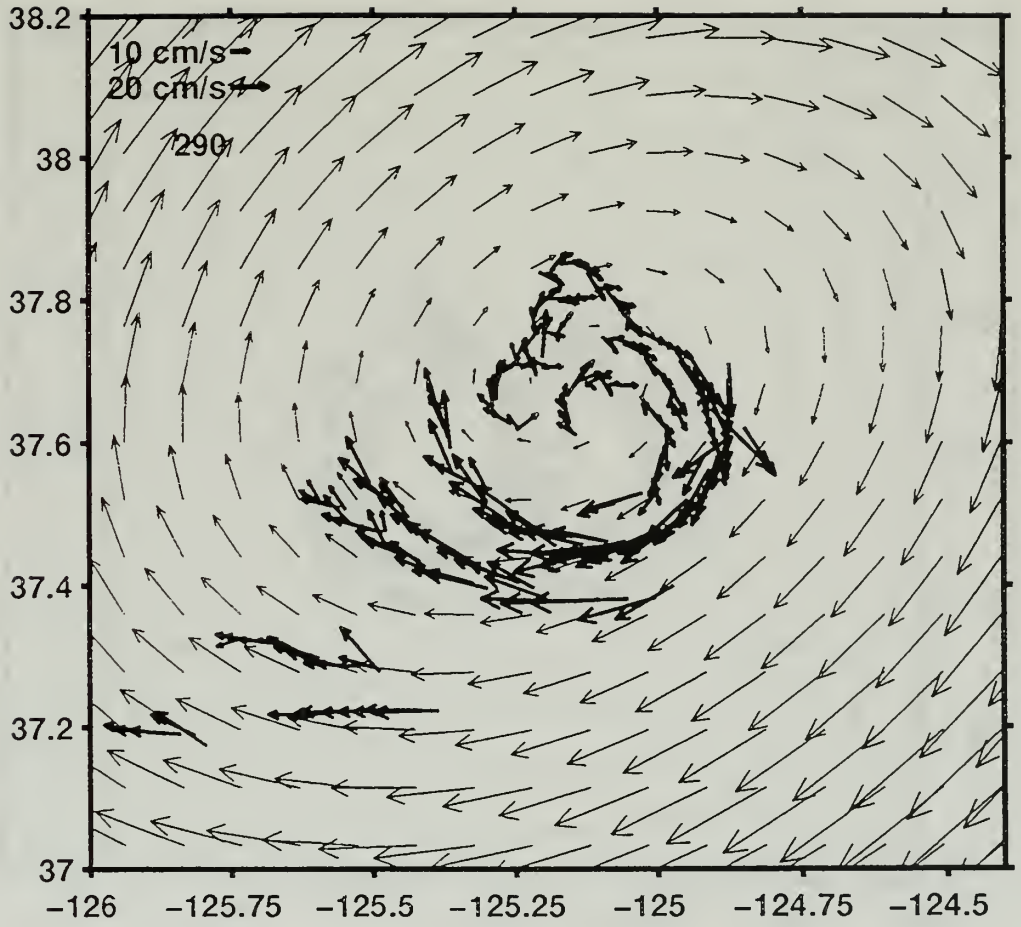


Figure 4.16 Drifter observations interpolated to one-tenth of a day overlaid on Sanderson technique's predicted eddy for Day 266.

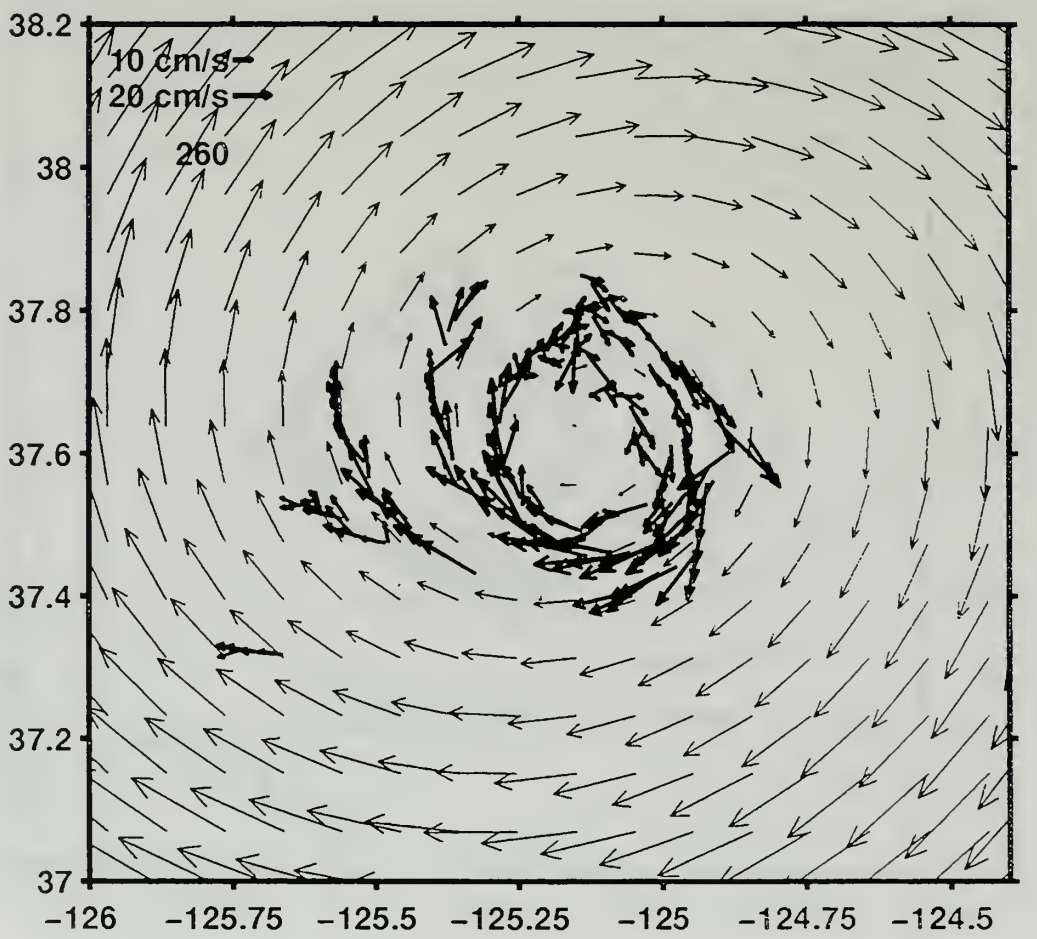


Figure 4.17 Drifter observations interpolated to one-tenth of a day overlaid on Sanderson technique's predicted eddy for Day 267.

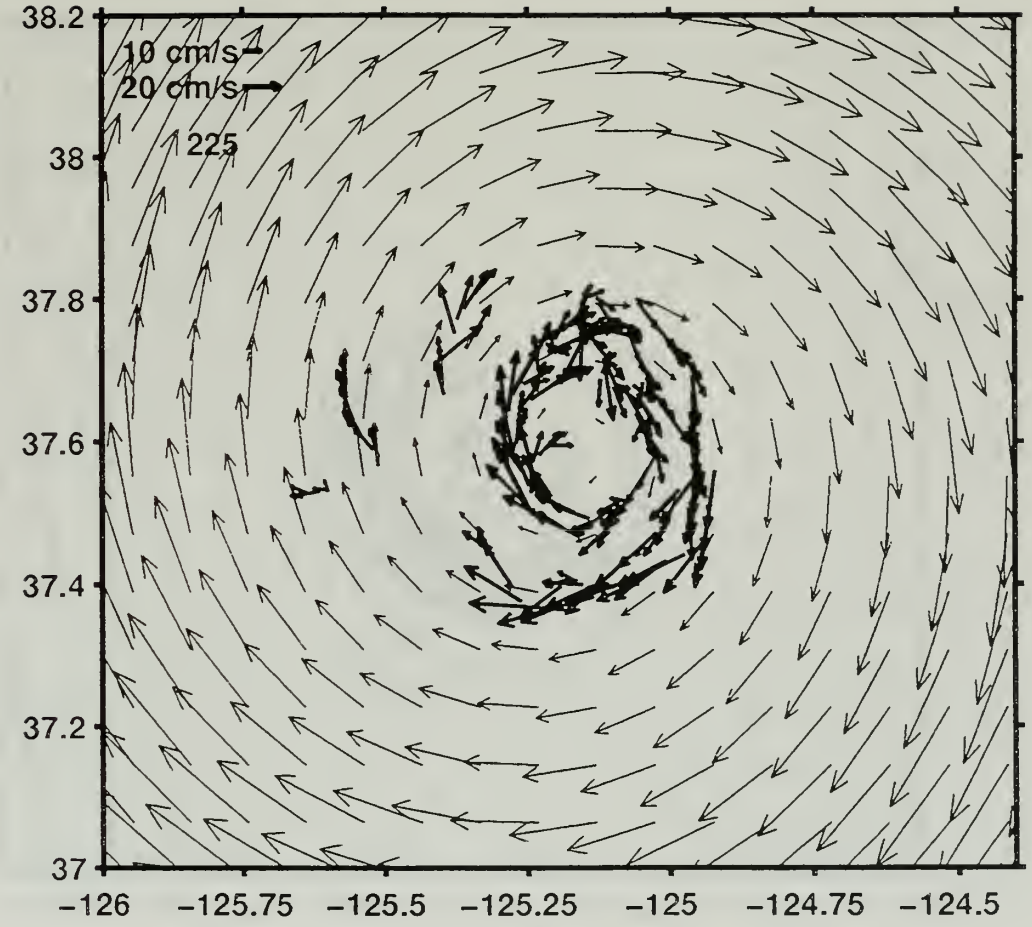


Figure 4.18 Drifter observations interpolated to one-tenth of a day overlaid on Sanderson technique's predicted eddy for Day 268.

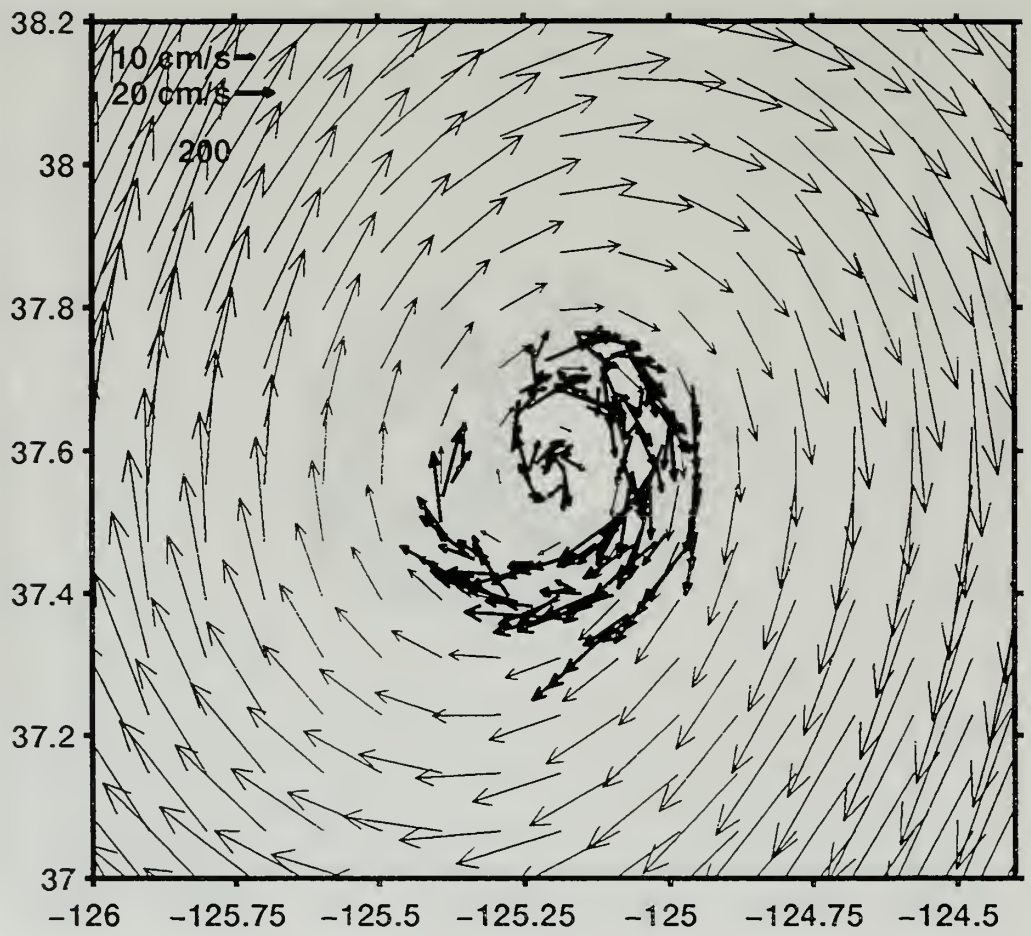


Figure 4.19 Drifter observations interpolated to one-tenth of a day overlaid on Sanderson technique's predicted eddy for Day 269.

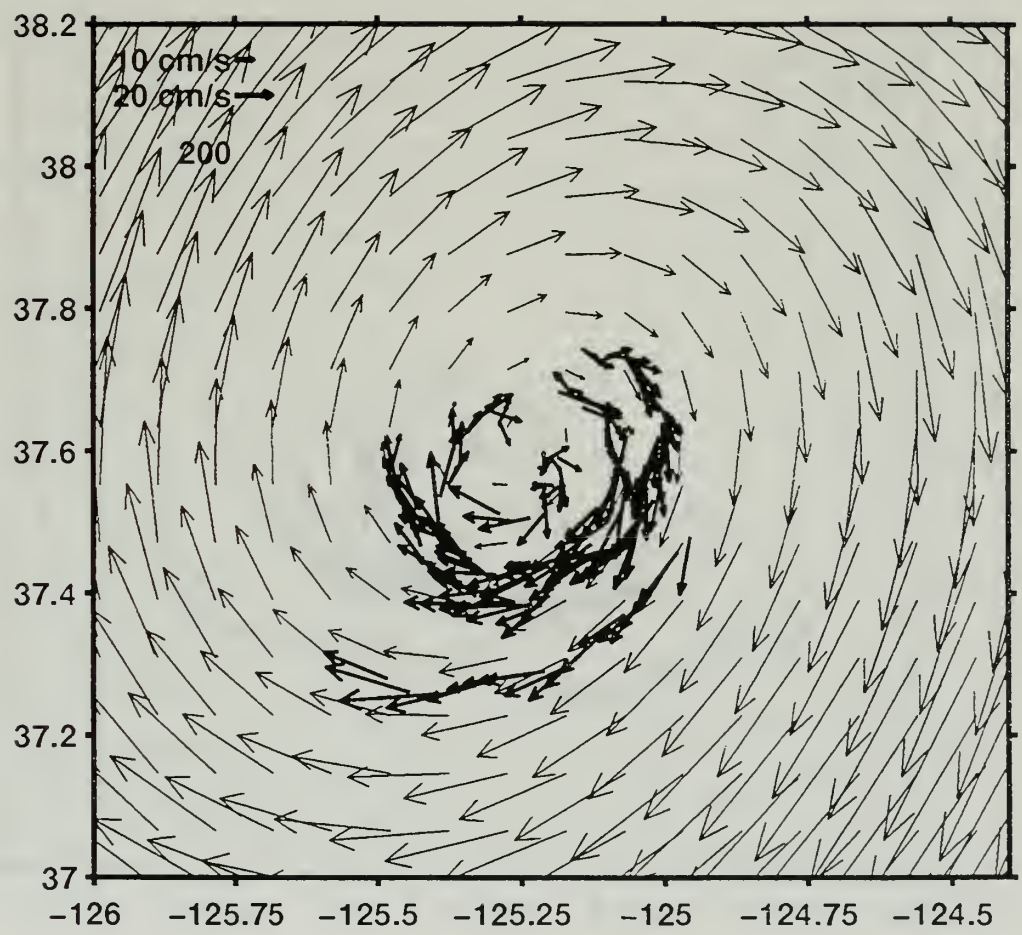


Figure 4.20 Drifter observations interpolated to one-tenth of a day overlaid on Sanderson technique's predicted eddy for Day 270.

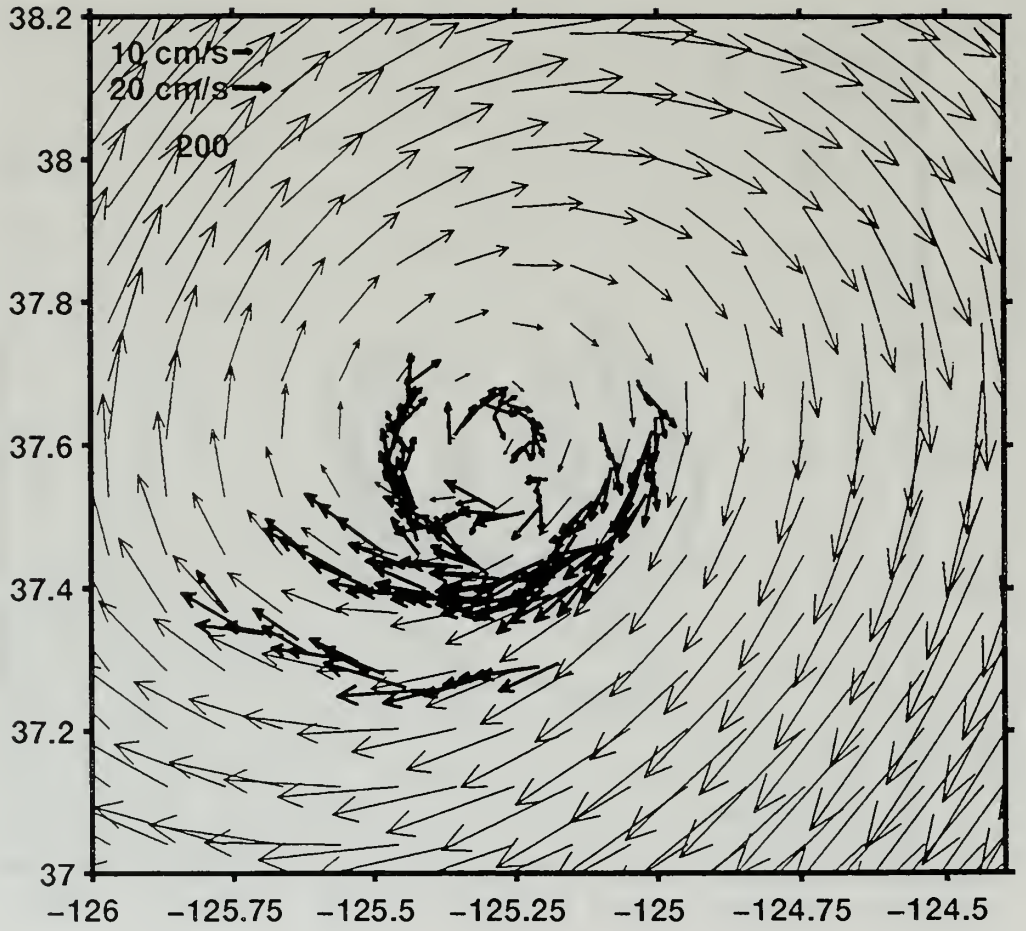


Figure 4.21 Drifter observations interpolated to one-tenth of a day overlaid on Sanderson technique's predicted eddy for Day 271.

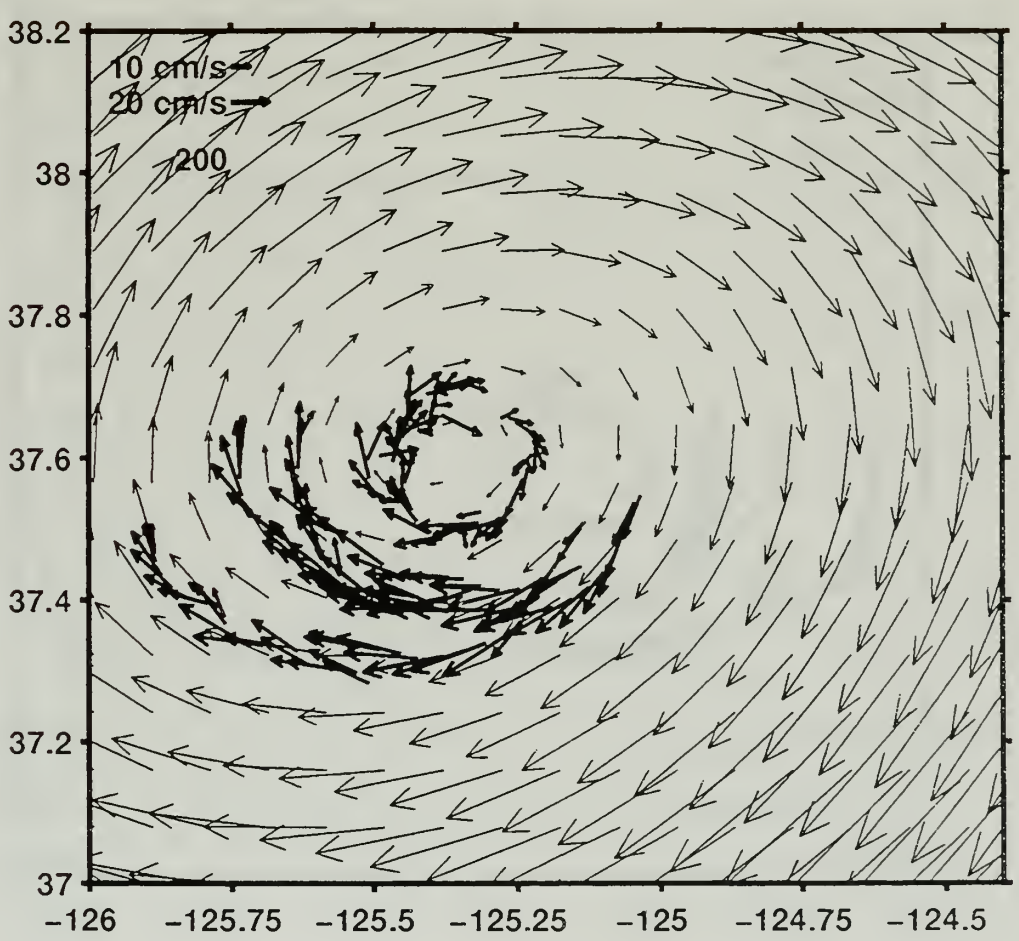


Figure 4.22 Drifter observations interpolated to one-tenth of a day overlaid on Sanderson technique's predicted eddy for Day 272.

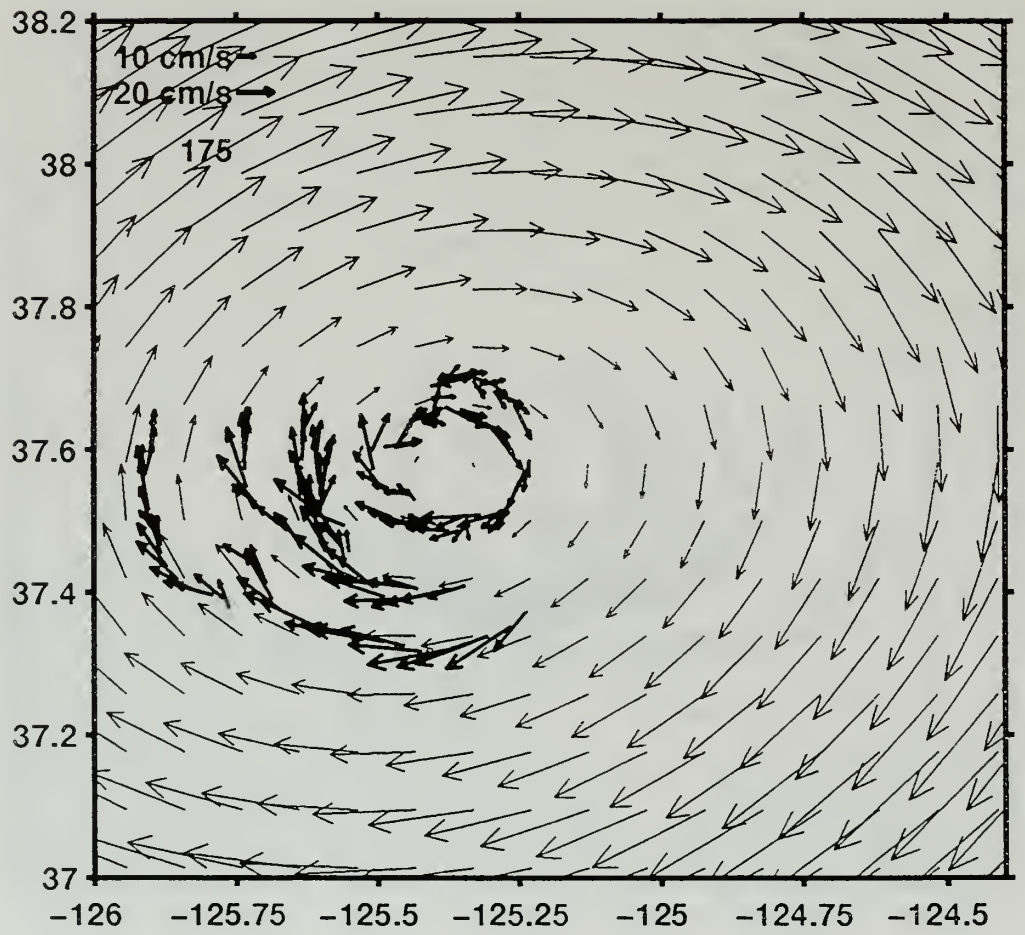


Figure 4.23 Drifter observations interpolated to one-tenth of a day overlaid on Sanderson technique's predicted eddy for Day 273.

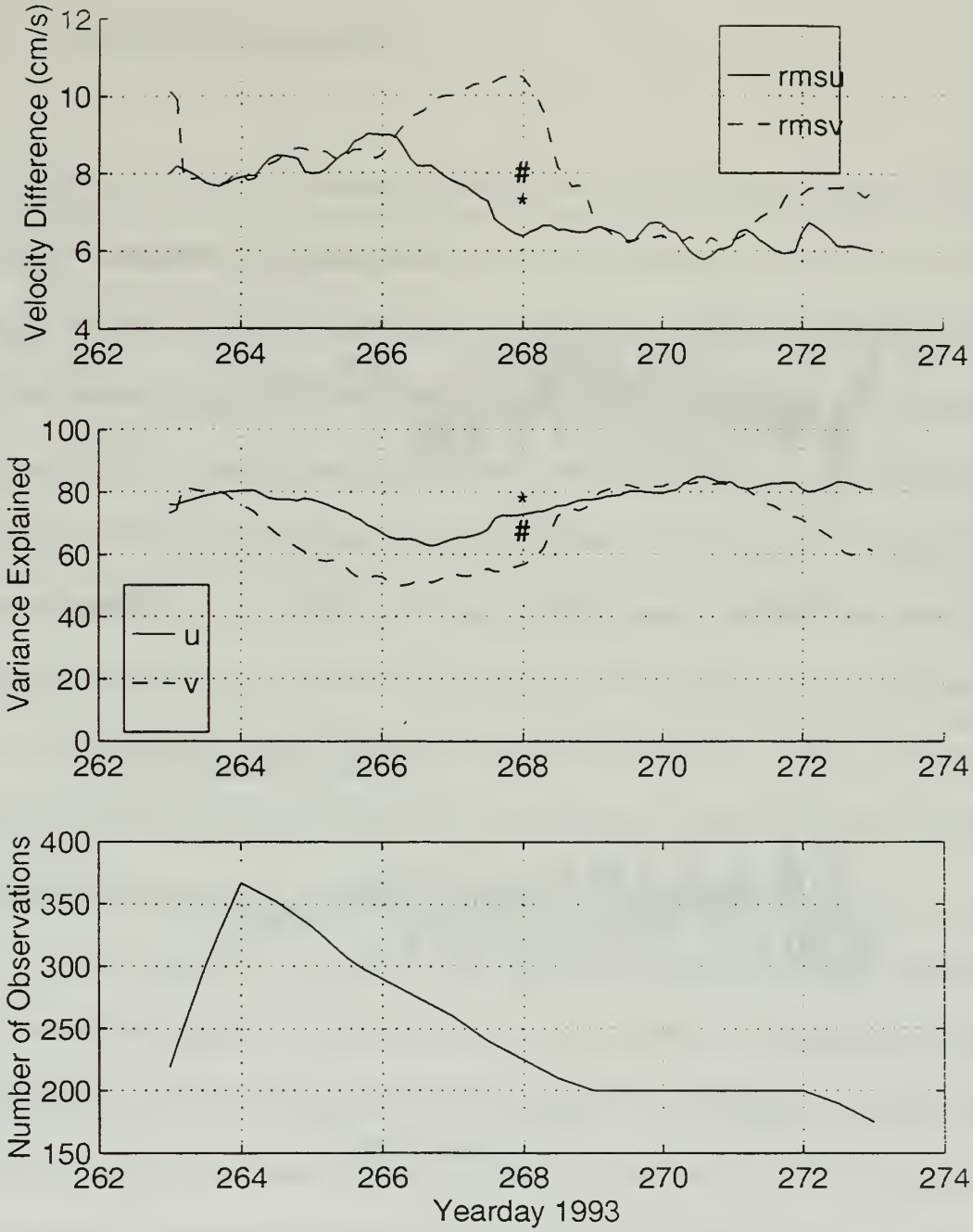


Figure 4.24 Rms velocity differences between actual observations and Sanderson-technique velocities (top), percent variance explained by the model velocities (middle), and the number of observations per day over the seven day time series (bottom) using 2-day fit lengths for the cyclonic eddy. Symbols denote east-west (*) and north-south(#) averages from single, 12-day fit.

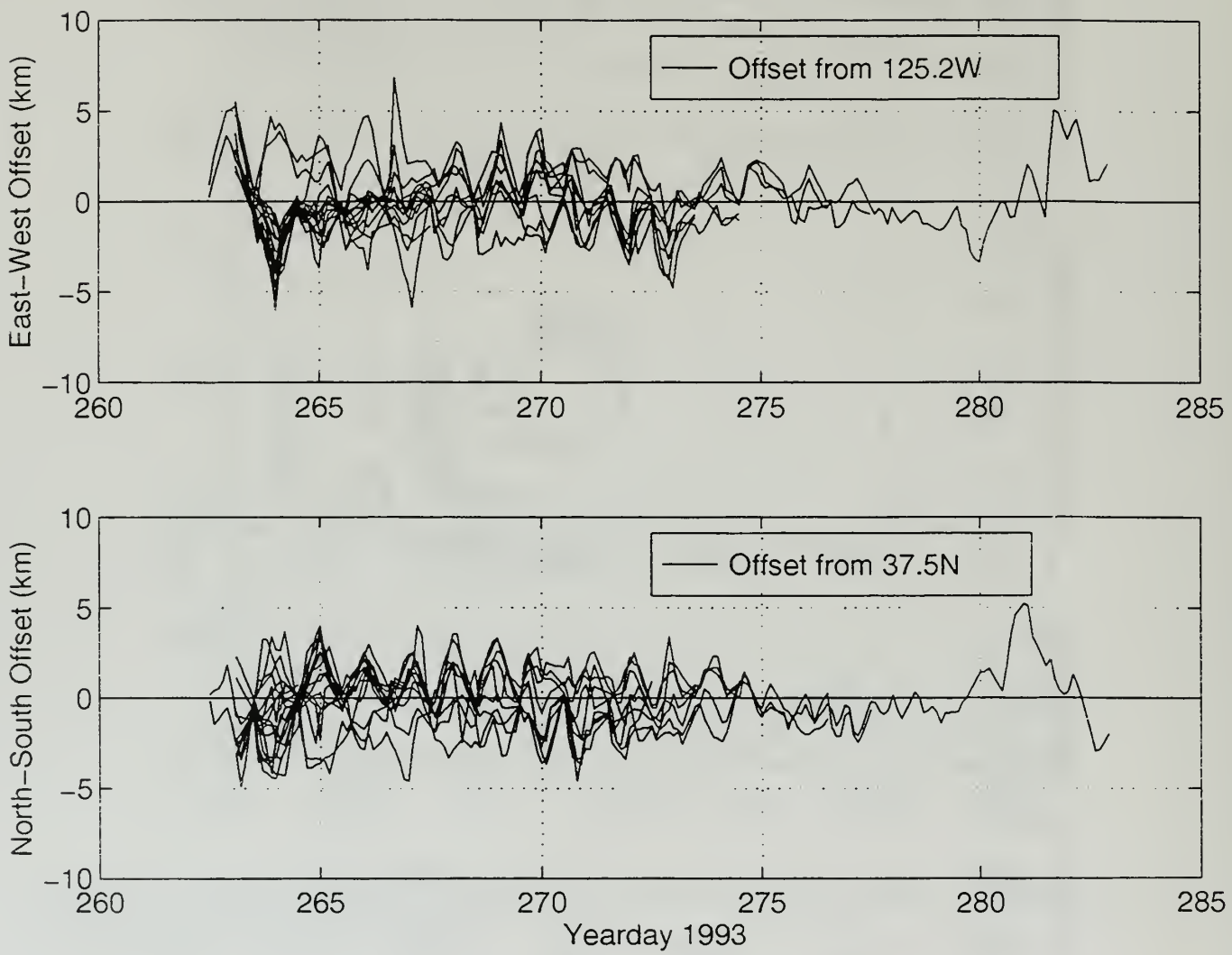


Figure 4.25 The RMS difference (in kilometers) of filtered versus unfiltered drifter positions in the east-west direction (top) and north-south direction (bottom).

# V. CONCLUSIONS

## A. SUMMARY OF RESULTS

Observations of the motions of drifters in the California Current System (CCS) were obtained during the Eastern Boundary Current (EBC) experiment in 1993. NOAA AVHRR satellite imagery and drifter trajectories were used to provide an annual description of the SST features and flow field in the CCS off the northern California coast. The winter season was marked by no visible upwelling or filament activity and small mesoscale instabilities associated with the poleward-flowing Davidson Current. After the spring transition in April, increasingly stronger upwelling and filament activity grew to dominate the coastal flow. Instabilities arising from the strengthening filaments, fueled the formation of eddies as noted in previous studies (Rienecker and Mooers, 1989b; Strub et al., 1991). After the fall transition, upwelling ceased and filaments rapidly decreased in size and intensity, until their complete disappearance by December.

Drifter trajectories were overlaid on the satellite imagery to provide both a qualatative and quantitative approach to the study of the mesoscale field. The trajectories not only highlighted visible mesoscale features, but allowed for quantitative estimates of eddy translation velocities and directions to compare to computed results. The July cyclonic eddy was observed to be translating at an average rate of 3.6 cm/s to the southwest for the three months it was observed. The September anticyclone was observed to be translating at 4.2 cm/s to the southwest, and the anticyclone north of the Point Arena filament was observed

to be nearly stationary. Calculated translation rates for the July and September eddies were very close to these observed rates, as indicated in Table 3.1.

Two eddies, a cyclonic eddy in July and an anticyclonic eddy in September were chosen from AVHRR imagery and hydrographic/ADCP surveys for more detailed analysis using data from drifter deployments of 13 and 24 instruments, respectfully. Drifter data from the two deployments were applied to a first-order linear regression technique developed by Sanderson (1995). The Sanderson technique was used to estimate the two eddy's translation rates and estimates of vorticity and divergence.

The Sanderson technique was used in two different ways in this study: 1) using all available drifter data over 7 (12) days from the cyclone (anticyclone) to obtain single, best-fit translation and rotation estimates and 2) using drifter data for 1-day (2-day) intervals from the cyclone (anticyclone) to investigate the short-term evolution of these eddy parameters. We conclude that this objective, least square technique performs well under conditions of uniform data distribution, such as for the multiple-day, multiple-drifter fits over 7 days or 12 days. In this case, translation and rotation estimates match those estimated, qualitatively, by comparing eddy location observations separated in time by weeks or months.

Using results from the shorter fit intervals, it is tempting to draw conclusions about eddy "spin-down" based on changes in the best-fit rotation period and translation rates. For example, the July cyclone appears to have reduced by half its rotation rate as it drew nearer to the Point Arena filament during the 7-day observation period. Similarly, the September anticyclone substantially reduced its southwestward translation velocity as it drew nearer to the same filament during the 12-day observation period. However, other indicators suggest

that these variations in the best-fit parameters may not be significantly greater than the noise due to inadequate and changing data distributions within the eddies. Inspection of the actual data distribution relative to the predicted eddy fields showed spatially biased sampling whose evolution correlated with changes in the percent variance accounted for in east-west and north-south velocity components. In short, the Sanderson technique (Sanderson, 1995) proved much more sensitive to the relative drifter location than he indicated. Sanderson had sought to eliminate this problem by explicitly regressing over time as well as space, but the technique fails to eliminate the measurement error due to poorly distributed drifter data.

The Sanderson technique did prove effective at reducing the effects of high frequency oscillations on eddy translation and vorticity estimates. In the case of the September anticyclone, low-pass filtered drifter trajectories compared with unfiltered trajectories showed that motions with periods in the inertial (20 hour) to diurnal range, and rms displacements of ~2 km, dominated the higher frequency oscillations. Estimated eddy parameters from the filtered data, however, tracked closely those from the unfiltered data (Figure 4.12) indicating that the Sanderson technique is capable of extracting mesoscale parameters in the presence of higher frequency noise. The one exception noted was that vorticity estimates from the filtered data were biased lower, suggesting the possibility that inertial rotations found their way into the results based on unfiltered data.

## B. RECOMMENDATIONS FOR FUTURE WORK

In order to more fully evaluate the data from both coherent deployments, model results from the Sanderson technique should be compared with those from existing models not requiring spatial derivatives, since these types of models are reliant upon proper buoy spacing. The model by Kirwan et al. (1984, 1988, 1990) and Kirwan (1992), which only depends upon higher-order time derivatives and does not take into account spatial derivatives, would serve as an excellent model for comparison of results.

Both models could also be used to evaluate the large anticyclonic eddy to the north of the Point Arena filament present at the start of August 1993. Drifters sampled that eddy in August and September. Other drifters were also advected into the eddy in late September after leaving the smaller anticyclone that was the focus of the second coherent deployment, making this one the longest observation of an eddy acquired during EBC. The data may suffer from the same buoy geometry biases as the coherent deployments, however.

Another factor which may have biased drifter data was the inclusion of the OSU drifter trajectories into the two coherent deployment datasets. This was desirable to increase the total number of observations and to achieve the research objectives of the coherent deployments. The OSU buoys were deployed with additional biological sensors and had drogues that were different from the standard WOCE-type drifters used by NPS and WHOI. Uniformity in drifting buoy designs, with buoy systems all having similar drag area ratios, is desirable but, more importantly, a more systematic evaluation of the influence of wind-

driven currents and wind-induced slip on these measurements and on the derived eddy parameters should be conducted.

Finally, although the EBC program has been the most comprehensive to date, there still has been no solely dedicated eddy study in the CCS such as the WCRE for Gulf Stream rings. A dedicated study should include a multidisciplinary approach with detailed hydrographic/ADCP surveys prior to a drifter deployment, such as in EBC, but also at regular intervals after the deployment. This would serve as a second comprehensive in-situ set of data on the studied eddy. Such a study would improve prediction capabilities by measuring eddy decay rates and providing clues to decay-causing processes, such as interaction with nearby filaments.

## LIST OF REFERENCES


Batteen, M. L., 1997: Wind-forced modeling studies of currents, meanders, and eddies in the California Current system. J. Geophys. Res., 102, 985-1010.

Beardsley, R. C. and S. J. Lentz, 1987: The Coastal Ocean Dynamics Experiment collection: An Introduction. J. Geophys. Res., 92, 1455-1463.

Bray, N. H. and C. L. Greengrove, 1993: Circulation over the shelf and slope off Northern California. J. Geophys. Res., 98, 18,119-18,146.

Brink, K.H., and T.J.Cowles, 1991: The Coastal Transition Zone program. J. Geophys. Res., 96, 14,637-14,647.

Brown, J. E. M., 1995: Drifter-based velocity statistics in the vicinity of the Azores Front. M.S. thesis, Naval Postgraduate School, 152 pp.

Chumbinho, R. P. A., 1994: Kinematics and Dynamics of a cyclonic eddy off PT. Arena, California. Phd Dissertation, Naval Postgraduate School, 84 pp.

Davis, R. E., 1985a: Drifter observations of coastal surface currents during CODE: The statistical and dynamical views. J. Geophys. Res., 90, 4756-4772.

Davis, R. E., 1985b: Drifter observations of coastal surface currents during CODE: The method and descriptive view. J. Geophys. Res., 90, 4741-4755.

Evans, R. H., K. S. Baker, O. B. Brown, and R. C. Smith, 1985: Chronology of Warm-Core Ring 82B. J. Geophys. Res., 90, 8803-8811.

Flierl, G. R. and R. P. Mied, 1985: Frictionally induced circulations and spin down of a warm- core ring. J. Geophys. Res., 90, 8917-8927.

Halide, H. and B. G. Sanderson, 1993: Determining flow field singularities from drifter trajectories. J. Geophys. Res., 98, 8413-8423.

Halliwell, G. R. , Jr., and J. S. Allen, 1987: The large-scale coastal wind field along the west coast of North America, 1981-1982. J. Geophys. Res., 92, 1861-1884.

Hickey, B. M., 1996: Western North America, Tip of Baja California to Vancouver Island. in The Sea, John Wiley, New York, in press.

Hickey, B. M., 1979: The California Current system-Hypothesis and facts. Prog. Oceanogr., 8, 191- 279.

Hooker, S. B. and D. B. Olson, 1984: Center of mass estimation in closed vortices: A verification in principle and practice. J. Atmos. Oceanic Technol., 1, 247-255.

Huyer, A., P. M. Kosro, J. Fleischbein, S. R. Ramp, T. Stanton, L. Washburn, F. P. Chavez, T. J. Cowles, S. D. Pierce, and R. L. Smith, 1991: Currents and water masses of the coastal transition zone off northern California, June to August 1988. J. Geophys. Res., 96, 14,809-14,831.

Huyer, A., E. J. C. Sobey, and R. L. Smith, 1979: The spring transition in currents over the Oregon continential shelf. J. Geophys. Res., 84, 6995-7011.

Joyce, T. M., 1985: Gulf Stream Warm-Core Ring Collection: An Introduction. J. Geophys. Res., 90, 8801-8802.

Kelly, K. A., R. C. Beardsley, R. Limeburner, K. H. Ruik, J. D. Paduan, and T. K. Chereskin, Variability of the near-surface eddy kinetic energy in the California Current based on altimetric, drifter and moored current data. in preparation for submission to J. Geophys. Res.

Kirwan, A. D., Jr., 1992: Corrections to 'Observed and simulated properties of loop current rings' by A. D. Kirwan et al. J. Geophys. Res., 97, 11,471-11,472.

Kirwan, A. D., Jr., A. W. Indest, J. Liu, and N. Clark, 1990: Ring evolution in general circulation models from path analysis. J. Geophys. Res., 95, 18,057-18,073.

Kirwan, A. D., Jr., 1988: Notes on the cluster method for interpreting relative motions. J. Geophys. Res., 93, 9337-9339.

Kirwan, A. D., Jr., J. K. Lewis, A. W. Indest, P. Reinersman, and I. Quintero, 1988: Observed and simulated kinematic properties of Loop Current rings. J. Geophys. Res., 93, 1189-1198.

Kirwan, A. D., Jr., W. J. Merrell, Jr., J. K. Lewis, R. E. Whitaker, and R. Legeckis, 1984: A model for the analysis of drifter data with an application to a warm core ring in the Gulf of Mexico. J. Geophys. Res., 89, 3425-3428.

Largier, J. L., B. A. Magnell and C. D. Winant, 1993: Subtidal circulation over the Northern California shelf. J. Geophys. Res., 98, 18,147-18,180.

Lynn, R. J. and J. J. Simpson, 1987: The California Current system: the seasonal variability of its physical characteristics. J. Geophys. Res., 92, 12947-12966.

Menke, W., 1984: Geophysical data analysis: Discrete inverse theory. Academic Press, Inc., Orlando, Fl., pp 260.

Molinari, R., and A. D. Kirwan, Jr., 1975: Calculations of differential kinematic properties from Lagrangian observations in the Western Caribbean Sea. J. Phys. Oceanogr., 5, 361-368.

Nelson, C. S., 1977: Wind stress and wind stress curl over the California Current, NOAA Tech. Rep., NMFS SSRF-714, 89 pp.

Niiler, P. P., J. D. Paduan, A. L. Sybrandy, and L. Sombardier, 1991: The WOCE/TOGA Lagrangian surface drifter. Proceedings of OCEANS 91, IEEE, Honolulu, HA.

Niiler, P. P., R. E. Davis, and H. J. White, 1987: Water-following characteristics of a mixed layer drifter. Deep-Sea Res., 34, 1867-1881.

Niiler, P. P. and J. D. Paduan, 1995: Wind-driven motions in the northeast Pacific as measured by Lagrangian drifters. J. Phys. Oceanogr., 25, 2819-2830.

Niiler, P. P., A. S. Sybrandy, K. Bi, P-M. Poulain, and D. Bitterman, 1995: Measurements of the water-following capability of Holey-sock and TRISTAR drifters. Deep-Sea Res., 1951-1964.

Olson, D. B., R. W. Schmitt, M. Kennelly, and T. M. Joyce, 1985: A Two-layer diagnostic model of the long-term physical evolution of warm-core ring 82B. J. Geophys. Res., 90, 8813-8822.

Paduan, J. D. and P. P. Niiler, 1990: A Lagrangian description of motion in northern California coastal transition filaments. J. Geophys. Res., 95, 18,095-18,109.

Poulain, P.-M., and P. P. Niiler, 1989: Statistical Analysis of the surface circulation in the California Current System using satellite-tracked drifters. J. Phys. Oceanogr., 19, 1588-1603.

Poulain, P.-M., A. Warn-Varnas, and P. P. Niiler, 1996: Near-surface circulation of the Nordic Seas as measured by lagrangian drifters. J. Geophys. Res., 101, 18,237-18,258

Reynolds, R.W., 1988: A real-time global sea surface temperature analysis. J. Climate, 1, 75-86.

Rienecker, M. M. and C. N. K. Mooers, 1989a: A summary of the OPTOMA program's mesoscale ocean prediction studies in the California Current system. in, Mesoscale/SynopticCoherent Structures in Geophysical Turbulence, edited by J. C. J. Nihoul and B. M. Jamart, pp. 519-548, Elsevier Sci., New York.

Rienecker, M. M. and C. N. K. Mooers, 1989b: Mesoscale eddies, jets, and fronts off Point Arena, California, July 1986. J. Geophys. Res., 94, 12,555-12,569.

Ring Group, 1981: Gulf Stream cold core rings: Their physics, chemistry and biology. Science, 212, 1091-1100.

Robinson, A. R., 1983: Overview and Summary of Eddy Science. in, Eddies in Marine Science, edited by A. R. Robinson, M. Ghil, R. Sadourny, J. Sundermann, pp 3-15, Springer-Verlag, Berlin Heidelberg.

Sanderson, B. G., 1995: Structure of an eddy measured with drifters. J. Geophys. Res., 100, 6761-6776.

Strub, P. T., P. M. Kosro, A. Huyer, and CTZ Collaborators, 1991: The nature of the cold filaments in the California Current system. J. Geophys. Res., 96, 14,743-14,768.

Strub, P. T., and C. James, 1995: The large-scale summer circulation of the California Current. Geophys. Res. Lett., 22, 207-210.

## INITIAL DISTRIBUTION LIST

| | No. Copies |
|---|---|
| 1. Defense Technical Information Center<br>8725 John J. Kingman Rd., STE 0944<br>Ft. Belvoir, VA 22060-6218 | 2 |
| 2. Dudley Knox Library<br>Naval Postgraduate School<br>411 Dyer Rd.<br>Monterey, CA 93943-5101 | 2 |
| 3. Library, Scripps Institution of Oceanography<br>Code C-075, UC-San Diego<br>La Jolla, CA 92093 | 1 |
| 4. Director, Naval Ocean. Div.<br>Naval Observatory<br>34th and Mass. Ave., NW<br>Washington, D. C. 20390 | 1 |
| 5. Dr. Jeffrey D. Paduan<br>Department of Oceanography<br>Code OC/PD<br>833 Dyer Rd.<br>Monterey, CA 93943-5000 | 1 |
| 6. Dr. Pierre-Marie Poulain<br>Department of Oceanography<br>Code OC/PN<br>833 Dyer Rd.<br>Monterey, CA 93943-5000 | 1 |
| 7. Dr. Pearn P. Niiler<br>Scripps Institution of Oceanography<br>UCSD, Code 0230<br>La Jolla, CA 92093-0230 | 1 |
| 8. Commanding Officer, Naval Oceanographic Office<br>1002 Balch Blvd.<br>Stennis Space Ctr., MS 39522 | 1 |
| 9. Commander, Naval Meteor. And Oceanography Command<br>1020 Balch Blvd.<br>Stennis Space Ctr., MS 39529-5005 | 1 |

10. Dr. Steve Ramp 1
Office of Naval Research
Code, 322 PO
800 N. Quincy St.
Arlington, VA 22217-5660

11. Dr. Robert Beardsley 1
Physical Oceanography
Woods Hole Oceanographic Institution
Woods Hole, MA 02543

12. Dr. Michael Kosro 1
College of Oceanography
Oceanography Admin Bldg. 104
Oregon State University
Corvallis, OR 97331-5503

13. Lt. James G. Sires 1
3936 Plantation Drive
Hermitage, TN 37076